TÉCNICO LISBOA

Cell-derived ECM loaded electrospun nanofibrous scaffolds for periodontal regeneration

Mafalda Silva Santos

Thesis to obtain the Master of Science Degree in

Biomedical Engineering

Supervisors: Dr. Marta Monteiro Silva Carvalho
Dr. João Carlos Fernandes da Silva

Examination Committee

Chairperson: Prof. Cláudia Alexandra Martins Lobato da Silva
Supervisor: Dr. Marta Monteiro Silva Carvalho
Member of the Committee: Dr. Ana Filipa Soares Pires

December 2022

Preface

The work presented in this thesis was performed at the Institute for Bioengineering and Biosciences of Instituto Superior Técnico (Lisbon, Portugal), during the period March-October 2022, under the supervision of Dr. João Carlos Fernandes da Silva and Dr. Marta Monteiro Silva Carvalho.

Declaration

I declare that this document is an original work of my own authorship and that it fulfills all the requirements of the Code of Conduct and Good Practices of the Universidade de Lisboa.

Acknowledgments

First of all, I would like to thank my amazing supervisors Dr. Marta Carvalho and Dr. João Silva, for their availability (specially for our improvised meetings), dedication and constant support throughout the thesis. I would like to thank Professor Joaquim Cabral for the opportunity to be part of the Stem Cell Engineering Research Group at iBB and Professor Frederico Ferreira for being integrated in the Bioengineering group. I would like to thank Professor Cláudia Lobato da Silva, Dr. Ana Fernandes and everyone from Lab 3, for the incredible working environment. I would like to thank my colleagues working in the cold Bioengineering Lab, particularly Dr. Fábio Garrudo for insightful contributions and support in the lab even at late working hours. I would also like to thank Rachel Cordeiro for the characterization analysis of the electrospun scaffolds, performed at CDRSP-Politécnico de Leiria and Frederico Barbosa for the last minute SEM analysis of some of my electrospun scaffolds.

I would like to thank for the funding received from the FCT projects "Exploiting the power of decellularized extracellular matrix to fabricate hierarchical biomimetic scaffolds to regenerate functional periodontal tissues" (PTDC/BTM-MAT/3538/2020) and "In silico models guiding in vitro biophysical stimulation of biomimetic hierarchical scaffolds: a computational modelling approach towards functional osteochondral regeneration" (PTDC/EME-SIS/0838/2021).

I would like to thank my group of friends at IST for their companionship during the 5 years of the Master and my partner for his astounding patience and company.

Abstract

Periodontitis is an inflammatory infection caused by bacterial plaque accumulation that affects the periodontal tissues supporting the tooth. Current treatments lack bioactive signals to induce tissue repair and coordinated regeneration of the periodontium, thus alternative strategies are needed to improve clinical outcomes. Cell-derived extracellular matrix (ECM) has been used in combination with biomaterials to enhance their biofunctionality for various tissue engineering (TE) applications. In this work, bioactive cell-derived ECM loaded electrospun polycaprolactone/chitosan (PCL/CTS) nanofibrous scaffolds were developed using lyophilized decellularized ECM (dECM) derived from human Periodontal Ligament Stem Cells (PDLSCs). This work's aims were to fabricate and characterize cell-derived ECM electrospun PCL/CTS scaffolds and assess their ability to enhance the osteogenic differentiation of PDLSCs, envisaging periodontal TE applications. Human PDLSCs were cultured and used for dECM production. PDLSCs and dECM were characterized regarding morphology, protein expression, and DNA, glycosaminoglycans and collagen contents. Osteogenic differentiation of PDLSCs was performed on PCL, PCL/CTS and PCL/CTS/ECM electrospun scaffolds for 21 days. The obtained results demonstrate that PCL/CTS/ECM scaffolds promoted cell proliferation compared to PCL and PCL/CTS scaffolds, while maintaining similar physical and mechanical properties of PCL/CTS scaffolds. PCL/CTS/ECM scaffolds enhanced the osteogenic differentiation of PDLSCs, confirmed by increased ALP activity and calcium deposition. PCL/CTS scaffolds showed higher levels of calcium deposition and cell mineralization than PCL scaffolds. Overall, results show that ECM loaded electrospun scaffolds enhanced the osteogenic differentiation and proliferation of PDLSCs. This work describes the first use of lyophilized cell-derived ECM loaded electrospun scaffolds for periodontal TE applications and highlights its potential as a promising therapeutic strategy for periodontitis.

Keywords

Cell-derived Extracellular Matrix; Electrospinning; Periodontal Ligament Stem Cells; Periodontal Regeneration; Tissue Engineering

Resumo

A periodontite é uma doença inflamatória causada por acumulação de placa bacteriana que afeta os tecidos periodontais que suportam o dente. Os tratamentos atuais carecem de sinais bioativos que induzem a reparação do tecido e a regeneração coordenada do periodonto, portanto estratégias alternativas são necessárias para melhorar resultados clínicos. Matriz extracelular (ECM) derivada de células tem sido usada com biomateriais para melhorar a sua biofuncionalidade para diversas aplicações de engenharia de tecidos (ET). Neste trabalho, suportes nanofibrosos bioativos de policaprolactona (PCL) e quitosano (CTS) com ECM derivada de células foram desenvolvidos usando ECM descelularizada (dECM) liofilizada derivada de células estaminais humanas do ligamento periodontal (PDLSCs). Os objetivos deste trabalho foram fabricar e caracterizar suportes eletrofiados de PCL/CTS com dECM e avaliar a sua capacidade de potenciar a diferenciação osteogénica de PDLSCs, com vista a aplicações em ET periodontal. PDLSCs humanas foram cultivadas e usadas para produzir dECM. PDLSCs e dECM foram caracterizadas quanto à sua morfologia, expressão proteica, e conteúdos de DNA, glicosaminoglicanos e colagénio. Diferenciação osteogénica de PDLSCs foi efetuada em suportes electrofiados de PCL, PCL/CTS e PCL/CTS/ECM durante 21 dias. Os resultados obtidos demonstram que suportes de PCL/CTS/ECM promoveram maior proliferação celular que suportes de PCL e PCL/CTS, ainda mantendo propriedades físicas e mecânicas semelhantes a suportes de PCL/CTS. Suportes de PCL/CTS/ECM potenciaram a diferenciação osteogénica de PDLSCs, confirmado por atividade ALP e deposição de cálcio aumentadas. Suportes de PCL/CTS mostraram níveis mais elevados de deposição de cálcio e mineralização celular do que suportes de PCL. Em geral, os resultados mostram que suportes eletrofiados com dECM potenciaram a diferenciação osteogénica e a proliferação de PDLSCs. Este trabalho descreve a primeira utilização de suportes eletrofiados com dECM liofilizada para aplicações em ET periodontal e sublinha o seu potencial como uma estratégia terapêutica promissora para a periodontite.

Palavras Chave

Matriz extracelular derivada de células; Electrofiação; Células Estaminais do Ligamento Periodontal; Regeneração Periodontal; Engenharia de Tecidos

Contents

List of Figures

List of Tables

Acronyms

AA	Acetic Acid
ALP	Alkaline Phosphatase
ASP	Asporin
ATR-FTIR	Attenuated Total Reflectance Fourier Transform Infrared Spectroscopy
BSA	Bovine Serum Albumin
CHL	Chloroform
CL	Crosslinking
CMP	Cementum Protein
COL	Collagen
CTS	Chitosan
DCM	Dichloromethane
DD	Degree of Deacetylation
DMEM	Dulbecco's Modified Eagle's Medium
DMMB	Dimethyl-Methylene Blue
DFSC	Dental Follicle Stem Cell
DPSC	Dental Pulp Stem Cell
DSC	Differential Scanning Calorimetry
ECM	Extracellular Matrix
EDX	Energy Dispersive X-Ray
FA	Formic Acid
FBS	Fetal Bovine Serum
FIB	Fibronectin
GAGs	Glycosaminoglycans

GEL	Gelatin
GTR	Guided Tissue Regeneration
HCl	Hydrochloric Acid
HFIP	Hexafluoroisopropanol
LAM	Laminin
MFD	Mean Fiber Diameter
MSC	Mesenchymal Stem/Stromal Cell
MW	Molecular Weight
OC	Osteocalcin
OPN	Osteopontin
OSX	Osterix
PBS	Phosphate Buffered Saline
PCL	Polycaprolactone
PDL	Periodontal Ligament
PDLSC	Periodontal Ligament Stem/Stromal Cell
PEG	Polyethylene Glycol
PFA	Paraformaldehyde
PHAL	Phalloidin
PLA	Polylactic Acid
PLGA	Poly(lactic-co-glycolic acid)
POSTN	Periostin
qRT-PCR	Quantitative Reverse Transcription-Polymerase Chain Reaction
RUNX2	Runt-related transcription factor 2
SEM	Scanning Electron Microscopy
SIAL	Sigma-Aldrich
TFA	Trifluoroacetic Acid
TFE	Trifluoroethanol
TGA	Thermogravimetric Analysis
UTS	Ultimate Tensile Strength

1

Aims and Objectives

Motivation

Periodontitis is a chronic inflammatory infection of the periodontium, the structure responsible for ensuring tooth attachment and stability. This infection is caused and sustained by bacteria from dental plaque accumulation. Periodontitis, in its advanced form, is characterized by the loss and destruction of the periodontium, which is consisted of periodontal ligament, root cementum and alveolar bone. The current treatments for periodontitis, such as bone grafts and membranes for guided tissue regeneration, fail to achieve periodontal ligament regeneration and integration of soft (periodontal ligament) and hard (cementum and alveolar bones) tissues. Alternative strategies to treat periodontitis that lead to a coordinated regeneration of all periodontal tissues are needed to improve clinical outcomes.

Specific Objectives

This work's main objective is to develop cell-derived ECM loaded electrospun polycaprolactone/chitosan nanofibrous scaffolds, using decellularized ECM derived from Periodontal Ligament Stem Cells (PDLSCs). Electrospun scaffolds with PDLSC-derived ECM were developed with the aim to mimic the structure, architecture and the composition of native periodontal tissue ECM. Cell-derived ECM creates a biomimetic microenvironment, which was combined with polycaprolactone/chitosan (PCL/CTS) electrospun scaffolds with the desired properties for periodontal regeneration. Each component involved in the development of the electrospun scaffolds was analysed and characterized. The multilineage differentiation capacity and expression of certain surface markers by PDLSCs were verified. PDLSCs and PDLSC-derived ECM were characterized, regarding morphology, ECM composition and expression of relevant ECM proteins. Electrospinning process was optimized to facilitate dECM incorporation in polymer solutions and to produce uniform PCL/CTS fibers with the desired mechanical properties. The physicochemical properties of electrospun scaffolds were assessed (e.g. structure, elemental composition, mechanical properties, contact angle) and the effects of CTS and dECM presence on the scaffolds' properties were determined. The biological effects of the scaffolds on the PDLSCs were evaluated and the influence of CTS and dECM on the biological effects of the scaffolds was assessed. PDLSC proliferation and osteogenic differentiation on electrospun scaffolds were analysed using various assays and stainings (e.g. Alamar Blue Cell Viability Assay, ALP activity quantification, gene expression analysis by qRT-PCR, Von Kossa and Alizarin Red Stainings). This work proposes a promising bioactive scaffold and aims to contribute to the development of novel strategies for periodontal tissue engineering.

Thesis Outline

This thesis is organized into six main chapters follows: In chapter 1, the aims and objectives of this work were laid out. Chapter 2 consists of important literature background necessary to understand this work. In chapter 3 all the materials and methods used to develop this project are detailed. In chapter 4 the results obtained are presented and analyzed. Chapter 5 contains further discussion of the results. Lastly, in chapter 6 the main conclusions are summarized and potential future work is discussed.

2

Introduction

Contents

2.1 The Periodontium

The periodontium is a complex structure composed of hard and soft tissues that support the tooth. It has an important role of ensuring tooth attachment to the bone of the jaw and allowing the teeth to withstand the forces of mastication. The periodontium consists of alveolar bone, root cementum and Periodontal Ligament (PDL). The anatomy of the periodontium is illustrated in figure 2.1.

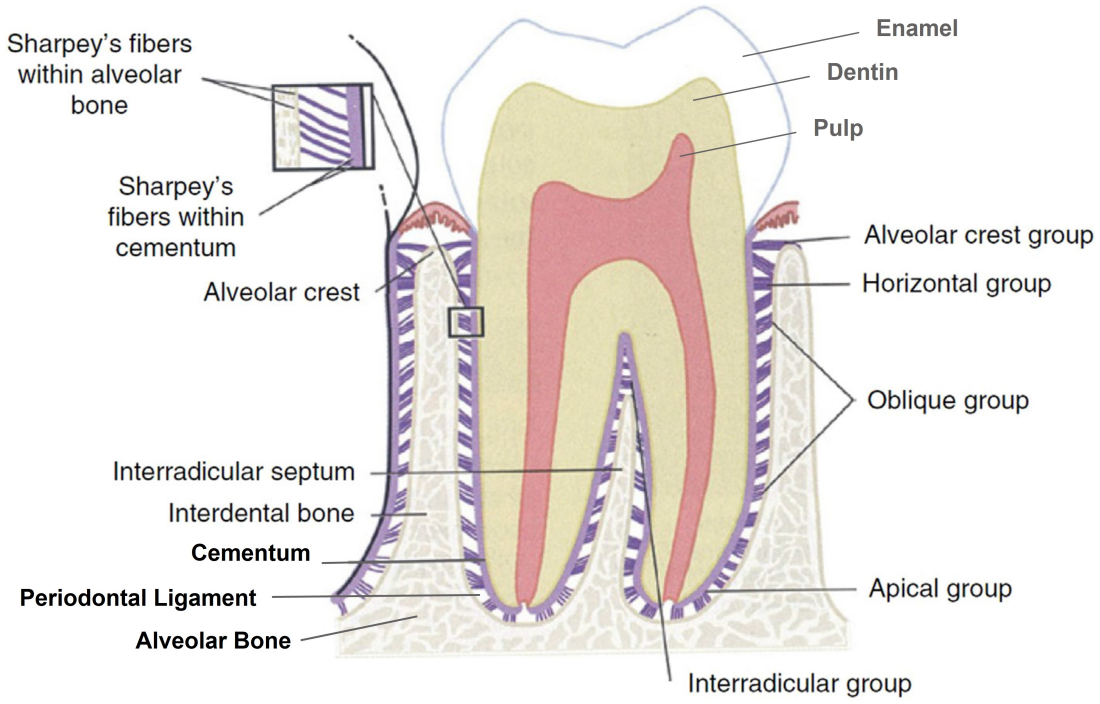

Figure 2.1: Schematic illustration of the periodontium's anatomy, adapted from [1].

2.1.1 Alveolar Bone

The alveolar bone is the part of the maxilla or mandible that contains the sockets that surround and anchor the teeth. The alveolar bone is a highly mineralized, hard tissue composed of 60% (w/w) inorganic material, 25% (w/w) organic material and 15% water. In the root of the teeth, the alveolar bone is connected to the root cementum through the PDL, as can be seen in figure 2.1. The alveolar bone is perforated by channels, which allow the passage of blood vessels and nerve fibers that extend to within the pulp of the teeth [1]. Similar to what occurs in other types of bones, alveolar bone is maintained through constant bone remodeling. Since the teeth are continuously making minor movements and there is a functional demand due to the forces of mastication, the alveolar bone undergoes constant remodeling. Bone remodeling relies on a balance between bone resorption and bone deposition, which is maintained by progenitor cells that can differentiate into osteoclasts (bone resorption) and osteoblasts (bone deposition) [5].

2.1.2 Cementum

The cementum is a hard, avascular connective tissue that covers the roots of teeth. It is located between the dentin and the PDL, as can be seen in figure 2.1. The primary function of the cementum is to anchor the PDL fibers. The cementum's composition is very similar to that of the alveolar bone, namely 65% (w/w) of inorganic material, 23% (w/w) of organic material and 12% of water. The organic material is constituted up to 90% of collagen type I. Interestingly, the majority of non-collagenous matrix proteins present in the cementum are also found in bone, namely fibronectin, osteocalcin, osteonectin and osteopontin [5].

The cementum can be classified in two types: acellular and cellular. The acellular cementum is located on the cervical part of the root, has PDL fibers inserted and provides attachment for the tooth. The cellular cementum is located on the apical part of the root and is composed of cementoblasts and cementocytes. This type of cementum is more rapidly formed than the acellular type and is produced as repair tissue to fill root fractures and resorptive defects [1, 5].

In periodontal regeneration, new cementum is formed from cementoblasts. Reports suggest that the PDL serves as a source of progenitor cells for cementoblasts involved in cementum formation, and also for osteoclasts and osteoblasts involved in bone remodeling [5].

2.1.3 Periodontal Ligament

The PDL is a complex, highly cellular, fibrous connective tissue located between the alveolar bone and the cementum, as can be seen in figure 2.1. The width of the PDL ranges between 100 and 400 µm, however it progressively decreases in thickness with age [5, 6].

The PDL is primarily responsible for providing support and mechanical stability to the teeth. It connects the cementum covering the tooth to the alveolar bone, ensuring the attachment of the tooth to the bone, while absorbing the shock from the considerable forces associated with mastication [6]. When characterized through tensile testing under loads between 1 and 5 N, the PDL demonstrated values of elastic modulus in the range between 0.607 and 4.274 MPa. Its elastic behavior is influenced by the loading rate, type of tooth, root level, and individual variation [7].

The extracellular compartment of the PDL is composed of highly aligned and organized collagen fiber bundles and non-collagenous matrix constituents, such as glycoproteins (e.g. Alkaline Phosphatase (ALP)) and proteoglycans [5]. The collagen fiber bundles provide the structural strength of the PDL and are mainly composed of collagen type I. The fibers and fibrils present in the PDL are of nano- to microsized order [1]. The extremities of the collagen fiber bundles are embedded in cementum or alveolar bone, and are referred to as Sharpey's fibers, as can be seen in figure 2.1. The collagen fiber bundles are termed principal fibers and can be divided into groups according to their specific location

and orientation to the tooth. The alveolodental ligament represents the majority of the PDL volume and is divided in: alveolar crest group, horizontal group, oblique group, apical group, and interradicular group (only in multirooted teeth), as seen in figure 2.1. This complex spatial organization of the principal fibers is essential for PDL function, enabling the protection of the tooth from the forces from mastication [5, 6].

Furthermore, the PDL is innervated and can act as a sensory receptor for regulating pressure on the teeth and proper positioning of the jaw during mastication.

Moreover, the PDL possesses an extensive blood supply and a diversity of cell populations, which include osteoblasts, osteoclasts, cementoblasts, fibroblasts, epithelial cells of Malassez, and progenitor cells. Another cell population that is present in the PDL are Periodontal Ligament Stem/Stromal Cells (PDLSCs), which serve as a source for renewable progenitor cells, which differentiate into osteoblasts, cementoblasts and fibroblasts. Due to the presence of these heterogeneous cell populations, the PDL serves as a cell reservoir for tissue homeostasis, repair and regeneration [5, 6]. Blood vessels present in the PDL provide nutrients necessary for the maintenance of the ligament and the hard tissues.

The unique structure and composition of the PDL is essential for the physiological functionalities of periodontal tissues. The PDL connects the root cementum to the alveolar bone and sustains a balance between formation and maintenance of the hard and soft tissues.

2.2 Periodontitis

Periodontitis is a chronic inflammatory infection of the periodontium. This infection is caused and sustained by bacteria from dental plaque accumulation. In early stages of the disease, there is inflammation only of the gingiva, known as gingivitis, which is reversible with effective oral hygiene. However, if left untreated, gingivitis can progress to periodontitis. Periodontitis in its advanced form is characterized by the loss and destruction of the periodontal tissues, including PDL, root cementum and alveolar bone, as can be seen in figure 2.2 [8–10]. This results in the loss of the tooth attachment to its supporting structures of the periodontium and in the formation of pockets surrounding the tooth. The symptoms of severe periodontitis include pain and discomfort during mastication, drifting and mobility of teeth and tooth loss [9, 10]. Periodontitis is the main cause of tooth loss, which is a global health problem representing a burden to society and the economy, particularly affecting older people [8].

Periodontitis is prevalent in adults, elderly populations and can also occur in children and adolescents. The prevalence of periodontal disease, which includes gingivitis and periodontitis, is estimated to range from 20% to 50% worldwide [9, 10]. This large range of estimated prevalence is due to the absence of a unique and consensual case definition among different countries and populations. Periodontitis can be characterized by the number of affected teeth, the magnitude of the pocket depth, the loss of tooth attachment capacity and the loss of alveolar bone. More severe forms of periodontitis are estimated to affect 10% of the population [10].

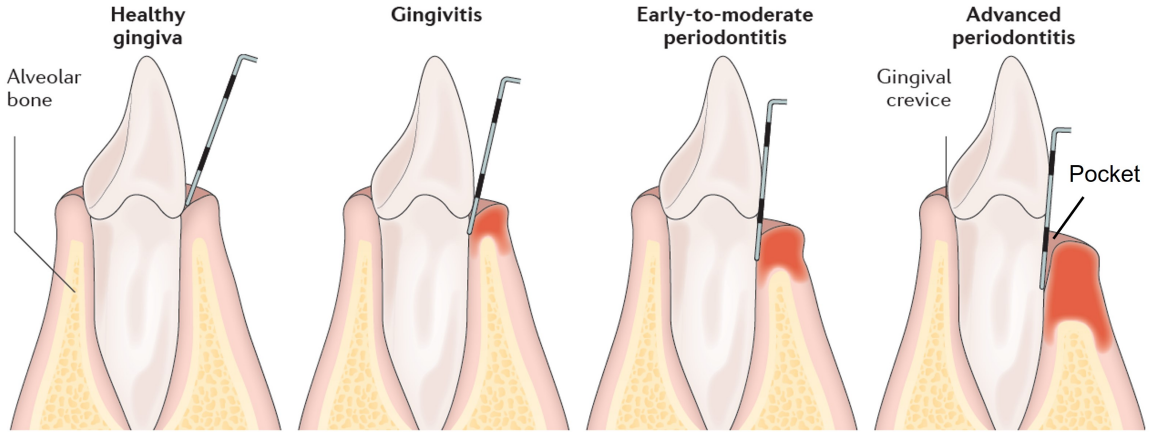

Figure 2.2: Schematic illustrations of the main stages of periodontal disease, adapted from [2].

Although bacterial plaque accumulation is the initiator of gingivitis, the host's susceptibility to disease progression plays an important role. In patients not susceptible to periodontitis the primary defense mechanisms are able to control the infection and the inflammation of the gingiva may persist indefinitely without progressing to periodontitis. On the other hand, the primary defenses of patients susceptible to periodontitis cannot contain the infection of the gingiva and the infection spreads to the periodontium [10]. The destruction of the periodontal tissues is in fact caused by host-derived mediators and enzymes from inflammatory cells in response to the bacterial infection of the periodontium. The inability to control the infection, allows it to further progress into the tooth root, deepening the pockets, resulting in tooth attachment loss and alveolar bone loss [9].

Gingivitis progresses to periodontitis in susceptible hosts. Patient susceptibility is significantly affected by risk factors that increase the probability of periodontitis development. The risk factors can be genetic or environmental. Genetic risk factors that increase the patient susceptibility to disease include defects of phagocytosis, which leads to an insufficient response to the bacterial infection, and enhanced enzyme production for a bacterial challenge, resulting in an excessive response with increased tissue damage [9]. Environmental or acquired risk factors include smoking, which is associated with decreased wound healing and reduced bacterial killing. Studies show that smokers are more likely to have severe periodontitis, present increased loss of alveolar bone and higher prevalence of tooth loss when compared to non-smokers [8, 9]. Poor oral hygiene is another risk factor, since it allows accumulation of dental plaque and is linked to increased severity of periodontitis [8]. In addition, diabetes mellitus is associated with severe periodontitis due to higher concentrations of inflammatory mediators compared to non-diabetic individuals. The severity and extent of periodontitis is directly influenced by the metabolic control of diabetic individuals [8, 10]. Finally, age is a potential risk factor, since the risk of periodontitis increases with the advancing age, with a higher prevalence of the disease in elderly populations [8].

2.3 Periodontitis Treatments

Initial stages of periodontitis can be treated with non-surgical procedures consisted of dental plaque and tartar removal with scaling and root planing [2, 9]. The main goal of these treatments is to control and reduce bacterial plaque accumulation. After the clinical removal of the dental plaque, patient should practice adequate oral hygiene to achieve a good clinical outcome [2]. Non-surgical treatments can be combined with adjunctive therapies, such as local drug delivery, systemic antibiotics and systemic host response modulation to improve treatment outcomes. Adjunctive drugs include antibiotics and antimicrobials that are directly administered to the periodontal pocket via a gel or fiber delivery system. Examples of systemic antibiotics are amoxicillin and metronidazole, which in combination result in pronounced clinical improvements [2]. Host response modulation can be particularly beneficial for susceptible patients to disease development. Host modulatory therapies influence the destructive components of the host response to reduce periodontal tissue destruction. These therapies include non-steroidal anti-inflammatory drugs; doxycycline that downregulates collagenases in inflamed periodontal tissues; and bisphosphonates, which reduce osteoclast activity and bone resorption [9].

Non-surgical treatments have been shown to reduce pocket depth and allow formation of new tooth attachment, which can be sufficient for early to moderate stages of periodontitis. However, in some cases and in advanced stages of the disease, surgical therapy is necessary to access sites deeper in the tooth root, to control the inflammation, to fully eliminate bacterial plaque and to stimulate the regeneration of lost periodontal tissues [2]. Pocket reduction surgery is a procedure that involves resecting soft and hard necrotic tissues. Regenerative surgery includes guided tissue regeneration and bone grafts.

2.3.1 Membrane Guided Tissue Regeneration

Guided Tissue Regeneration (GTR) is based on the use of a mechanical barrier membrane that prevents epithelial cells and fibroblasts from migrating into the defect site, while maintaining sufficient space for the regeneration of all the periodontal tissues, namely alveolar bone, cementum and PDL [3, 11]. There are two types of membranes already available that can be used for periodontal regeneration: non-degradable and degradable membranes. Currently available non-degradable membranes include polytetrafluoroethylene membranes, such as Cytoplast TXT-200, however they require a second surgery for their removal. To avoid additional surgeries, there are degradable membranes in the market, which are composed of synthetic polymers such as polycaprolactone, polylactic acid and polyglycolic acid, and of natural polymers like collagen, for example from porcine collagen, which is used in the Bio-Gide commercially available membrane. However, current GTR membranes have limitations such as low attachment to the adjacent tissues, which can expose the defect site and allow bacteria infiltration; lack of antibacterial properties and poor ability to enhance the regeneration of all the periodontal tissues [3, 11].

The limitations of the current membranes need to be addressed and new improved membranes need to be developed that meet all the criteria for ideal GTR membranes, specifically the following: biocompatibility; non-immunogenicity as to not trigger adverse reactions; biodegradability without release of toxic byproducts; cell-occlusivity to exclude specific cell types and ease of use in clinical setting. They should also possess appropriate surface area and high porosity for cell attachment, proliferation and differentiation; mechanical strength to stay in place for at least 4-6 weeks and to maintain space for the slow regenerating periodontium, and bioactivity to accelerate tissue repair and induce a coordinated regeneration of all the periodontal tissues, that is cementum, alveolar bone and PDL [3, 11, 12]. Considering the slow regenerating alveolar bone, bone grafts can be used to fill the defect site. GTR membranes can be combined with bone grafts, to prevent membrane collapse, as illustrated in figure 2.3.

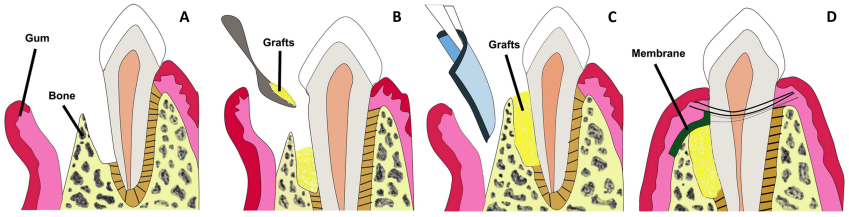

Figure 2.3: Schematic illustration of a GTR membrane combined with a bone graft for periodontal regeneration. (A) Loss of PDL and alveolar bone, resulting in a periodontal defect. (B) Bone graft placed in the defect site. (C) Placement of GTR membrane over the grafts. (D) Wound closure and sewing. Adapted from [3].

2.3.2 Bone Grafts

Bone grafts are transplanted into bone defects, where they promote bone healing either alone or in combination with other materials. Their main function is to provide mechanical support and enhance bone regeneration [13]. Bone grafts need to have four essential properties for achieving successful bone regeneration: osseointegration, which refers to the graft's ability to bind to the bone's surface; osteogenesis, that is the formation of new bone through osteoblasts present in the graft; osteoconductivity which is the graft's ability to generate a scaffold on which host cells can grow; and osteoinductivity that translates to the graft's ability to recruit host stem cells into it and induce their differentiation into osteoblasts through local proteins and growth factors. Unfortunately, current bone grafts mainly fulfill only the osteoconductivity property, by serving as a structure for regeneration processes to occur [13].

There are three types of bone grafts: autografts, allografts and xenografts. Autografts are composed of grafting material that is removed from one part of the patient's body to fill that same patient's bone defect. Since the source of the graft is the patient himself, there are no immunogenicity issues. In addition, these grafts present high osteogenesis, osteoconductivity and osteoinductivity. However, autografts are limited to small bone defects, associated with donor site injury and present more significant surgical risks, such as infection, inflammation and pain. In allografts and xenografts the source of the graft is not

the same patient as it is in autografts, thus, there are potential complications due to graft versus host responses. Allografts are composed of grafting material from compatible living donors or from cadaveric bone sources that is used fresh, frozen or freeze-dried. Fresh and frozen allografts show higher osteoinductivity, but also a higher risk of a host immune response and disease transmission. On the other hand, freeze-dried allografts present lower immunogenicity, but also lower osseointegration and decreased structural strength. Xenografts are composed of grafting material from other species, other than human, for example bovine or porcine. The xenografts are processed to be only constituted by a porous structure of inorganic components of bovine bone that highly resemble the human bone, provide mechanical support and present osteoconductivity [13].

Although some bone grafts might present almost all four essential properties for successful bone regeneration, that success is influenced by the grafts biocompatibility, biodegradability, structural integrity and porosity [13]. Moreover, the grafts are envisaged for bone formation only, thus neglecting periodontal ligament regeneration. Not only is osseointegration important, but also the attachment of newly formed bone to a regenerated PDL, that in turn connects the newly formed bone to the cementum of the tooth. Besides bone grafts, also GTR membranes fail to achieve PDL regeneration and integration of soft (PDL) and hard tissues (alveolar bone, cementum). If the PDL is not regenerated, there is no connection between cementum and alveolar bone and the tooth will eventually be lost, due to the lack of attachment of the teeth to the bone. These regenerative procedures are still exposed to clinical failures due to the lack of bioactivity to induce a coordinated regeneration of all the periodontal tissues, that is cementum, alveolar bone and PDL. Therefore, new strategies that promote a hierarchical structure regeneration of the entire periodontium are needed to improve clinical outcomes.

2.4 Tissue Engineering for Periodontal Regeneration

Tissue engineering makes use of cells, scaffolds, and biochemical factors to facilitate tissue regeneration (figure 2.4). Tissue engineering strategies use or manipulate one or more of these mediators with the aim of promoting the regeneration of lost tissues. Various tissue engineering strategies for periodontal regeneration have been reported in the literature, proposing alternatives to the current regenerative treatments of bone grafts and GTR membranes used in periodontal regeneration.

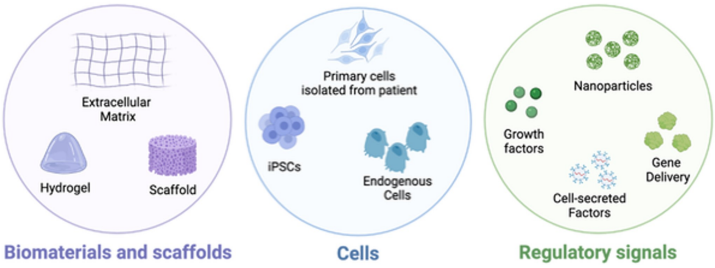

Figure 2.4: Mediators used in tissue engineering strategies. Adapted from [4].

2.4.1 Cell Sources

2.4.1.A Mesenchymal Stem/Stromal Cells

Mesenchymal Stem/Stromal Cells (MSCs) are multipotent cells with the capacity to self-renew and differentiate into the adipogenic, chondrogenic and osteogenic lineages. MSCs grow adhered to plastic and present a fibroblast-like morphology [14]. MSCs can be isolated from a broad range of sources: adult bone marrow, adipose tissue, synovial tissue and umbilical cord. Moreover, MSCs present immunomodulatory properties and are able to set up a regenerative microenvironment for tissue progenitors, due to their anti-apoptotic, anti-fibrotic, angiogenic and mitotic properties. Also their hypoimmunogenicity demonstrates that MSCs exhibit great potential for clinical applications in cell-based therapies [15, 16].

The Mesenchymal and Tissue Stem Cell Committee of the International Society for Cellular Therapy proposed three minimal criteria for defining multipotent MSCs: adherence to plastic; positive expression of CD73, CD90 and CD105 surface markers, and lack of expression of hematopoietic markers (CD14, CD34 and CD45) and class-II major histocompatibility complex (MHC) molecules (i.e. HLA-DR); and capability of differentiating into mesodermal lineages (adipocytes, osteoblasts and chondrocytes) [14].

Considering the hypoimmunogenicity and immunomodulatory properties, MSCs are promising candidates for tissue engineering applications. MSCs derived from adult tissues present no ethical or legal concerns, can be expanded *in vitro* and used in tissue engineering strategies. Current stem cell-based therapies rely mainly on the delivery of cells that were expanded *in vitro* to the periodontal defect site with the goal of promoting regeneration [17]. This delivery can be performed using single-cell suspensions injected into the defect site, which represents a simple and minimally invasive procedure [18]. Bone marrow-derived MSCs (BMMSCs) have been injected into rat periodontal defect models and showed capacity to exert anti-inflammatory and immunomodulatory effects and promote periodontal regeneration, since MSCs can differentiate into the osteogenic lineage [17–19]. However, injection of single-cell suspensions have drawbacks, including: poor engraftment, significant decrease in cell number after implantation, spreading to surrounding tissues and loss of cell fate control [18].

2.4.1.B Periodontal Ligament Stem/Stromal Cells

As previously mentioned, an important cell population present in the PDL are PDLSCs. These cells serve as a source for renewable progenitor cells, which differentiate into osteoblasts, cementoblasts and fibroblasts, responsible for bone, cementum and PDL formation [5]. Stem cells have also been isolated from the dental pulp and the dental follicle. The dental follicle is a loose connective tissue that surrounds the enamel and the dental pulp of the developing tooth germ before tooth eruption, hence Dental Follicle Stem Cells (DFSCs) also give rise to progenitors of osteoblasts, cementoblasts and PDL cells [20].

PDLSCs were first isolated from the human PDL in 2004 by Seo and colleagues [21]. PDLSCs

can self-renew and differentiate into the adipogenic, chondrogenic and osteogenic lineages, similar to MSCs. Seo *et al.* demonstrated that PDLSCs have an immunophenotype similar to BMMSCs, with positive expression of STRO-1 and CD146, and the capacity to develop into cementoblast-like cells *in vitro*, and cementum/PDL-like tissue *in vivo* [21]. PDLSCs also showed the capacity to form collagen fibers, similar to Sharpey's fibres, connecting to the cementum-like tissue, suggesting the potential to regenerate PDL tissue. Interestingly, both PDLSCs and Dental Pulp Stem Cells (DPSCs), show a higher number of population doublings than BMMSCs in culture [21].

Since PDLSCs were shown to be highly proliferative and capable of regenerating cementum/PDL-like tissues, interest was raised regarding their potential for use in periodontal tissue regeneration as a stem cell-based therapy to treat periodontal defects. Their regenerative capacity was studied in dental defects using several animal models (e.g. rat, miniature pig and beagle dog defect models) and results showed that PDLSCs had potential to form soft and hard periodontal-like structures and to promote periodontal regeneration [19, 21–24]. PDLSCs are very important for periodontal tissue engineering strategies. In addition to single-cell suspensions, another possible stem-cell based approach is the delivery of monolayer or stacked cell sheets. Cell sheets remain intact as whole due to cellular junctions and Extracellular Matrix (ECM). This technique is based on harvesting confluent cultured cells without any enzyme, which is easier to be implemented than cell suspensions and results in minimized cell loss and cell viability [17, 18]. Interestingly, a study compared cell injection and cell sheet transplantation of human DPSCs in swine periodontal bone defect models. The results showed that both approaches were able to significantly regenerate periodontal bone, however, the cell sheet transplantation exhibited higher bone regeneration capacity [25]. Nevertheless, cell sheets require a longer culture period, are fragile if cells are not confluent enough, attach weakly to hard tissues and cell sheets that are too thick present necrotic cells. These limitations may be addressed with the use of biomaterial scaffolds.

2.4.2 Scaffolds

2.4.2.A Decellularized ECM

The ECM is a complex structure that surrounds and supports cells within all tissues and organs. It is composed of structural proteins, including collagens and non-collagenous proteins, such as osteopontin, osteocalcin and alkaline phosphatase (ALP); specialized proteins, which include fibronectin and laminin; Glycosaminoglycans (GAGs) (e.g. chondroitin sulfate), and proteoglycans [26]. The ECM provides an appropriate microenvironment that supports cell adhesion, migration, proliferation and differentiation. The ECM also has the adequate mechanical strength, namely rigidity and compressibility, to ensure the structural stability of the tissues. Each tissue source has an ECM comprised of unique compositional and topographical features. The structure of the ECM has important implications in cell migration, gene expression, and differentiation. The cells actively remodel and reshape the ECM, degrade and secrete

the ECM's components, thus sculpting their surrounding microenvironment. ECM proteins associate with cell receptors, such as integrins, that can directly activate intracellular signalling pathways. Moreover, the cellular functions can also be regulated through mechanotransduction, i.e. the transduction of mechanical signals, since the cells show distinct responses according to the stiffness and elasticity of the ECM. The ECM composition and distribution of its constituents vary notably with the type of tissue and can change during tissue development and due to pathological conditions [27].

Tissue-engineering scaffolds focus on the development of biomaterials that can mimic the native ECM's structure and composition, in an attempt to recreate the *in vivo* microenvironment to facilitate tissue regeneration. However, it is extremely challenging to determine and recreate the exact composition of native ECM, which is essential when developing biomimetic scaffolds. Considering the importance of ECM and its tissue-specific composition, using decellularized ECM is an alternative approach to more closely mimic the specific *in vivo* microenvironment, including its complex bioactivity. Decellularized ECM can be classified as cell-derived and tissue-derived. Tissue-derived ECM is obtained through the decellularization of human or animal tissues and organs. However, this strategy presents some limitations such as the limited availability of tissues, the destruction of complex matrix structures by harsh mechanical and chemical decellularization processes, possible immunogenic responses caused by ECM from xenogeneic and allogeneic sources, and the potential transmission of pathogens [28–30].

Cell-derived ECM consists of secreted ECM by cells cultured *in vitro*. Considering the ECM's tissue-specific composition, cell-derived ECM presents additional advantages over tissue-derived ECM, namely that cell-derived ECM can mimic the composition of native ECM from tissues that are hard to isolate, for example stem cell niches. Furthermore, cell-derived ECM can be isolated through gentle decellularization processes, can have pathogen content easily eliminated, can be derived from autologous cells and can be used for surface modification of biomaterial scaffolds, resulting in improved bioactivity [28–30].

Cell-derived ECM has been used as scaffolds in tissue engineering, since it mimics the *in vivo* microenvironment. Carvalho *et al.* demonstrated that the use of cell-derived ECM resulted in higher cell metabolic activity of MSCs and enhanced osteogenic potential, confirmed by increased ALP activity and expression of osteogenic genes, compared with tissue culture polystyrene [31]. Yang *et al.* showed that the use of cell-derived ECM significantly increased the proliferation rate of chondrocytes and promoted a better chondrogenic differentiation profile in comparison to tissue culture plastic [32]. Cell-derived ECM influences cell proliferation and differentiation through physical, mechanical and chemical cues. Although cell-derived ECM supports cell adhesion and proliferation, it has insufficient mechanical properties, thus it is often combined with biomaterials. Kang *et al.* showed that scaffolds containing human umbilical vein endothelial cells (HUVECs) derived ECM enhanced osteogenic differentiation of human MSCs compared with scaffolds without ECM, which suggests that cell-derived ECM maintains the potential to create a biomimetic microenvironment that enhances osteogenic differentiation, while, through

the combination with biomaterial scaffolds, also offers mechanical support [33].

2.4.2.B Nanofibrous Scaffolds

Tissue-engineered scaffolds made of synthetic polymers, such as polycaprolactone (PCL), Polylactic Acid (PLA), Poly(lactic-co-glycolic acid) (PLGA) and Polyethylene Glycol (PEG), or of natural polymers, such as chitosan (CTS), Gelatin (GEL), Collagen (COL), Zein and Alginate have been studied for periodontal regeneration. Synthetic polymers offer tailorable and reproducible structural properties, which allows mass production. Although they present good mechanical properties, they have slow degradation rates and poor biological properties. Natural polymers have high biocompatibility and advantageous bioactivity, associated with enhanced cell adhesion, proliferation and matrix production. Synthetic and natural polymers can be combined to address their limitations and obtain scaffolds with the advantageous characteristics of both polymer types [3, 11, 12].

Nanofibrous scaffolds possess unique properties, such as high surface area to volume ratio, porosity and interconnectivity which favor cell attachment and proliferation and also enable nutrient and waste exchange. Electrospinning is a technique for fabricating continuous fibers with Mean Fiber Diameter (MFD) ranging from few nanometers to micrometers. Cumulative fibers form non-woven fibrous membranes that mimic the morphology of ECM proteins therefore facilitating cell attachment, proliferation and differentiation. Electrospinning allows the production of fibrous scaffolds with controllable fiber diameter, fiber orientation, porosity and surface characteristics [3, 11, 12].

The electrospinning technique is simple, cost-effective and requires four main components: a syringe containing a polymeric solution, a spinneret with a metallic needle, a high-voltage power supply and a grounded metal collector. The syringe with the polymeric solution is placed in a pump, which ejects the solution and controls its flow rate. The solution is ejected through the metallic needle that is connected to the high voltage power supply. The power supply is also connected to the metal collector and an electrostatic field is formed between the needle and the collector. The high voltage makes the droplets formed at the needle tip by the polymeric solution electrically charged. The droplets are stretched with electrostatic forces that counteract the solution's surface tension into an elongated shape, known as the Taylor cone, from which a jet of charged fluid is pulled towards the grounded collector. The electrospun polymeric fibers deposit and solidify in the collector, the solvent evaporates during the electrospinning process, resulting in dry fibers on the collector that accumulated form fibrous scaffolds [3, 11].

Essentially, electrospinning uses a polymeric solution to fabricate fibers in a high electrostatic field. There are various factors that influence the characteristics of the collected electrospun fibers and these factors can be divided in three categories: solution parameters, process parameters and environmental parameters. The solution parameters include solution concentration, solution viscosity, solution surface tension, polymer solubility and polymer molecular weight. The process parameters consist of the volt-

age, solution flow rate, needle inner diameter, needle to collector distance and type of collector. The environmental parameters comprise temperature and humidity [11]. The effects of all these parameters that influence the electrospinning process are summarized and described in table 2.1.

Table 2.1: Effects of electrospinning parameters on the characteristics of electrospun fibers.

Parameter	Effect on the produced electrospun fibers
Polymer MW	Increased polymer molecular weight (MW) results in an increase in fiber diameter. The molecular weight influences the solution viscosity.
Polymer solubility	Polymer solubility is important for the formation of continuous fibers. Poor polymer solubility hinders fiber formation.
Solution concentration	An increase of the polymer concentration in the solution, leads to an increase of the fiber diameter. If the concentration is too high, the fibers can be discontinuous.
Solution viscosity	Increased solution viscosity, as a result of high polymer MW and/or high polymer concentration in the solution, results in increased fiber diameter. However, solutions with very low or very high viscosity can difficult or impede electrospinning.
Solution surface tension	An increase in the solution surface tension results in an increase of the fiber diameter and it facilitates the formation of beads.
Voltage	The fiber diameter decreases with increasing voltage, due to increased solvent evaporation. However if the applied voltage is too high or too low the diameter distribution will be heterogeneous and fibers are not uniform.
Flow rate	The fiber diameter increases with increasing flow rate. The fibers form beads, if the flow rate is too high.
Needle inner diameter	Needles with smaller inner diameters give rise to finer fibers.
Needle-collector distance	The fiber diameter decreases as needle to collector distance increases. If this distance is too small, it can lead to bead formation.
Collector type	The use of static collectors results in random fibers. Rotating collectors or two parallel plate collectors allow aligned fiber formation.
Temperature	An increase in temperature results in decreasing solution viscosity and surface tension, and, consequently, decreased fiber diameter.
Humidity	Depending on the polymer, humidity can increase or decrease the fiber diameter. Increased humidity facilitates the formation of beads on the fibers.

By using the most adequate polymers and through the optimization and consideration of all the parameters that influence the characteristics of electrospun fiber, it is possible to produce electrospun polymeric fibrous scaffolds with the most appropriate properties for a specific application. Electrospinning has been used in various tissue engineering strategies, including periodontal tissue engineering, since electrospun fibrous scaffolds are highly suitable for the development of periodontal GTR barrier membranes. Nanofibrous scaffolds resemble the natural fibrous ECM, which has been shown to enhance cell attachment, proliferation and differentiation. The high porosity with small pore size can prevent the migration of fibroblasts across the nanofibrous scaffolds, which is vital feature of a GTR membrane [3]. Through the use of optimized electrospinning parameters and the combination of carefully selected synthetic and natural polymers, nanofibrous scaffolds can meet the criteria of an ideal GTR membrane: biodegradable, biocompatible, with good mechanical properties and osteoinductive. In addition to their resemblance to natural ECM, the scaffolds can be further complemented with additives, such as bioceramics and growth factors, to enhance their biological effects. Therefore these scaffolds might have the

capacity to recruit host stem and progenitor cells and promote their proliferation and differentiation into fibroblasts, osteoblasts, and cementoblasts, thus regenerating all the periodontal tissues. Extensive research has been done regarding the development of electrospun scaffolds for periodontal regeneration, which is illustrated in table 2.2 along with the specific features and main results from each study.

Table 2.2: Overview of electrospun scaffolds for PDL regeneration with human cells and *in vitro/in vivo* tests.

Polymers	Solvents	MFD	Alignment	Cells	Tests	Results	Year; Ref
CTS; PEG	AA; H_2O; DMSO	410 ± 163 nm 288 ± 107 nm	aligned non-aligned	MG63; ES-MPs	*In vitro*	Cells attached and viable; ↑ mineral deposition in non-aligned fibers	2017; [34]
PCL	AA	1252 nm	non-aligned	PDLSCs	*In vitro*	Cell sheet formed; Cell growth	2020; [35]
PCL	CHL	10 ± 3 µm	non-aligned	DFSCs	*In vitro*	Fibroblastic differentiation	2016; [36]
PCL//PEG shell//core	HFIP//H_2O	0.5-1.5 µm	non-aligned	PDLSCs	*In vitro*	↑ Osteogenic differentiation due to Enamel Matrix Derivative in the core	2021; [37]
PLA; calcium alginate	CHL	250 ± 90 nm	non-aligned	PDLCs; BMMSCs	*In vitro*	Alginate enhanced cell adhesion and mineralization in BMMSCs	2020; [38]
PCL; COL	HFIP	9.59 ± 2.40 µm	aligned non-aligned	PDLSCs;	*In vitro*	Aligned fibers: ↑ Col I, Col III, POSTN Non-aligned: ↑ ALP, OPN expression	2017; [39]
COL; CTS; PCL	HFIP FA	239 ± 26 nm	non-aligned	PDLCs	*In vitro* *In vivo*	↑ viable cells due to CTS; ↑ ALP, OC and new bone formation in rat defect	2020; [40]
GEL; PEG	AA; H_2O; EtOAc	528 ± 17 nm	non-aligned	BMMSCs &/or PDLCs	*In vitro*	↑ porosity → ↑ viable cells; ↑ POSTN and OPN expression in cocultures	2022; [41]
PCL GEL	DCM/DMF PBS	599 ± 95 nm 590 ± 167 nm	aligned non-aligned	PDLSCs	*In vitro* *In vivo*	Aligned Fibers: ↑ collagen, ↑ new & oriented PDL fibers, ↑ POSTN levels	2019; [42]
PCL; GEL	HFIP	≈ 1.1 µm ≈ 1.5 µm	aligned non-aligned	PDLSCs	*In vitro* *In vivo*	Both: ↑ OPN, OC; Non-aligned: ↑ ALP Aligned: ↑ POSTN; new oriented fibers	2022; [43]
PCL//GEL; shell//core	HFIP	≈ 400 nm	non-aligned	PDLSCs	*In vitro*	Antibacterial + ↑ ALP & mineralization due to MgO NPs in the core	2021; [44]
PCL; GEL	HFIP; AA	355 ± 181 nm	non-aligned	PDLSCs	*In vitro* *In vivo*	↑ cell proliferation, ALP & new bone in rat defect due to CeO_2 NPs.	2022; [45]
PCL; PEG	DMF; CHL	522 ± 159 nm	non-aligned	PDLSCs	*In vitro*	↑ ALP, RUNX2, OC gene expression	2021; [46]
Polyurethane	DCM; DMF	200 - 300 nm	non-aligned	DPSCs	*In vitro*	↑ drug content→ ↓ cell viability	2020; [47]
PLGA	HFIP	165 ± 60 nm	non-aligned	PDLCs	*In vitro* *In vivo*	fibroblast growth factor-2 → ↑ viable cells; ↑ Col I; ↓ root surface resorption	2020; [48]
PCL	TCM	≈ 0.5 - 2.0 µm	non-aligned	PDLSCs	*In vitro*	↑ ALP activity, Col I & OC expression due to dentin non-collagenous proteins	2020; [49]
Zein; GEL	HFIP	≈ 1.5 - 2.5 µm	non-aligned	PDLSCs	*In vitro* *In vivo*	HA→ ↑ ALP, OC, RUNX2 expression; ↑ mineralization; ↑ new bone formation	2019; [50]
PCL	CHL	≈ 2.0 - 3.5 µm	non-aligned	PDLSCs	*In vitro* *In vivo*	Simvastatin→ ↑ mineralization, Col I & ALP; cementum-like tissue formed	2020; [51]
PLGA	HFIP	922 nm	non-aligned	PDLSCs	*In vitro* *In vivo*	DMOG→ ↑ VEGF; nSi→ ↑ ALP, OC, OPN; induced angio- & osteogenesis	2021; [52]
PCL; PLGA	TFE	≈ 1.0 - 2.0 µm	non-aligned	PDLCs	*In vitro* *In vivo*	DA + COL + PFI-2→ ↑ ALP, OC, OSX, RUNX2; new bone & cementum formed	2022; [53]
SF; PEG	LiBr; H_2O	300 - 400 nm	non-aligned	PDLCs	*In vitro*	Sonication+↓ PEG→ ↑ cell proliferation	2019; [54]
PLGA; wool keratin	TCM; DMF	614 ± 126 nm	non-aligned	PDLCs	*In vitro*	ORN or bFGF→ ↑ proliferation; ↑ ALP; cytocompatible but ↓ with ↑ ORN/bFGF	2020; [55] [56]
PCL; GEL	HFIP	551 ± 206 nm	non-aligned	DPSCs	*In vitro*	Antibacterial due to Zinc Oxide; cytocompatible (but ↓ with ↑ ZnO)	2015; [57]
PCL	HFIP	micrometer size	non-aligned	PDLSCs	*In vitro* *In vivo*	0.5% ZnO→ ↑ RUNX2, OCN expression; ↑ ALP activity; bone formation in defect	2018; [58]
PLA CTS	CHL AA	200 nm	non-aligned	BMMSCs PDLCs	*In vitro*	↑ CTS→ ↑ hydrophilic; ↑ OPG, RUNX2 in BMMSCs; but ↑ TLR4 in PDLCs	2018; [59]
Zein; GEL	HFIP	950 ± 356 nm	non-aligned	PDLSCs	*In vitro*	GEL→ ↑ cell proliferation; ↑ ALP activity	2017; [60]
COL CTS	HFIP HFIP/TFA	159 ± 59 nm	non-aligned	PDLCs	*In vitro* *In vivo*	↑ viable cells; ↑ RUNX2, OPN, OC, ALP expression; ↑ bone regeneration *in vivo*	2017; [61]
SF; PEG	LiBr; H_2O	≈ 500nm	non-aligned	PDLCs	*In vitro*	↑ GEL→ ↑ cell proliferation; antibacterial due to vancomycin loaded GEL NSs	2017; [62]
PCL	HFIP	150 - 300 nm	non-aligned	PDLCs	*In vitro*	↑ drug→ antibacterial, but ↓ viable cells	2016; [63]
PCL; COL	HFIP	200 nm	non-aligned	PDLCs	*In vitro* *In vivo*	rCMP1 → ↑ CMP1; ↓ OCN, OPN; ↑ cementum & ↓ bone formed in defect	2016; [64]

Acronyms used in table 2.2 that are not in the list of acronyms: DMSO: Dimethyl sulfoxide; MG63: a bone osteosarcoma cell line; ES-MPs: embryonic stem cell-derived mesenchymal progenitor cells; DMF: Dimethylformamide; MgO: Magnesium Oxide; CeO_2: Cerium Oxide; EtOAc: Ethyl acetate; VEGF: Vascular Endothelial Growth Factor; nSi: Nanosilicate; DMOG: Dimethyloxalylglycine; DA: Dopamine; SF: Silk Fibroin; TCM: Trichloromethane; HA: Hydroxyapatite; bFGF: basic fibroblast growth factor; ORN: Ornidazole; NPs: nanoparticles; BMMSCs: bone marrow-derived MSCs; OPG: Osteoprotegerin; TLR4: Toll-like receptor 4; LiBr: Lithium Bromide; NSs: nanospheres; rCMP: recombinant CMP

Table 2.2 summarizes the findings of the literature research carried out in Scopus with the keywords: periodontal regeneration; electrospinning, fibers and synonyms or alternative words. The exclusion criteria were the following: published before 2015; electrospinning was not used; human cell culture was not performed on the electrospun scaffolds. One polymer that has been extensively used and is present in the majority of scaffolds displayed in table 2.2 is polycaprolactone.

2.4.3 Polycaprolactone-Chitosan Scaffolds

Polycaprolactone (PCL) is a FDA-approved, biodegradable and biocompatible synthetic material that has been extensively used in biomedical applications [12]. PCL has good mechanical properties suitable for tissue engineering and has been shown to support adhesion and proliferation of MSCs and promote osteogenic differentiation [65, 66]. PCL is hydrophobic and has a slow degradation rate (2-3 years), which means it may not match perfectly the rate of new tissue formation. Therefore, it can be blended with other polymers to improve hydrophilicity and expedite degradation [3, 11, 12].

Chitosan (CTS) is a natural hydrophilic polymer obtained through the deacetylation of chitin, which can be extracted from crustaceans' shells. CTS is biodegradable, biocompatible and possesses antibacterial properties. Its antibacterial activity is due to the positively charged protonated amino groups that interact with the negatively charged bacterial cell wall causing cell disruption [67]. In addition, CTS is associated with enhancement of the osteogenic differentiation of cells [3,68]. However, it is highly challenging to electrospun CTS alone, due to its polycationic nature in solution. The high electric field results in repulsive forces among CTS ionic groups, which inhibit the formation of continuous fibers. [69,70] Moreover, CTS fibers have poor mechanical properties and rapid degradation. Hence it is usually combined with other polymers, specially synthetic polymers that provide mechanical support [3, 11, 66].

Through the preparation of PCL-CTS blends, it is possible to combine the advantageous characteristics of both polymers. PCL provides PCL-CTS scaffolds mechanical stability, while CTS contributes with biodegradability, hydrophilicity and antibacterial activity. The antibacterial activity of chitosan is influenced by its Degree of Deacetylation (DD) and Molecular Weight (MW). Although, the influence of MW has been investigated in the literature, the conclusions are contradictory. When studying chitosan with MW under 400 kDa, the antibacterial effect on *Staphylococcus aureus* was enhanced with increased MW, but the antibacterial effect of chitosan on *Escherichia coli* was decreased with increased MW [67]. The DD of chitosan has a clear effect on the antibacterial activity of CTS, namely the higher the DD, the higher the positive charge of protonated amino groups, thus the stronger the antibacterial activity [67]. Commercial chitosan from Sigma-Aldrich (SIAL) is available in three different ranges of MW: low molecular weight chitosan (50,000-190,000 Da); medium molecular weight chitosan (190,000-310,000 Da); and high molecular weight chitosan (310,000-375,000 Da), all presenting DD between 75% and 85%.

There are various possibilities to prepare PCL-CTS blends for electrospinning. PCL can be easily dis-

solved in numerous solvents: Hexafluoroisopropanol (HFIP), Trifluoroethanol (TFE), Formic Acid (FA), Acetic Acid (AA), Dichloromethane (DCM) and Chloroform (CHL). Chitosan can be dissolved in HFIP, AA solutions, FA/AA mixtures, Trifluoroacetic Acid (TFA) and TFA/DCM mixtures. PCL-CTS blends can be prepared in two different ways; either two separate PCL and CTS solutions are prepared and then blended together, or only one solution is prepared with both polymers added at the same time or the second polymer added after dissolution of the first. PCL-CTS blend electrospun fibers have already been fabricated for a number of applications. Table 2.3 summarizes some examples from the literature.

Table 2.3: Examples of electrospun scaffolds prepared from PCL-CTS blends previously reported in the literature.

PCL type	CTS type	PCL solvent	CTS solvent	Polymer concentrations	Electrospinning parameters	MFD	Year; Ref
Mn = 80 kg/mol	medium MW (SIAL)	FA/AA 7:3 v/v	FA/AA 7:3 v/v	PCL 6 wt% + CTS 20 wt%	20-25kV; 17.5cm; 0.25ml/h	191 ± 54 nm	2022; [71]
Mn = 80 kg/mol	medium MW (SIAL)	TFE	TFA	PCL 16 wt% + CTS 5 wt%	12kV; 20cm; 1ml/h; 23G	207 ± 56 nm	2022; [72]
Mn = 80 kg/mol	low MW (SIAL)	FA/AA 6:4 v/v	FA/AA 6:4 v/v	PCL 14 wt% + CTS 1.4 wt%	27kV; 18cm; 1ml/h; 21G	200-300 nm	2022; [73]
Mn = 80 kg/mol	low MW (SIAL)	DCM	DCM	PCL 10 wt% + CTS 3 wt%	rotating collector; 3ml/h; 18G	4.80 ± 1.373 µm	2021; [74]
Mn = 80 kg/mol	low MW (SIAL)	FA/AA 3:2 v/v	FA/AA 3:2 v/v	PCL 12 wt% + CTS 2 wt%	11kV; 20cm; 0.3ml/h	137.28 ± 1.38 nm	2021; [75]
Mn = 80 kg/mol	medium MW (SIAL)	FA/AA 3:2 v/v	FA/AA 3:2 v/v	PCL 12 wt% + CTS 2 wt%	22kV; 20cm; 0.5ml/h	277.68 ± 1.55 nm	2021; [75]
Mn = 80 kg/mol	MW ≈ 100,000 Da	TFA	TFA	PCL 8 wt% + CTS 3.5 wt%	18kV; 22cm; 0.41ml/h; 21G	447 ± 87.69 nm	2020; [76]
Mn = 80 kg/mol	MW = 150-300 kDa	AA	AA	PCL 12 wt% + CTS 3 wt%	18kV; 15cm; 0.4ml/h	96.4 ± 41.1 nm	2020; [77]
Mn = 80 kg/mol	MW ≈ 100,000 Da	TFA	TFA	PCL 10 wt% + CTS 6 wt%	14kV; 22cm; 0.37ml/h; 21G	281 ± 105 nm	2019; [78]
Mn = 80 kg/mol	CTS from crab shell	FA/AA 3:2 v/v	FA/AA 3:2 v/v	PCL 12.5 wt% + CTS 5/10 wt%	18-30kV; 16-20cm; 0.1-0.7ml/h	453/434 ± 150 nm	2018; [79]
Mn = 70-90 kg/mol	medium MW (SIAL)	FA/AA 70:30 v/v	FA/AA 70:30 v/v	PCL 12wt% + CTS 2wt% (1:2)	15kV; 14cm; 0.1ml/h; 22G	159 ± 34.9 nm	2018; [80]
Mn = 80 kg/mol	medium MW (SIAL)	FA/AA 7:3 v/v	FA/AA 7:3 v/v	PCL 6wt% + CTS 1.2wt%	20kV; 12.5cm; 0.3ml/h; 21G	57 ± 24 nm	2018; [81]
Mn = 80 kg/mol	MW = 200-300 kDa	FA/AA 70:30 v/v	FA/AA 70:30 v/v	PCL 10wt% + CTS 0.5/1/1.5wt%	10kV; 10cm; 0.2ml/h; 16G 13kV; 10cm; 0.2ml/h; 16G 17kV; 10cm; 0.2ml/h; 16G	180 ± 69 nm (0.5wt%) 123 ± 40 nm (1 wt%) 114 ± 20 nm (1.5wt%)	2018; [82]
Mn = 70-90 kg/mol	low MW (SIAL)	HFIP	TFA/DCM 70/30 v/v	PCL 12wt% + CTS 4wt% (1:1)	25kV; 15cm; 0.5ml/h; 20G	120 ± 20 nm	2017; [83]
Mn = 70-90 kg/mol	MW = 500 kDa	AA/H_2O 90:10 v/v	AA/H_2O 90:10 v/v	PCL 2wt% + CTS 2wt%	18kV; 25cm; 0.3ml/h; 23G	890 ± 364 nm	2017; [84]
Mn = 70-90 kg/mol	low MW (SIAL)	HFIP	HFIP	Blends with 5/10/25% w/w CTS	13-20kV; 10cm; 1-2ml/h; 23G	100-400 nm	2017; [85]
Mn = 80 kg/mol	MW = 1000 kDa	TFE	TFA	PCL 10wt% + CTS 5wt%	22kV; 15cm; 0.5ml/h; 23G	250-450 nm	2017; [86]
Mn = 70-90 kg/mol	medium MW (SIAL)	HFIP/AA 9:1 w/w	HFIP/AA 9:1 w/w	PCL 3wt% + CTS 0.15wt%	25kV; 20cm; 5ml/h; 20G	150 ± 62 nm	2016; [87]
Mn = 70-80 kg/mol	CTS from shrimp shell	Acetone/FA 7:3 v/v	Acetone/FA 7:3 v/v	PCL 10wt% + CTS 2wt%	16kV; 20cm; 1ml/h; 21G	0.5–2.0 µm	2015; [88]
Mn = 80 kg/mol	medium MW (SIAL)	HFIP	HFIP	PCL 10wt% + CTS 0.5wt%	15kV; 10.5cm; 0.4ml/h; 21G	432 ± 207 nm	2014; [89]

In PCL-CTS blends, it has been observed that when using acetic acid/formic acid mixtures different viscosities and electrical conductivity depend on the acid proportion, namely a decrease in AA concentration results in an increased solution conductivity and production of finer fibers [90, 91]. Furthermore, the increase of CTS concentration causes a strong increase in solution viscosity. Solutions with a very high viscosity often impede the electrospinning process. CTS dissolves in TFA, which destroys the strong interactions between the chitosan molecules, and DCM can be added to offer stability to the electrospinning process for the production of CTS fibers [90, 91]. Dissolving a determined concentration of CTS in TFA or TFA/DCM yields a less viscous solution, when compared to the FA/AA system. Urbanek *et al.* compared the properties of PCL-CTS blends prepared with HFIP and FA/AA (1:1 v/v). With HFIP finer fibres were obtained with brittle and hydrophilic character, typical for the chitosan component. Fibers fabricated with FA/AA showed formation of chitosan salts, which caused decreased mechanical properties and hydrophilicity [91]. To enhance the mechanical properties of PCL-CTS fibers, crosslinking can be used. Glutaraldehyde in vapor-phase has been used to crosslink electrospun PCL-CTS nanofibrous membranes and even CTS electrospun fibers [76, 78, 83]. Aldehydic groups of the glutaraldehyde form stable imine bonds with free amino groups of CTS. [92]

PCL and CTS have already been used together in strategies for periodontal tissue engineering. PCL electrospun fibers were coated with drug loaded CTS nanoparticles to serve as vehicles for the administration of antibiotics [93, 94]. Khodir *et al.* developed PCL fibers with homogeneously distributed

CTS nanoparticles loaded with tetracycline, that provided good attachment and proliferation of human MSCs and increased cell viability in comparison to PCL control fibers, independently of the drug's concentration [94]. Guarino *et al.* used amoxicillin loaded CTS nanoparticles in PCL fibers and verified antibacterial activity against *Staphylococcus aureus* and *Escherichia coli* [93]. Zupančič *et al.* developed a double-layer nanofibrous mat composed of a CTS layer with ciprofloxacin, and a PCL layer with metronidazole, showing antibacterial activity against *Escherichia coli* due to the release of the incorporated antibiotics [95]. Demir *et al.* dip-coated PCL fibers loaded with metronidazole in a CTS solution, which lead to increased hydrophilicity and degradation rate [96]. Shalumon *et al.* fabricated PCL-CTS blend nanofibers with incorporated bioactive glass and hydroxyapatite nanoparticles that showed enhanced ALP activity of human periodontal ligament fibroblasts due to the presence of nanoparticles. PCL-CTS without nanoparticles provided good attachment and proliferation of human periodontal ligament fibroblasts and exhibited increased ALP activity [97]. Gümüşderelioğlu *et al.* treated porous chitosan membranes with glycerol solution to prevent its shrinkage and brittle behaviour, thus obtaining a flexible and easily manipulated membrane [98]. This membrane was envisaged as a scaffold to place in the periodontal pocket and possessed two functionalized surfaces, a porous surface with hydroxyapatite to be in contact with degraded cementum and a nonporous surface with electrospun PCL nanofibers to act as a barrier membrane [98]. Similarly, Sundaram *et al.* developed a bilayered construct consisted of PCL electrospun fibers to mimic and regenerate PDL, and a CTS scaffold with calcium sulfate to regenerate alveolar bone [36]. Zhang *et al.* combined various layers of PCL-Gelatin nanofibers with a CTS solution and lyophilized the assembly to obtain multilayer scaffolds [99]. These scaffolds showed enhanced cell viability of human gingival fibroblasts and collagen deposition by the cells. *In vivo* tests in rats demonstrated good biocompatibility, low immunogenicity and good cellular barrier effect of scaffolds, which showed no cell infiltration [99]. Similarly, Jiang *et al.* obtained lyophilized scaffolds from PCL-PEG nanofibers embedded in a CTS solution and evaluated their *in vivo* performance in rat periodontal defect model. The aligned PCL-PEG nanofibers resulted in higher expression of periostin and significant formation of tooth-supporting mineralized tissue in the regenerated periodontium [100].

2.5 Combination of Scaffolds with cell-derived dECM

Bioactive additives, such as ceramics, drugs, growth factors and proteins, can be incorporated into scaffolds to enhance their properties, including biocompatibility, antibacterial activity and osteogenic properties. Table 2.2 demonstrates that various strategies have used additives, including growth factors, hydroxyapatite, metal oxides, small molecules and proteins. Cell-derived ECM is a reservoir of proteins and growth factors that influence cell proliferation and differentiation. Considering the enhanced cell proliferation and promoted osteogenic differentiation resulting from the use of decellularized cell-derived ECM, one strategy is the incorporation of ECM in scaffolds, such as electrospun nanofibers.

2.5.1 Cell-derived dECM loaded electrospun scaffolds

Cell-derived ECM has insufficient mechanical properties to support and regenerate hard tissues, such as alveolar bone. Therefore, it can be combined with electrospun scaffolds that ensure good mechanical properties while the cell-derived ECM enhances their biofunctionality and bioactivity.

Some studies have already shown promising results on the use of cell-derived ECM in periodontal tissue engineering applications. Heng *et al.* demonstrated that the use of PDLSC-derived ECM as a scaffold alone promoted rapid adhesion and spreading of seeded DPSCs *in vitro*, increased DPSCs proliferation and enhanced osteogenic differentiation in comparison to tissue culture polystyrene [101]. Jiang *et al.* placed PDLSC-sheets on top of PCL/gelatin nanofibers and then decellularized the constructs. Decellularized cell sheets, with and without nanofibers, showed periodontium regeneration potential in rat periodontal defects, confirmed by formation of new bone, cementum and PDL *in vivo* [102]. Farag and colleagues transfered PDLSC-sheets onto melt electrospun PCL membranes and then decellularized the constructs [103, 104]. Decellularized cell sheets were shown to maintain the ECM intact, retain growth factors, and support recellularization by allogenic PDLSC *in vitro* [103]. The decellularized cell-sheets also demonstrated enhanced expression of osteogenic genes by PDLSCs compared to PCL scaffolds alone. Decellularized cell-sheets were biocompatible *in vivo* and supported periodontal attachment in a rat periodontal defect model [104].

PDLSC-derived ECM has not yet been extensively researched in the literature. All the studies reported in the literature developed strategies to decorate electrospun scaffolds with ECM by seeding cells onto the fibers, allowing them to grow followed by decellularization to obtain the ECM-decorated electrospun fibers. A different approach, which has not been used in periodontal tissue engineering, consists on the production of cell-derived ECM in regular *in vitro* cell culture dishes, its collection, followed by lyophilization (freeze-drying) to obtain ECM powder that can be incorporated in the polymeric solutions used in electrospinning to generate fibers with incorporated cell-derived ECM particles. This strategy has already been done for bone tissue engineering and fibers with incorporated ECM demonstrated enhanced cell proliferation and osteogenic differentiation of MSCs compared to fibers without ECM [65].

In the previously mentioned works, solely the expression of Collagen I and Fibronectin were evaluated in decellularized PDLSC-derived ECM and electrospun fibers only served as a simple enhancement of the mechanical properties, which were not assessed. The characterization of electrospun fibers with PDLSC-derived ECM and the assessment of the effects from the ECM incorporation on the fibers' properties still remain to be performed. Electrospun scaffolds with cell-derived ECM can be developed with the aim to mimic the structure, architecture and composition of native ECM, instead of only focusing on the composition. Cell-derived ECM creates a biomimetic microenvironment, that enhances cell proliferation and osteogenic differentiation, which should be combined with electrospun nanofibrous scaffolds with the desired structural/mechanical properties for periodontal regeneration.

3

Materials and Methods

Contents

3.1 PDLSC Culture and Characterization

3.1.1 Isolation and Culture of PDLSCs

The human PDLSCs used in this work were part of the cell bank available at the Stem Cell Engineering Research Group, Institute for Bioengineering and Biosciences (iBB) at Instituto Superior Técnico (IST). PDLSCs were isolated from periodontal samples provided by Clinica Egas Moniz, according to protocols established at iBB-IST. The PDL tissue was harvested from the roots of healthy human teeth, extracted at the clinic. Isolated PDLSCs were stored frozen in liquid/vapor nitrogen tanks until further use.

PDLSCs were thawed and plated on T-75 cm^2 flasks and well plates using low glucose Dulbecco's Modified Eagle's Medium (DMEM) [Gibco] supplemented with 10% Fetal Bovine Serum (FBS) MSC qualified (Gibco) and 1% antibiotic-antimycotic (A/A, Gibco). Cells were cultured at 37℃ and 5% CO_2 in a humidified atmosphere. Medium renewal was performed every 3 to 4 days. All experiments were performed using cells between passages 3 and 6. To perform cell passaging, PDLSCs were washed once with Phosphate Buffered Saline (PBS) solution (Gibco), detached using a 0.05% trypsin solution (Gibco) and counted using the Trypan Blue exclusion method (Gibco).

3.1.2 Multilineage Differentiation and Stainings

To assess the multilineage differentiation capacity of PDLSCs, the cells were differentiated *in vitro* into the adipogenic, chondrogenic and osteogenic lineages, using appropriate differentiation media. Cells that were not cultured with differentiation media were used as control samples. All samples were stained and then imaged using bright-field microscopy or fluorescence microscopy (Leica DMI3000B).

Adipogenic Differentiation: PDLSCs were seeded at a density of 3000 cells/cm^2 on 24-well plates with DMEM + 10% FBS + 1% A/A. Once the cells reached confluence, half of the wells were cultured in adipogenic differentiation medium for 21 days, whilst the other half remained cultured in DMEM. The adipogenic differentiation medium consisted of basal differentiation medium (StemPro™ Adipogenesis Differentiation Kit, Gibco), to which 10% v/v adipogenic supplement from the Kit and 1% v/v A/A was added. Medium was renewed every 3 to 4 days. After 21 days, the media were removed, cells were washed once with PBS, fixed with 4% Paraformaldehyde (PFA) [SIAL] for 20 min at room temperature and incubated with Oil Red O solution (0.3% in isopropanol, SIAL) for 1 h at room temperature, protected from light. Oil Red O stains lipid reserves, which allows the detection of lipid droplet formation as a result of the adipogenic differentiation. After staining, cells were washed with milliQ water and observed under the microscope (Leica DMI3000B).

Chondrogenic Differentiation: PDLSCs were seeded as 10 µl droplets at a density of $10x10^6$ cells/ml on ultra-low attachment 24-well plates (Corning) with DMEM + 10% FBS+ 1% A/A. The plates were placed in the incubator for 1 h to partially dry the droplets, facilitating aggregate formation. To half

of the wells chondrogenic differentiation medium was gently added, whilst to the other half DMEM + 10% FBS + 1% A/A. The chondrogenic differentiation medium consisted of basal differentiation medium (MesenCult^{TM} Chondrogenic Differentiation Kit, Stemcell Technologies), to which 5% v/v chondrogenic supplement from the Kit and 1% v/v A/A was added. Medium was renewed every 3 to 4 days. After 21 days, the media were removed, aggregates were washed once with PBS, fixed with 4% PFA for 20 min at room temperature and incubated with 1% Alcian Blue solution (SIAL, in 0.1 N HCl) for 1 h at room temperature, protected from light. Alcian Blue stains polysaccharides such as sulfated glycosaminoglycans present in cartilage, therefore it allows the detection of chondrocyte activity. After staining, aggregates were washed 3 times with PBS and observed under the microscope (Leica DMI3000B).

Osteogenic Differentiation: PDLSCs were seeded at a density of 3000 cells/cm^2 on 24-well plates with DMEM + 10% FBS + 1% A/A. Once the cells reached confluence, half of the wells were cultured in osteogenic differentiation medium for 21 days, whilst the other half remained cultured in DMEM. The osteogenic differentiation medium consisted of the medium used for PDLSC culture (DMEM + 10% FBS + 1% A/A) further supplemented with 10 mM β-glycerophosphate (SIAL), 50 µg/ml ascorbic acid (SIAL) and 10 nM dexamethasone (SIAL). Medium was fully renewed every 3 to 4 days. After 21 days, the media were removed, cells were washed once with PBS, fixed with 4% PFA for 20 min at room temperature and stained with Alizarin Red, Alkaline Phosphatase/Von Kossa and Xylenol Orange stainings. Alizarin Red staining allows the visualization of calcium deposits in red. ALP staining detects ALP activity, which is a byproduct of osteoblast activity. Von Kossa staining allows the identification of mineralization, indicating the presence of calcium phosphate through black precipitates. Xylenol Orange staining also confirms the presence of calcium deposits. For Alizarin Red staining, cells were incubated with a 2% Alizarin Red solution (SIAL) for 1 h at room temperature, protected from light. After staining, cells were washed 6 times with milliQ water and observed under the microscope. For ALP staining, cells were incubated with Fast Violet solution (SIAL) and Naphthol AS-MX Phosphate Alkaline solution (SIAL) in a final concentration of 4% for 45 min at room temperature, protected from light. After this staining, cells were washed with milliQ water, and incubated with 2.5% silver nitrate solution (SIAL) for 30 min at room temperature, protected from light, to perform the Von Kossa staining. After this staining, cells were washed twice with milliQ water and observed under the microscope. For Xylenol Orange staining, cells were incubated with a 20 mM Xylenol orange solution (SIAL) for 1 h at room temperature, protected from light. After staining, cells were washed with milliQ water and observed by fluorescence microscopy.

3.1.3 Flow Cytometry Analysis

The immunophenotype of PDLSCs was analyzed with flow cytometry using a panel of mouse anti-human monoclonal antibodies for the expression of CD73, CD90, CD105, CD34, CD45, CD146 and CD106 (Biolegend). PDLSCs (2.5x10^6 cells/ml) were incubated with each antibody for 20 min at room

temperature, protected from light. Then cells were washed with PBS, centrifuged at 1500 rpm for 5 min and fixed with 4% PFA. Flow cytometry analysis was performed using FACScalibur flow cytometer (Becton Dickinson) and CellQuest^{TM} software (Becton Dickinson). A minimum of 10 000 events were collected for each sample. The obtained data was analyzed using Flowing Software (University of Turku).

3.1.4 Immunocytochemistry Analysis

The presence and distribution of several ECM proteins, namely fibronectin, collagen I, laminin, asporin, osteopontin and osteocalcin, were analyzed in PDLSCs, through immunofluorescent staining.

Cells were seeded on 24-well plates and expanded for 10 days in DMEM + 10% FBS + 1% A/A. Medium was renewed every 3 to 4 days. After the 10 days, the medium was removed, cells were washed once with PBS, fixed with 4% PFA for 20 min at room temperature and the immunofluorescent stainings were performed. Briefly, cells were incubated for 5 min with a 1% Bovine Serum Albumin (BSA) [SIAL] solution in milliQ water and then incubated for 45 min with a blocking solution composed of 0.3% Triton-X-100 (SIAL), 1% BSA and 10% FBS in PBS to permeabilize the cells and prevent non-specific staining. The primary antibodies Fibronectin (FIB), Collagen I (Col I), Laminin (LAM), and Asporin (ASP) were diluted 1:400, Osteopontin (OPN) was diluted 1:200 and Osteocalcin (OC) 1:50 in the aforementioned blocking solution. The primary antibody solutions were added to the respective wells and left incubating overnight at 4℃. One well of the 24-well plates had only one primary antibody from the following: fibronectin (ab6328, Abcam), collagen I (ab34710, Abcam), laminin (ab11575, Abcam), asporin (PA5-28124, Thermo Fisher Scientific), osteopontin (MA5-17180, Thermo Fisher Scientific) and osteocalcin (MAB1419, R&D Systems). After overnight incubation, the primary antibody solution was removed, cells were washed once with 1% BSA, the secondary antibodies diluted 1:500 in 1% BSA were added and left incubating for 1 h at room temperature, protected from light. The secondary antibodies were goat anti-rabbit IgG Alexa Fluor 546 (Thermo Fisher Scientific) for wells with collagen I, laminin, asporin, goat anti-mouse IgG Alexa Fluor 546 (Thermo Fisher Scientific) for wells with osteopontin and osteocalcin, and goat anti-mouse IgG Alexa Fluor 488 (Thermo Fisher Scientific) for wells with fibronectin. Finally, secondary antibody solutions were removed, cells were washed with PBS, the cells' nuclei were counterstained with 1.5 µg/ml DAPI solution (SIAL) for 5 min and then washed with PBS. Immunofluorescent stainings of the cells were observed by fluorescence microscopy (Leica DMI3000B).

3.1.5 Cell Morphology

Similar to section 3.1.4 cells were seeded on 24-well plates and expanded for 10 days in DMEM + 10% FBS + 1% A/A. Medium was renewed every 3 to 4 days. After the 10 days, the medium was removed, cells were washed once with PBS, fixed with 4% PFA for 20 min at room temperature and then

permeabilized with a 0.1% Triton X-100 solution for 10 min. Phalloidin (PHAL) [Thermo Fisher Scientific] was diluted 1:250 in PBS, added to the cells and left incubating for 45 min at room temperature, protected from light. Then, cells were washed with PBS, stained with 1.5 µg/ml DAPI solution for 5 min and then washed with PBS. Cells were observed by fluorescence microscopy (Leica DMI3000B).

3.2 Decellularized ECM Production and Characterization

3.2.1 Decellularized cell-derived ECM Production

PDLSCs were seeded at a density of 3000 cells/cm^2 on 6-well plates with DMEM + 10% FBS + 1% A/A. Cells were expanded for 10 days and medium was renewed every 3 to 4 days. After the 10 days, the medium was removed and cells were washed once with PBS. The ECM was isolated following a decellularization protocol, which was based on previously reported methods [31–33, 105]. The wells of the plates were decellularized by adding a 0.5% Triton X-100 (SIAL) + 20 mM ammonium hydroxide (NH_4OH, Honeywell) PBS solution and incubating for 5 min at room temperature. After confirming the occurrence of complete cell lysis and presence of ECM on the wells' surface through microscopic observation, ECM was gently washed 3 times with milliQ water. With milliQ water in the wells, the ECM was detached using a cell scrapper (Corning) and collected in falcon tubes. The contents of the falcon tubes were lyophilized (freeze-dried) to obtain ECM in powder form to use in the electrospinning procedure and in characterization or quantification assays.

3.2.2 Immunocytochemistry Analysis

Analog to 3.1.4, the presence and distribution of several ECM proteins were analyzed in the decellularized cell-derived ECM. Cells were seeded on 24-well plates and expanded for 10 days in DMEM + 10% FBS + 1% A/A. Medium was renewed every 3 to 4 days. After the 10 days, the medium was removed, cells were washed with PBS and the wells of the plates were decellularized using the protocol described in 3.2.1. After gently washing the ECM 3 times with milliQ water, the wells were fixed with 4% PFA for 20 min at room temperature and the immunofluorescent stainings were performed, as described in 3.1.4. In addition to the ECM proteins, the ECM was also stained for Phalloidin, as described in 3.1.5. Immunofluorescent stainings of the decellularized ECM were observed by fluorescence microscopy.

3.2.3 DNA/GAG/Collagen Quantification

The amount of DNA, GAGs and collagen present in samples before and after decellularization was quantified using adequate biochemical assays. PDLSCs were seeded at a density of 3000 cells/cm^2 on 6-well plates with DMEM + 10% FBS + 1% A/A. Cells were expanded for 10 days and medium was renewed

every 3 to 4 days. Afterwards, the medium was removed and cells were washed once with PBS. For samples corresponding to before decellularization, cells were detached using a 0.05% trypsin solution, centrifuged with milliQ water to form a pellet and the supernatant was removed almost completely with micropipette without disturbing the pellet. For samples corresponding to after decellularization, the ECM was collected as described in section 3.2.1 and lyophilized. All samples were in falcon tubes that had been previously weighted to allow the determination of the weight of the lyophilized samples. In each quantification assay, three samples of each condition (before and after decellularization) were used.

DNA quantification: DNA present in samples was quantified using Quant-iT PicoGreen dsDNA Reagent and Kit (Thermofisher Scientific). Following the manufacturer's instructions, a 1X TE buffer was prepared, the Quant-iT PicoGreen dsDNA Reagent was diluted 1:200 in 1X TE buffer and a 2 µg/ml DNA stock solution was prepared by diluting the kit's lambda DNA standard 1:50 in 1X TE buffer. In a 96-well plate, diluted forms of the 2 µg/ml DNA stock solution were pipetted at eight distinct concentrations, to make up standards for a calibration curve. Samples were diluted in 1X TE buffer and added to the 96-well plate. The PicoGreen solution was added to all the wells and left incubating for 2-5 min at room temperature, protected from light. The fluorescence was then measured on a plate reader (Infinite 200 Pro; Tecan) at an excitation/emission wavelength of 480/520 nm. All samples and standards were run in triplicate. The DNA content of the samples was estimated using the prepared calibration curve.

GAG quantification: The amount of GAGs in samples was determined using Dimethyl-Methylene Blue (DMMB) assay. This assay requires the preparation of two main solutions: DMMB assay dilution buffer and DMMB stock solution. The DMMB assay dilution buffer consists of a 50 mM Sodium Phosphate (SIAL), 2 mM N-acetyl cysteine (SIAL) and 2 mM EDTA (SIAL) solution in milliQ water, whose pH was adjusted to 6.5 with 1 M Hydrochloric Acid (HCl). For the DMMB stock solution, 16 mg of 1,9-Dimethyl-Methylene Blue zinc chloride double salt (SIAL) was dissolved overnight in 5 ml reagent grade 100% ethanol (Thermo Fisher Scientific). The DMMB stock solution consists of 975ml milliQ water, 2.73 g Sodium Chloride (SIAL), 3.04 g Glycine (SIAL), 0.69 ml concentrated HCl (11.6 M, Honeywell) and 5 ml DMMB solution. The DMMB stock solution had its pH adjusted to 3.0 with 1 M Sodium Hydroxide solution and its volume then adjusted to 1 liter with milliQ water. The first step of this assay is to digest the samples. For this purpose 1 mg of Papain (P4762, SIAL) was dissolved in 10 ml of DMMB assay dilution buffer and then added to the samples in the falcon tubes, which were digested for 16-18h at 60℃. In a 96-well plate, diluted forms of a 40 µg/ml chondroitin-6-sulfate (SIAL) solution in DMMB assay dilution buffer were pipetted at seven distinct concentrations, to make up standards for a calibration curve. The digested samples were vortexed and pipetted in the 96-well plate. DMMB stock solution was added to all the wells, and left incubating for 5 min at room temperature, protected from light. The absorbance was measured on a plate reader (Infinite 200 Pro; Tecan) at 525 nm. All samples and standards were run in triplicate. The GAG content of the samples was estimated using the prepared calibration curve.

Collagen quantification: The collagen content of samples was quantified using Hydroxyproline Assay Kit (SIAL). Hydroxyproline is a major component of collagen, therefore hydroxyproline concentration in samples was measured, following the manufacturer's instructions, to determine the collagen content of the samples. Samples were homogenized with water and concentrated HCl (11.6M, Honeywell) was added. Samples were hydrolyzed at 120℃ for 3h, then centrifuged at 10.000g for 3 min and the supernatant was transferred to a 96-well plate. The plate was placed in an oven at 60℃ to dry the samples. In a 96-well plate, diluted forms of a 0.1 mg/ml hydroxyproline solution were pipetted at six distinct concentrations, to make up standards for a calibration curve. The assay requires the preparation of two solutions using the components present in the kit: Chloramine T/Oxidation Buffer Mixture and Diluted DMAB reagent. First, the Buffer Mixture was added to all sample and standard wells and left incubating for 5 min at room temperature. Then, the Diluted DMAB reagent was added to all wells and left incubating for 90 min at 60℃. The absorbance was then measured on a plate reader (Infinite 200 Pro; Tecan) at 560 nm. Standards were run in duplicate and samples were run in triplicate. The collagen content of the samples before and after decellularization was estimated using the prepared calibration curve.

3.2.4 Scanning Electron Microscopy

Round cover glasses (13 mm diameter, VWR) were sterilized with ethanol and placed under UV light for 45 min. Afterwards, cover glasses were washed with PBS and placed inside an incubator at 37℃ to dry the remainder of the PBS. In a 12-well plate, cover glasses were placed one per well, in the center of the well. PDLSCs were seeded on top of the cover glasses at a density of 6000 cells/cm^2 with DMEM + 10% FBS + 1% A/A. Cells were expanded for 10 days and medium was renewed every 3 to 4 days. After the 10 days, the medium was removed, cells were washed with PBS and the wells of the plates were carefully decellularized to not detach the ECM from the cover glasses. After gently washing the ECM 3 times with milliQ water, the wells were fixed with 4% PFA for 20 min at room temperature. After fixation, samples were dehydrated using ethanol gradient solutions (20%, 40%, 60%, 80%, 90% and 100% (v/v)). The ECM samples were structurally characterized using a Scanning Electron Microscope (Phenom ProX G6 Desktop SEM, Thermo Fisher Scientific). The samples were first coated with a gold/palladium layer, and were then imaged at several magnifications using an accelerating voltage of 10kV or 15kV.

3.3 Fabrication of Electrospun Scaffolds

Poly (ε-caprolactone) (PCL, Mn = 70000-90000 Da, SIAL) was dissolved at 13% w/v in 1,1,1,3,3,3-hexafluoro-2-propanol (HFIP, Tokyo Chemical Industry) under agitation in a rocking platform (VWR) for 2.5 h at room temperature. The solvents used to dissolve chitosan were Trifluoroacetic acid (TFA, Honeywell) and Dichloromethane (DCM, Honeywell). Medium molecular weight chitosan (CTS, Mn =

190,000-310,000 Da, SIAL) was dissolved at 1%, 2%, 3%, 4% and 5% w/v in TFA/DCM (70/30 v/v) solvent mixture and stirred for 1.5 h at 250 rpm in a water bath at 50 ℃ using a magnetic stirrer. Glass vials containing CTS solutions were well closed and isolated with parafilm and tape to avoid solvent evaporation during CTS dissolution at 50 ℃.

In this work, three main solutions are prepared to be used in electrospinning: PCL 13% w/v solution, PCL-CTS blend solution and PCL-CTS-ECM blend solution. PCL and CTS solutions were blended together to obtain a 70/30 (v/v) PCL-CTS blend solution, followed by agitation overnight in a rocking platform to produce a homogeneous solution. For instance, to obtain a 5 ml PCL-CTS blend solution, 3.5 ml of PCL solution and 1.5 ml of CTS solution are blended. To prepare a PCL-CTS-ECM solution, lyophilized cell-derived ECM was incorporated into the CTS solution (1 mg/ml) and dispersed through agitation for 15 min at 300 rpm using a magnetic stirrer. Then, PCL and CTS-ECM solutions were blended together to obtain a 70/30 (v/v) PCL-CTS blend solution, followed by agitation overnight in a rocking platform to produce a homogeneous PCL-CTS-ECM solution. Due to CTS presence in the fibers, PCL-CTS and PCL-CTS-ECM scaffolds were crosslinked with glutaraldehyde (GA) vapor (25% v/v, SIAL) for 24 h in a desiccator to ensure their stability.

Fibrous scaffolds were fabricated using electrospinning. Each solution (5 ml) was loaded into a 10 ml plastic syringe (Henke Sass Wolf), placed in a pump and connected to a PTFE tube (VWR), which was attached to a 21G stainless steel needle (0.8 mm inner diameter; Monoject Blunt Cannula 21G; Covidien). A simplified scheme of the electrospinning setup used in this work can be seen in figure 3.1.

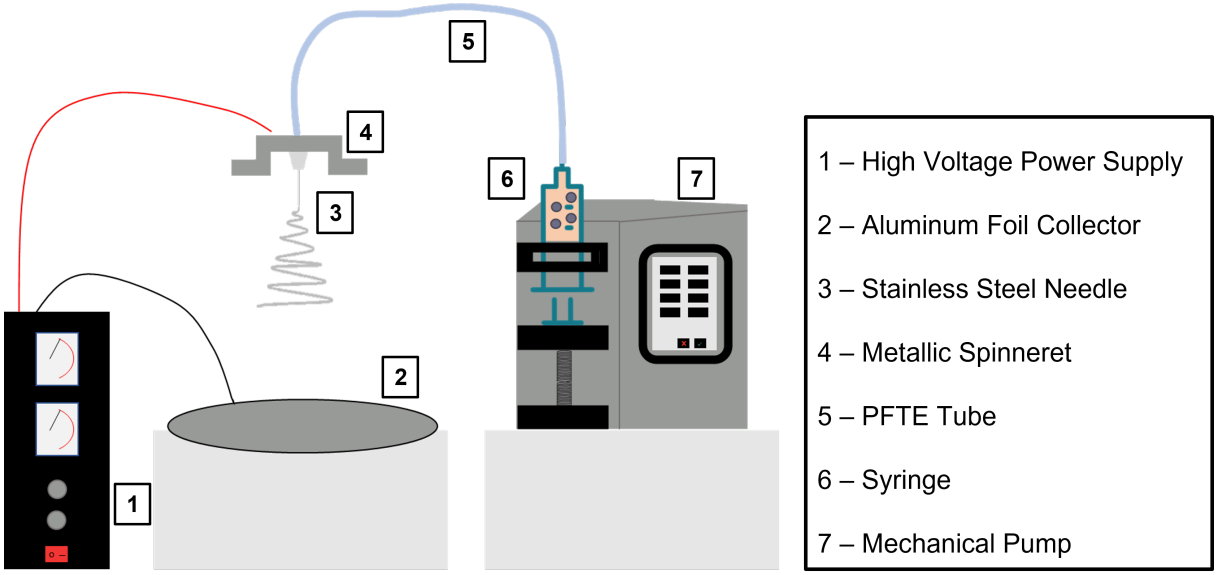

Figure 3.1: Simplified scheme of the electrospinning setup used.

During the electrospinning process for all solutions, a controlled flow rate of 0.5 ml/h, an applied voltage of 24 kV and a distance of 22 cm between needle tip and aluminum foil collector were used.

These parameters were optimized in order to obtain beadless electrospun fibers with the desired fiber diameters. The different electrospun fibrous scaffolds were produced under the same electrospinning parameters and ambient conditions. For the initial optimization scaffolds (PCL control and blends with 5 different CTS concentrations), temperature and relative humidity varied between 21–22℃ and 30-40%, respectively, and electrospinning was performed for 1.5 h to ensure thickness of each scaffold. After optimization and selection of the CTS concentration of 5%, all scaffolds onwards were electrospun for 2.5 h with temperature and relative humidity varying between 23–24℃ and 30–40%, respectively.

3.4 Characterization of Electrospun Scaffolds

3.4.1 Scanning Electron Microscopy and Energy Dispersive X-Ray Analysis

Electrospun fibers were structurally characterized through Scanning Electron Microscopy (SEM) using a Phenom ProX G6 Desktop SEM (Thermo Fisher Scientific). Electrospun fibers either deposited on top of round cover glasses (VWR) placed on the collector during the electrospinning procedure, or were fixed to the cover glasses using an adhesive silicone glue (Silastic Medical Adhesive Silicone, Type A; Dow Corning). Before imaging, samples were coated with a gold/palladium layer. The samples were imaged at several magnifications, using an accelerating voltage of 10kV or 15kV. The average fiber diameters of the various fibrous scaffolds were determined by measuring 100 individual fibers per scaffold from five different SEM images using ImageJ software (ImageJ 1.53k, National Institutes of Health, USA).

Energy Dispersive X-Ray (EDX) analysis was performed on all scaffolds that were structurally characterized using the Desktop SEM, since this microscope was equipped with an energy dispersive X-Ray spectroscopy (EDS) detector. The EDX analysis conducted was used to identify the different elements present in the various fibrous scaffolds, to determine variations between scaffolds and to confirm the presence of the polymers and ECM in their composition.

3.4.2 Attenuated Total Reflectance Fourier Transform Infrared Spectroscopy

Attenuated Total Reflectance Fourier Transform Infrared Spectroscopy (ATR-FTIR) analysis was performed at CDRSP - Politécnico de Leiria using a Bruker AlphaP FTIR spectrometer with Attenuated Total Reflectance (ATR) platinum–diamond coupling. FTIR spectra were obtained from PCL, PCL-CTS and PCL-CTS-ECM fibrous scaffolds with and without Crosslinking (CL); and from the individual materials, namely PCL, CTS and ECM, in order to confirm their presence in the electrospun scaffolds. Transmittance spectra were obtained with a spectral resolution of 4 cm^{-1} and in the range 4000 to 400 cm^{-1}. All spectra were then normalized using the maximum and minimum transmittance values of each individual spectrum.

3.4.3 Thermal Properties Analysis

Differential Scanning Calorimetry (DSC) Analysis was performed at CDRSP - Politécnico de Leiria on a Simultaneous Thermal Analyzer, STA 6000 system (Perkin Elmer). Samples of the used polymers, namely PCL and CTS, and of PCL, PCL-CTS and PCL-CTS-ECM fibers with crosslinking (CL) were weighed in alumina pans (6-8 mg per sample) and heated from 20℃ to 200℃ at a heating rate of 10℃/min. The analysis was performed under a nitrogen atmosphere with a flow rate of 20 ml/min. DSC analysis was performed in triplicates. The thermal degradation of the polymers and the fibers was evaluated using Thermogravimetric Analysis (TGA) mode on the STA 6000 system. The samples were heated from 50℃ to 600℃ at a heating rate of 10℃/min. This analysis was also performed in triplicates and under a nitrogen atmosphere with a flow rate of 20 ml/min.

3.4.4 Contact Angle

The contact angles of PCL, PCL-CTS and PCL-CTS-ECM fibers were measured using a DSA25 Drop Shape Analyzer (Krüss) in the sessile drop method. Droplets of distilled water were placed on the surface of the various fibrous scaffolds and the contact angles were measured. For each condition, the contact angles were measured in 3 individual fiber samples (N=3).

3.4.5 Mechanical Tensile Testing

The mechanical properties of electrospun scaffolds were assessed through uniaxial tensile testing at room temperature using a mechanical tester (Univert Model UV-200-01, CellScale Biomaterials Testing), with a 10 N load cell and a 3 mm/min displacement rate. For each condition, ten different test specimens (N=10) were cut as rectangular strips with a length of 30 mm, width of 10 mm and thickness of 0.1 mm. The rectangular strips of fibers were then fixed with tape to carton molds, as illustrated in figure 3.2(a). Prior to testing, the dimensions of the rectangular samples were measured and the samples were placed well aligned in the grips of the mechanical tester, as seen in figure 3.2(b).

The experimental data was collected and processed using the UniVert software, and was analyzed using Microsoft Excel. Tensile stress and strain were computed to plot stress-strain curves. Tensile stress, σ, was obtained by dividing the measured values of force by each specimen's cross-sectional area: $\sigma = \frac{F}{A}$. The cross-sectional area is determined by the width and thickness of the scaffold. Tensile strain, ε, was obtained by dividing the registered displacement values by the initial length of the specimen: $\varepsilon = \frac{h}{h_0}$ The Young's modulus of each specimen was obtained from the slope of the initial linear portion (0-15%) of the stress-strain curve. The Ultimate Tensile Strength (UTS) corresponded to the stress on the maximum of the stress-strain curve. The ultimate elongation was computed by dividing the displacement on the maximum of the curve by the original length of the specimen.

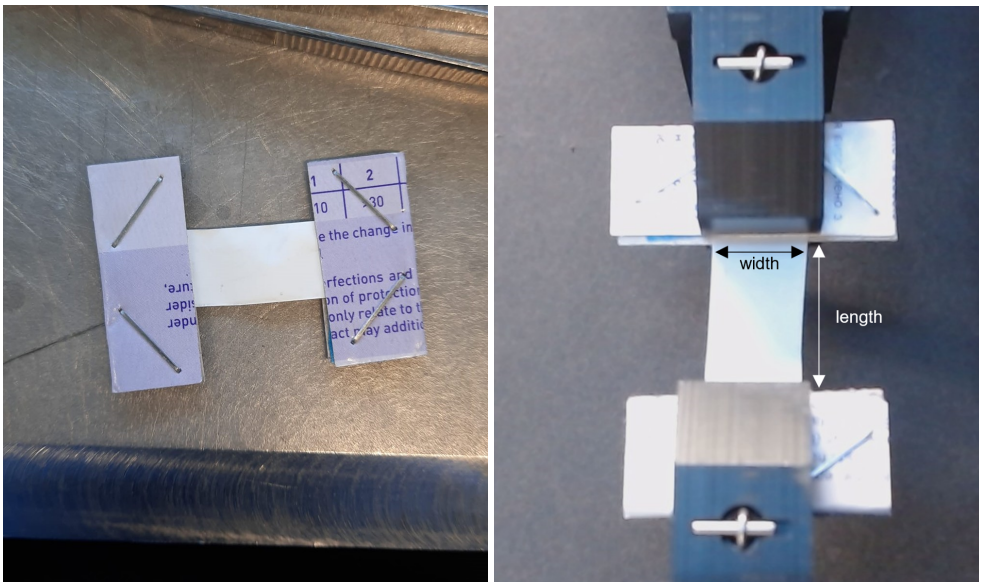

(a) Example of a prepared test specimen **(b)** Sample mounted on Univert tester

Figure 3.2: Examples of test specimens used for mechanical tensile testing and dimensions

3.5 *In Vitro* Cell Culture on Electrospun Scaffolds

3.5.1 Scaffold Preparation and Sterilization

PCL, PCL-CTS and PCL-CTS-ECM fibers with crosslinking were fixed to round cover glasses (13 mm diameter, VWR) using an adhesive silicone glue (Silastic Medical Adhesive Silicone, Type A; Dow Corning), which is biocompatible. The glued fibers were left overnight to properly adhere and to dry the glue. Cover glasses with fixed fibers were placed in petri dishes (Corning) and the scaffolds were sterilized with UV light for 30 min, as seen in figure 3.3. The scaffolds were then washed three times with a solution of PBS and 1% (v/v) A/A. In each wash, scaffolds remained submerged in the solution for 1 h before proceeding to the next wash. Scaffolds were left in PBS + 1% A/A until performing cell seeding.

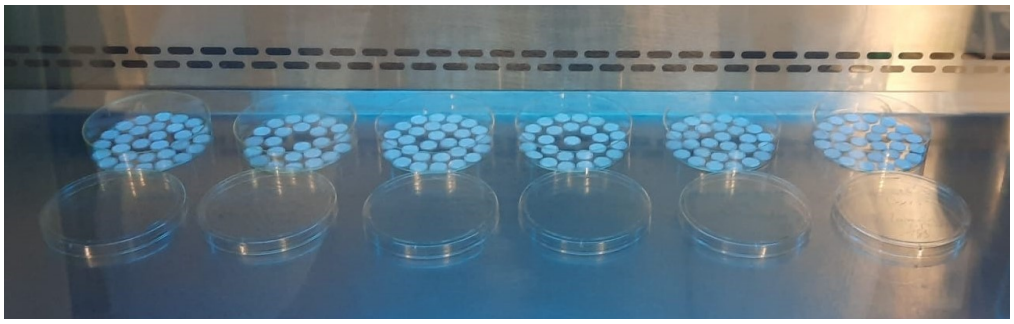

Figure 3.3: Sterilization of electrospun PCL, PCL-CTS and PCL-CTS-ECM scaffolds with UV light

Before performing cell seeding, the scaffolds were placed in ultra-low attachment 24-well plates to ensure that the cells only grew on the surface of the scaffold. The scaffolds were washed one more time with PBS + 1% A/A, immersed in DMEM + 10% FBS + 1% A/A and incubated for 1 h at 37℃.

3.5.2 PDLSC Seeding and Culture on Electrospun Scaffolds

After removing the medium, in which the scaffolds were immersed, PDLSCs were seeded as 20 µl droplets, at a density of 50.000 cells per scaffold. The seeded scaffolds were incubated at 37℃ and 5% CO_2 in a humidified atmosphere for 3h without culture medium, in order to promote initial cell adhesion. Osteogenic medium, whose composition is described in section 3.1.2, was then added to all scaffolds. PDLSCs were cultured on the scaffolds for 21 days and medium was fully renewed every 3 to 4 days.

3.5.3 Assessment of Electrospun Scaffolds Biological Performance

3.5.3.A PDLSC Proliferation on Scaffolds

The proliferation of PDLSCs on electrospun scaffolds was evaluated using AlamarBlue Cell Viability Assay (Thermo Fisher Scientific). This non-toxic assay was performed on days 1, 7, 14 and 21 following the manufacturer's instructions. When performing this assay, a 10% (v/v) AlamarBlue solution in DMEM + 10% FBS + 1% A/A medium was added to the scaffolds and incubated at 37℃ and 5% CO2 in a humidified atmosphere for 3 h. The fluorescence was then measured on a plate reader (Infinite 200 Pro; Tecan) at an excitation/emission wavelength of 560/590 nm. For each experimental group (PCL, PCL-CTS and PCL-CTS-ECM), the fluorescence was measured for 6 independent scaffolds (N=6) in triplicates and acellular electrospun scaffolds were used as blank controls. The collected fluorescence intensity values were correlated with the number of viable PDLSCs present on the electrospun scaffolds through a previously obtained calibration curve.

3.5.3.B Immunocytochemistry Analysis and Cell Morphology

Similar to section 3.1.4 and section 3.2.2, the presence of several proteins was analyzed in PDLSCs cultured on electrospun scaffolds after 21 days of culture. The proteins analyzed were collagen I, asporin, osteopontin, osteocalcin, periostin and cementum protein-1. The scaffolds were washed once with PBS, fixed with 4% PFA for 20 min at room temperature and immunofluorescent stainings were performed. Cells were permeabilized with 1% BSA and non-specific staining was prevented using a blocking solution, as described in section 3.1.4. The primary antibodies asporin, osteopontin, Periostin (POSTN) and Cementum Protein (CMP)-1 were diluted 1:100, collagen I was diluted 1:200 and osteocalcin 1:50 in the blocking solution. The primary antibody solutions were added to the respective wells and left incubating overnight at 4℃. One scaffold had only one primary antibody from the following: collagen I

(ab34710, Abcam), asporin (PA5-28124, Thermo Fisher Scientific), osteopontin (MA5-17180, Thermo Fisher Scientific), osteocalcin (MAB1419, R&D Systems), periostin (ab14041, Abcam) and cementum protein 1 (PA5-63462, Thermo Fisher Scientific). After overnight incubation, the primary antibody solution was removed, cells were washed once with 1% BSA, the secondary antibodies diluted 1:200 in 1% BSA were added and left incubating for 1 h at room temperature, protected from light. The secondary antibodies were goat anti-rabbit IgG Alexa Fluor 546 (Thermo Fisher Scientific) for scaffolds with collagen I, asporin, periostin and cementum protein, and goat anti-mouse IgG Alexa Fluor 546 (Thermo Fisher Scientific) for scaffolds with osteopontin and osteocalcin. Finally, secondary antibody solutions were removed, cells were washed with PBS, the cells' nuclei were counterstained with 1.5 µg/ml DAPI solution (SIAL) for 5 min and then washed with PBS.

To assess the morphology of the PDLSCs on the electrospun scaffolds, cells were stained with Phalloidin, similar to section 3.1.5. After fixation with PFA, cells were permeabilized with a 0.1% Triton X-100 solution for 10 min. Phalloidin (Thermo Fisher Scientific) was diluted 1:100 in PBS, added to the cells and left incubating for 45 min at room temperature, protected from light. Then, cells were washed with PBS, stained with 1.5 µg/ml DAPI solution for 5 min and then washed with PBS. All immunofluorescent stainings were observed by fluorescence microscopy (Leica DMI3000B).

Assessment of PDLSCs' Osteogenic Differentiation on Electrospun Scaffolds

3.5.3.C ALP Activity Assay

ALP activity after 21 days of PDLSCs osteogenic differentiation on scaffolds was quantified using QuantiChrom ALP Assay Kit (BioAssays Systems) according to the manufacturer's guidelines. The scaffolds were washed with PBS and then incubated with a 0.1% Triton X-100 solution overnight at room temperature under orbital agitation. Afterwards, a 2.5% Magnesium Acetate and 1% p-nitrophenyl phosphate solution in Assay Buffer was added to the samples. All the components necessary for this solution are present in the ALP quantification kit. ALP hydrolyzes p-nitrophenyl phosphate, which generates a yellow colored product. The absorbance of the samples was then measured on a plate reader (Infinite 200 Pro; Tecan) at 405nm. Multiple measurements were performed with 4-minute gaps for a total of 40 minutes, in order to compute the difference in absorbance between the different time points. The obtained values of absorbance were normalized to the number of PDLSCs present on each scaffold. For each experimental group (PCL, PCL-CTS and PCL-CTS-ECM), the absorbance was measured for three independent scaffolds (N=3) and collected in triplicates.

3.5.3.D ALP/Von Kossa Stainings

ALP staining detects ALP activity. Von Kossa staining allows the identification of mineralization, indicating the presence of calcium phosphate through black precipitates. After 21 days of osteogenic differentiation, the electrospun scaffolds were washed once with PBS, fixed with 4% PFA for 20 min at room temperature and the ALP and Von Kossa stainings were performed as described in section 3.1.2. First, for ALP staining, scaffolds were incubated with Fast Violet solution (SIAL) and Naphthol AS-MX Phosphate Alkaline solution (SIAL) in a final concentration of 4% for 45 min at room temperature, protected from light. After this staining, scaffolds were washed with milliQ water, and observed under the microscope. Afterwards, scaffolds were incubated with 2.5% silver nitrate solution (SIAL) for 30 min at room temperature, protected from light, to perform the Von Kossa staining. After this staining, scaffolds were washed twice with milliQ water and observed under the microscope.

3.5.3.E Alizarin Red Staining and Quantification

Alizarin Red staining allows the visualization of calcium deposits in red. After 21 days of culture, the scaffolds were washed once with PBS, fixed with 4% PFA for 20 min at room temperature and the Alizarin Red staining was performed as described in section 3.1.2. For each experimental group (PCL, PCL-CTS and PCL-CTS-ECM), three scaffolds (N=3) were incubated with a 2% Alizarin Red solution (SIAL) for 1 h at room temperature, protected from light. After staining, scaffolds were washed four times with milliQ water and observed under the microscope. Afterwards, the water was removed and the Alizarin Red bound to the scaffolds was dissolved with a 10% (w/v) cetylpyridinium chloride (CPC) solution under orbital agitation for 1 h. In a 96-well plate, diluted forms of a 1000 µg/ml Alizarin Red solution in 10% (w/v) CPC were pipetted at nine distinct concentrations, to make up standards. These diluted forms were used to build a standard curve and to determine the maximum absorption wavelength of Alizarin Red dissolved in 10% CPC by measuring absorbance values from 500-600nm in increments of 1nm. Then, the absorbance of the standards and the dissolved samples were measured on a plate reader (Infinite 200 Pro; Tecan) at 550nm. All standards and samples were run in triplicate.

3.5.3.F Biomineralization Quantification

The mineralization of PDLSCs on the scaffolds after 21 days of osteogenic differentiation was assessed and quantified using OsteoImage Mineralization Assay (Lonza). This fluorescent assay allows the quantification of cell mineralization, due to the specific binding of the Staining Reagent to the hydroxyapatite portion of bone-like nodules deposited by cells. Following the manufacturer's instructions, a 1X Wash Buffer was prepared and the Staining Reagent was diluted 1:100 in Staining Reagent Dilution Buffer. For each experimental group (PCL, PCL-CTS and PCL-CTS-ECM), three scaffolds (N=3) were washed

once with PBS, fixed with 4% PFA for 20 min at room temperature and washed once with 1X Wash Buffer. Afterwards, the diluted staining reagent was added to the scaffolds and left incubating for 30 min at room temperature, protected from light. Then, scaffolds were washed three times with 1X Wash Buffer, leaving the wash buffer in the wells for 5 min per wash. The fluorescence was then measured on a plate reader (Infinite 200 Pro; Tecan) at an excitation/emission wavelength of 492/520 nm. The green fluorescent staining of the cells was also observed by fluorescence microscopy (Leica DMI3000B).

3.5.3.G Scanning Electron Microscopy and Energy Dispersive X-Ray Analysis

The cell morphology of the PDLSCs present on the electrospun scaffolds was also analysed with SEM using Phenom ProX G6 Desktop SEM. After 21 days of osteogenic differentiation, scaffolds were washed once with PBS, fixed with 4% PFA for 20 min and dehydrated using ethanol gradient solutions (20%, 40%, 60%, 80%, 90% and 100% (v/v)). Then, the samples were incubated for 1 h in hexamethyldisilazane (HDMS) and left to air dry inside a fume hood. Scaffolds were coated with a gold/palladium layer and then analysed with SEM as previously described. EDX analysis was performed with an accelerating voltage of 10kV, using the Desktop SEM on the electrospun scaffolds after 21 days of PDLSCs osteogenic differentiation, with the aim to detect the presence of mineralization on the scaffolds.

3.5.3.H Gene Expression Analysis

Total RNA was extracted using the RNeasy Mini Kit (QIAGEN) following the manufacturer's instructions. Briefly, after 21 days of osteogenic differentiation, scaffolds were washed twice with PBS and then incubated with RLT lysis buffer under orbital agitation for 1 h. Afterwards, total RNA was isolated according to the manufacturer's protocol. Total RNA was quantified using a Nanodrop (NanoVue Plus, GE Healthcare). cDNA was synthesized from the purified RNA using High-Capacity cDNA Reverse Transcription kit (Thermofisher Scientific). Reaction mixtures (20 µL) were incubated in a thermal cycler (96-well T-100 Thermal Cycler, Biorad) for 5 min at 25℃, 20 min at 46℃ and 1 min at 95℃ and then were maintained at 4℃.

The Quantitative Reverse Transcription-Polymerase Chain Reaction (qRT-PCR) was performed using NZYSpeedy qPCR Green Master Mix (2x), ROX plus (NZYTech) and StepOnePlus real-time PCR system (Applied Biosystems). Target genes included ALP, Runt-related transcription factor 2 (RUNX2), COL I, OC, CMP1 and Osterix (OSX). Primer sequences used in the qRT-PCR analysis are presented in table 3.1. All reactions were carried out at 95℃ for 10 min, followed by 40 cycles of 95℃ for 15 s and 60℃ for 1 min. All samples were analyzed in triplicates. Target gene expression was primarily normalized to the housekeeping gene glyceraldehyde 3-phosphate dehydrogenase (GAPDH) and then determined as a fold change relative to the baseline expression of the target gene measured in undifferentiated PDLSCs at day 0, prior to scaffold seeding (Control).

Table 3.1: Sequences of primers used for qRT-PCR analysis.

Gene	Sequence
GAPDH	Fwd: 5'-GGTCACCAGGCTTTTA-3' Rev: 5'-CCTGGAAGATATGGGA-3'
ALP	Fwd: 5'-ACCATTCCCACGTCTTCACATTT-3' Rev: 5'-AGACATTCTCTCGTTCACCGCC-3'
RUNX2	Fwd: 5'-AGATGATGACACTGCCACCTCTG-3' Rev: 5'-GGGATGAAATGCTTGGGAACT-3'
Col I	Fwd: 5'-CATCTCCCCTTCGTTTTTGA-3' Rev: 5'-CCAAATCCGATGTTTCTGCT-3'
OC	Fwd: 5'-TGTGAGCTCAATCCGGACTGT-3' Rev: 5'-CCGATAGGCCTCCTGAAGC-3'
CMP1	Fwd: 5'-ACATCAAGCACTGACAGCCA-3' Rev: 5'-GTTGATCTCCGCCCATAAGC-3'
OSX	Fwd: 5'-CTGGACATGACACACCCCTAT-3' Rev: 5'-GCTGGATTAAGGGGAGCAAAG-3'

3.6 Statistical Analysis

All experiments were conducted in triplicate (N=3), unless specified otherwise. The statistical analysis of the data was performed in GraphPad Prism 9 software using one-way ANOVA, followed by Tukey post-hoc test. Data was considered to be statistically significant when the p-values obtained were less than 0.05 (95% confidence intervals, *$p < 0.05$).

4

Results

Contents

4.1 PDLSC and Decellularized ECM Characterization

4.1.1 Multilineage Differentiation of PDLSC

PDLSCs were successfully differentiated into the adipogenic, chondrogenic and osteogenic lineages, as can be seen in figure 4.1. Oil Red O staining showed lipid droplets in red in differentiated cells. Alcian Blue staining was noticeably blue on the rim of the aggregate, confirming presence of GAGs. Alizarin red staining confirmed calcium deposition in red in differentiated cells compared to undifferentiated cells. Xylenol Orange staining further confirmed the presence of calcium deposits, showing a slight increase in red fluorescence, highlighted with white arrows in figure 4.1, compared to undifferentiated cells. ALP staining interestingly showed lower levels of ALP activity in red in differentiated cells. Undifferentiated PDLSCs already have osteogenic potential and visibly stain for ALP. The Von Kossa staining should have shown mineralized extracellular matrix deposits in black on cells differentiated into the osteogenic lineage. However, differentiated cells showed a brown coloured stain, not observed in undifferentiated cells. This staining was performed on multiple wells with cells differentiated for 21 days in osteogenic medium, and the images were similar, showing this brown coloured stain, as seen in figure 4.2. Interestingly, some regions of the wells also showed intensely brown spots, as shown in figure 4.2.

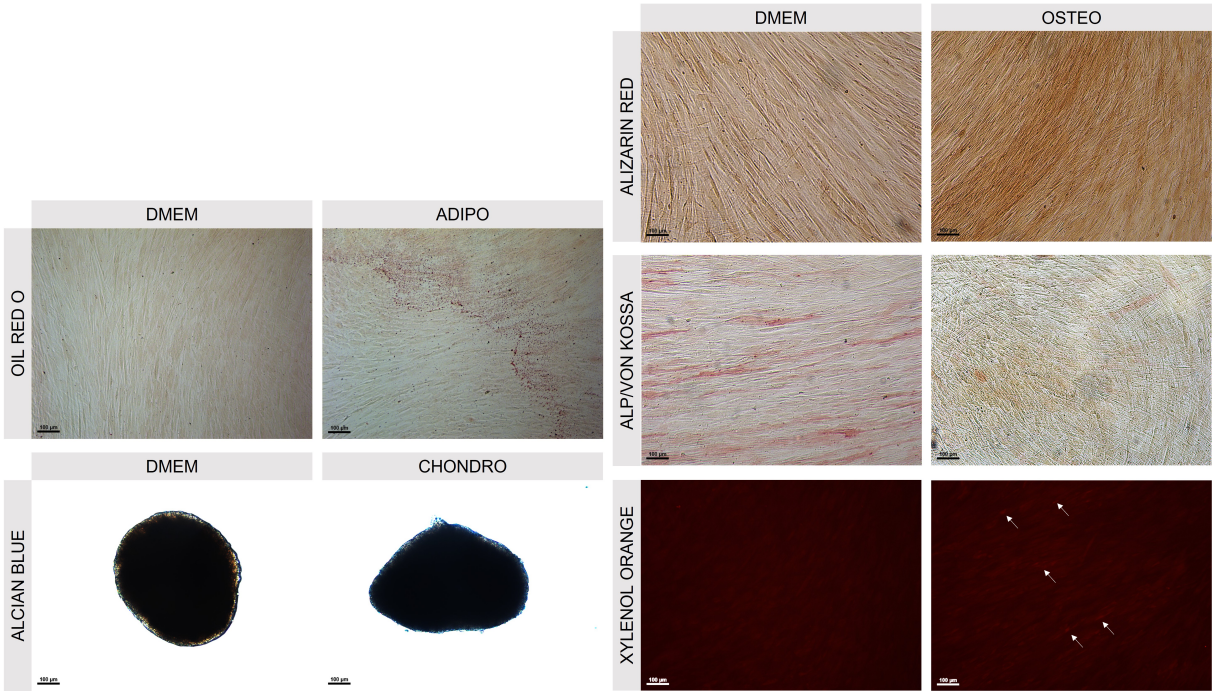

Figure 4.1: Multilineage differentiation of PDLSCs. Adipogenic differentiation (ADIPO) was detected by Oil Red O staining. Chondrogenic differentiation of aggregates (CHONDRO) was confirmed with Alcian Blue staining. Osteogenic differentiation (OSTEO) was verified through 3 distinct stainings: Alizarin Red, ALP/Von Kossa and Xylenol Orange. All stainings were also performed on controls (DMEM), corresponding to PDLSCs cultured in DMEM + 10% FBS + 1% A/A. Scale bar 100 µm.

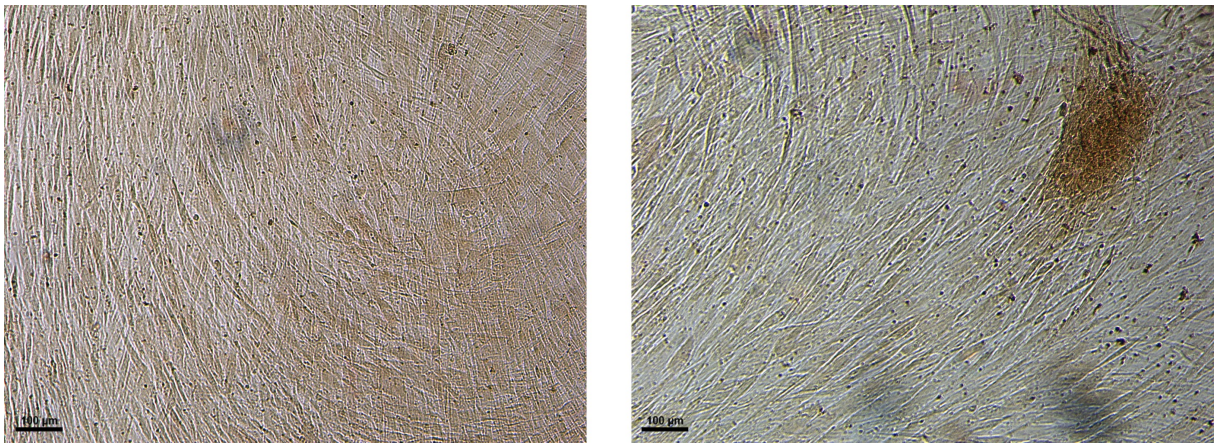

Figure 4.2: ALP/Von Kossa Staining of PDLSCs after osteogenic differentiation. Scale bar 100 µm.

4.1.2 Flow Cytometry of PDLSC

Results from the flow cytometry analysis of the immunophenotype of PDLSCs (figure 4.3) demonstrated positive expression of surface markers associated to MSCs, namely CD73 (98.33%), CD90 (99.98%), and CD105 (84.59%). However CD106, also known as vascular cell adhesion molecule-1 (VCAM-1), was negatively expressed by PDLSCs. In addition, PDLSCs also did not express hematopoietic stem cell surface markers CD34 and CD45. Lastly, PDLSCs exhibited positive expression of CD146 (68.36%), which is an endothelial cell marker also known as melanoma cell adhesion molecule (MCAM). The positive expression of this marker has already been used in the identification of PDLSCs [21].

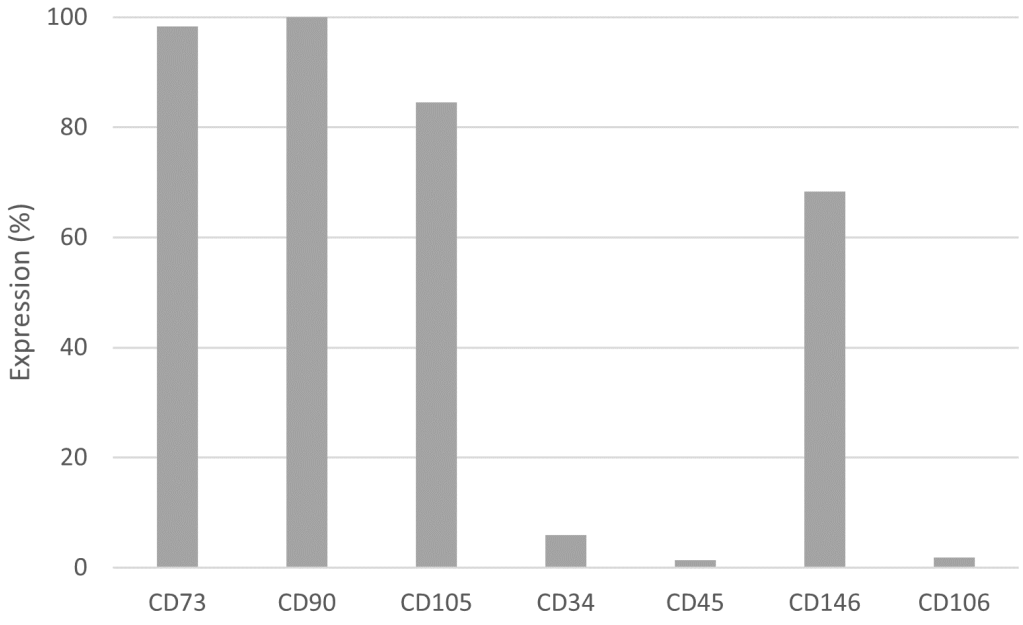

Figure 4.3: Immunophenotype of PDLSCs analyzed by flow cytometry.

4.1.3 Cell and ECM Morphology

Before decellularization, PDLSCs were fully confluent and displayed a fibroblast-like morphology similar to MSCs, as seen in figure 4.4(a). After the decellularization process, it is possible to confirm the presence of a fibrillary network of ECM through bright-field microscopy, as exemplified in figure 4.4(b).

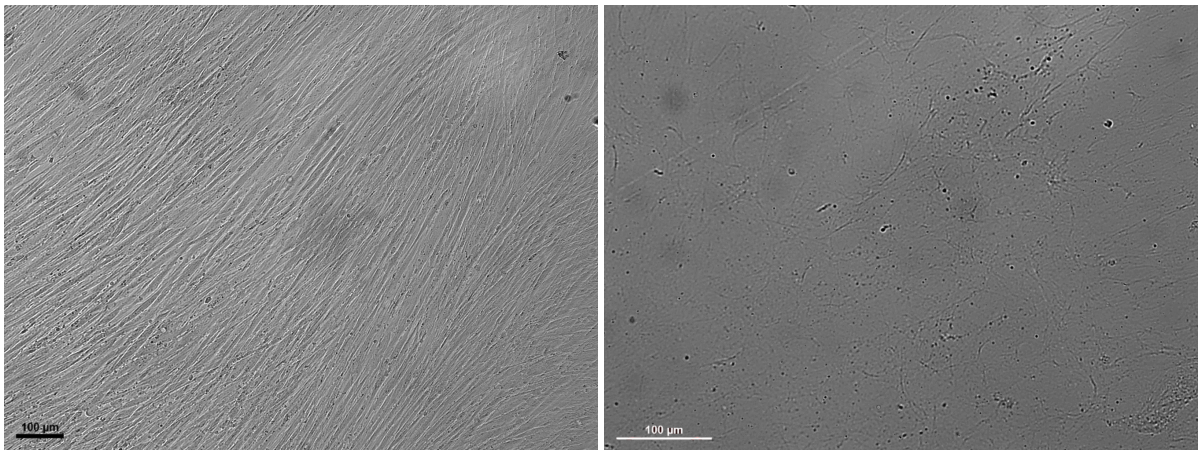

(a) Bright field image of PDLSCs. Scale bar 100 µm. **(b)** Bright field image of dECM. Scale bar 100 µm.

Figure 4.4: Bright field images of confluent PDLSCs and of decellularized cell-derived ECM.

Before decellularization, PDLSCs possessed well-defined cell nuclei and cytoskeleton, as seen in figure 4.5. After decellularization, only the ECM that was secreted by the cells remained, therefore no cell nuclei or actin filaments are visible in figure 4.5, confirming the success of the decellularization.

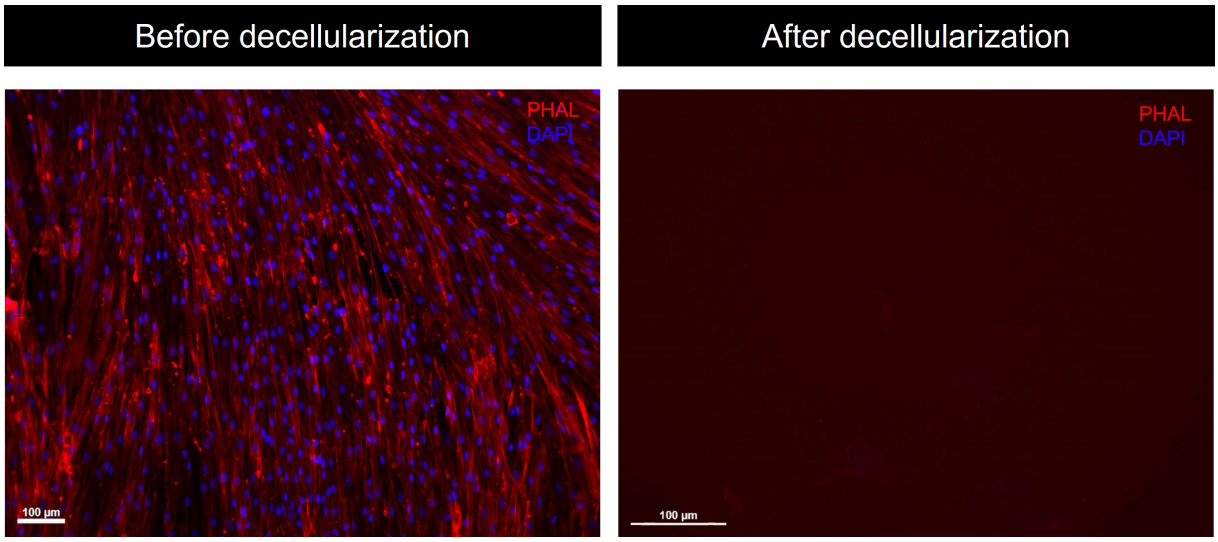

Figure 4.5: Cell morphology assessment by DAPI-Phalloidin staining before and after decellularization. The cytoskeleton actin filaments were stained with phalloidin (PHAL, red) and nuclei were stained with DAPI (blue). Scale bars 100 µm.

PDLSCs were successfully plated and expanded on top of round cover glasses, as can be observed in figure 4.6(a). After decellularization, ECM remained attached to the round cover glasses, as seen in figure 4.6(b), which enabled the posterior visualization of ECM through SEM.

Regarding microscopic visualization of the PDLSCs and the decellularized ECM, cells were always observed using a 10X magnification, whilst the decellularized ECM was always imaged using a 20X magnification to allow a more clear and detailed visualization.

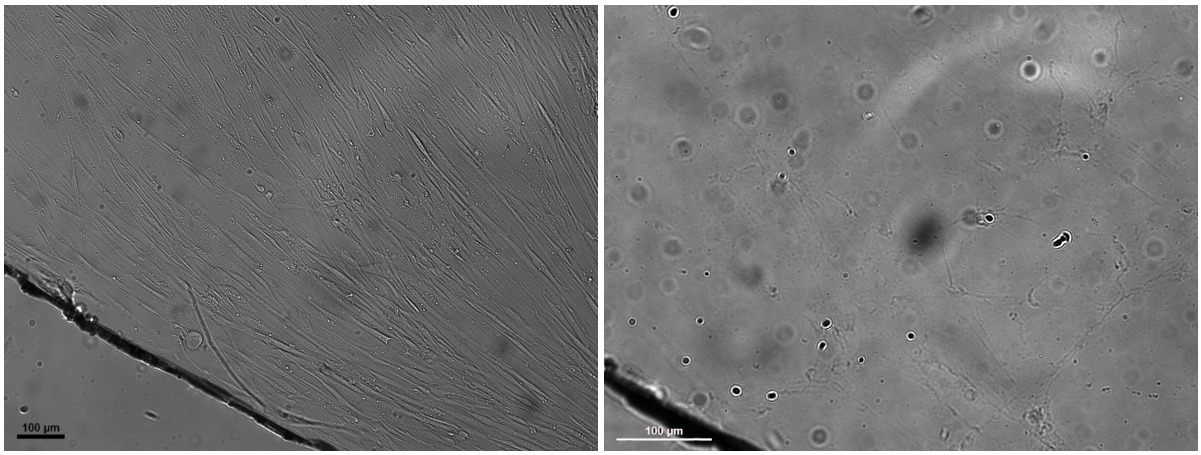

(a) PDLSCs on a cover glass. Scale bar 100 µm. **(b)** ECM on a cover glass. Scale bar 100 µm.

Figure 4.6: Bright field images of PDLSCs adhered to a round cover glass and of cell-derived ECM on a round cover glass after decellularization. Scale bars 100 µm.

The microscale features of the decellularized cell-derived ECM were assessed by SEM analysis. SEM further confirmed that the ECM possesses a fibrillary structure, as seen in figure 4.7(a). Interestingly, it was observed that ECM can form some agglomerates that have a porous-like structure.

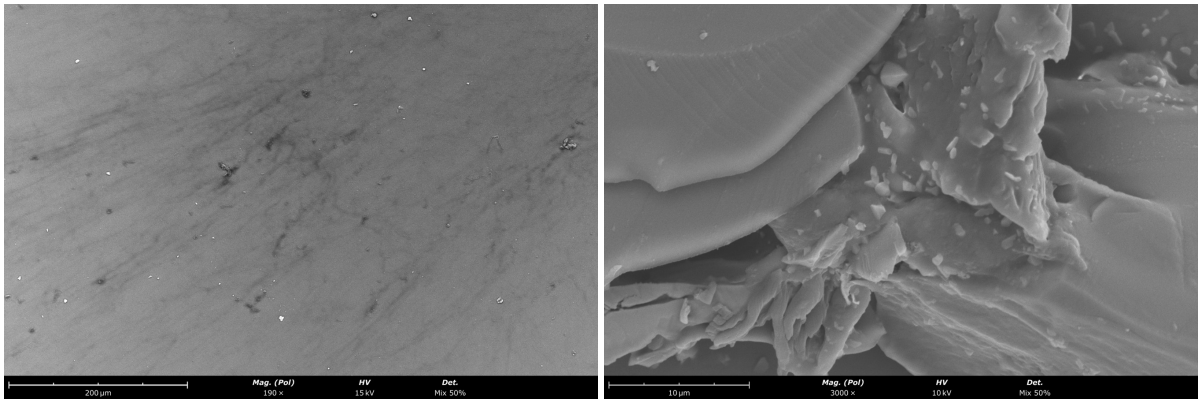

(a) Broad SEM image of ECM. Scale bar 200 µm. **(b)** SEM image of an agglomerate. Scale bar 10 µm.

Figure 4.7: SEM images of decellularized ECM on round cover glasses at different magnifications.

4.1.4 Immunocytochemistry Analysis

Immunofluorescent staining images (figure 4.8) confirm that PDLSCs express collagen I, fibronectin and laminin before decellularization. After decellularization, cell-derived ECM maintained the expression of these three common ECM proteins. It can be observed that the ECM possesses a fibrillary structure composed of collagen I, fibronectin and laminin.

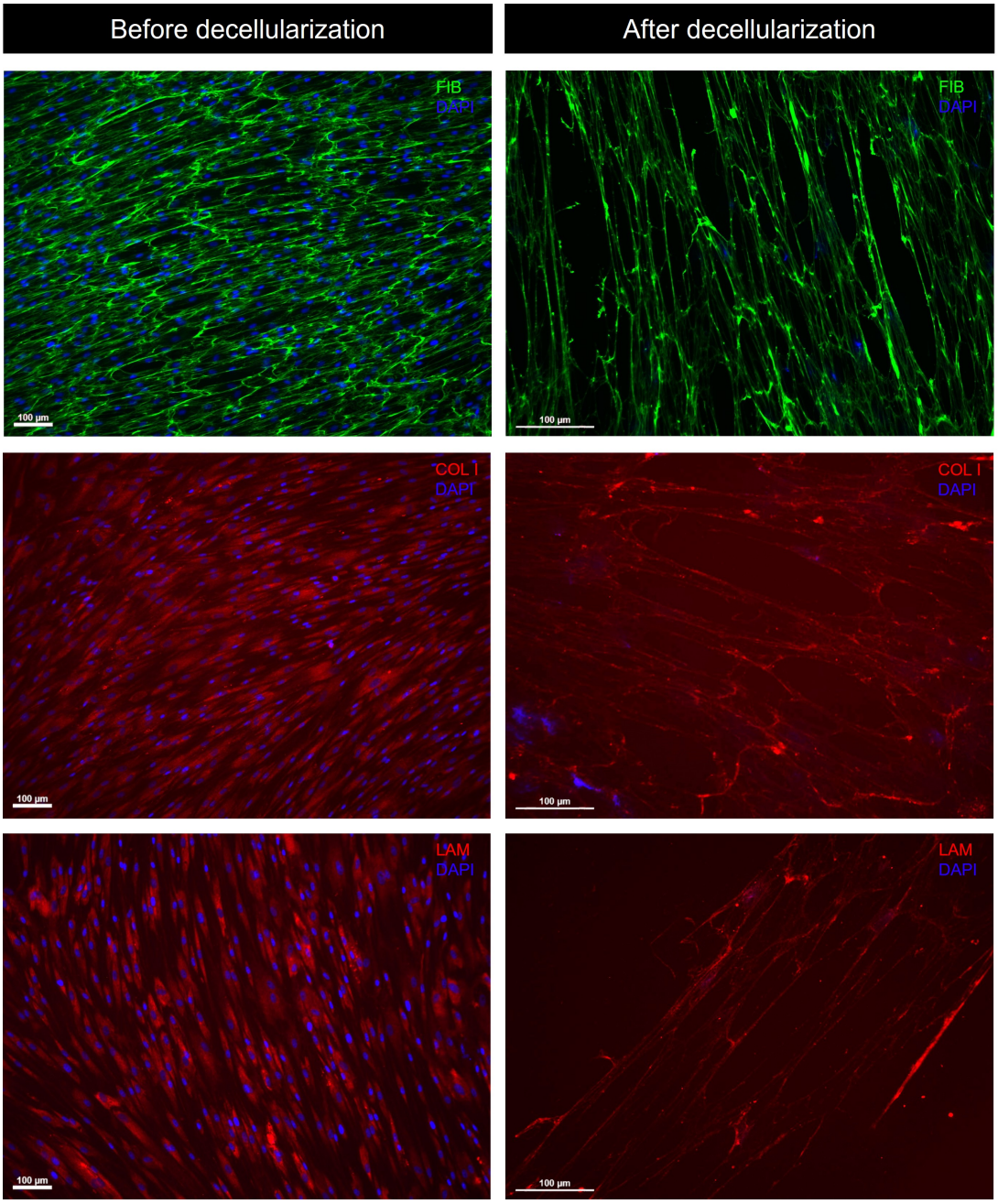

Figure 4.8: Characterization of PDLSCs and ECM by immunocytochemistry analysis. Immunofluorescent staining images before and after decellularization of three main ECM proteins: fibronectin (FIB, green), collagen I (COL I, red) and laminin (LAM, red). Nuclei stained with DAPI (blue). Scale bars 100 µm.

Immunofluorescent staining images (figure 4.9) confirm that PDLSCs express asporin, osteopontin and osteocalcin before decellularization. Asporin is a protein associated with the PDL [106, 107]. Osteopontin and osteocalcin are key osteogenic markers and two non-collagenous proteins present in bone ECM [108]. After decellularization, cell-derived ECM maintained the expression of these three proteins.

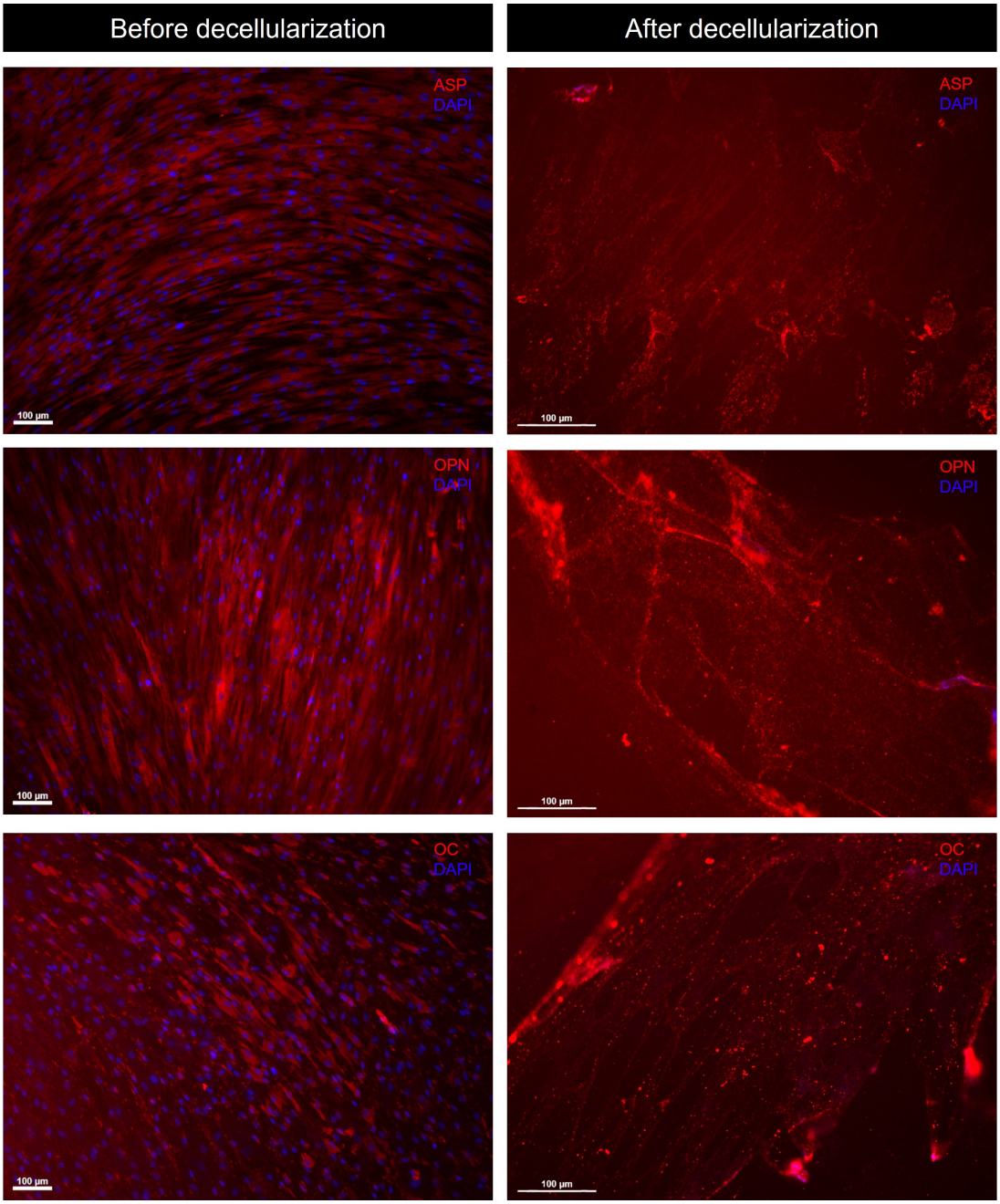

Figure 4.9: Characterization of PDLSCs and ECM by immunocytochemistry analysis. Immunofluorescent staining images before and after decellularization of three proteins expressed in the PDL tissue: asporin (ASP, red), osteopontin (OPN, red) and osteocalcin (OC, red). Nuclei stained with DAPI (blue). Scale bars 100 µm.

4.1.5 DNA/GAG/Collagen Quantification in dECM

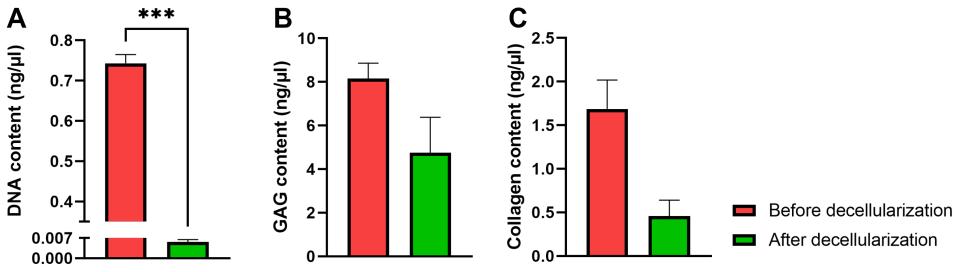

Figure 4.10: Quantified contents of DNA (A), GAGs (B) and collagen (C). Each quantification was performed on three different samples (N=3) for both conditions (before and after decellularization); *** $p < 0.001$.

After decellularization, cell-derived ECM retained to some extent the GAG and collagen content present before decellularization (figure 4.10), similar to what is reported in the literature [105, 109]. On the other hand, DNA content is almost completely diminished, confirming successful decellularization.

4.2 Characterization of Electrospun Scaffolds

4.2.1 Optimization of Electrospun Scaffolds

Initially the preparation of the solutions involved experimenting various solvents. Using the commonly used solvent system FA/AA (70:30 v/v, [71, 80, 82]), the solutions were very viscous, which would difficult the preparation of PCL-CTS blends with accurate proportions and would also hinder the complete dispersion of the ECM within the blend solution. Taking this into account, PCL was dissolved in HFIP, which yields a viscous solution, and CTS in TFA/DCM, which results in a more liquid solution that facilitates the dispersion of ECM. After choosing the solvents, PCL-CTS blends prepared using CTS solution with 5 different CTS concentrations (1%, 2%, 3%, 4%, 5%) were electrospun and the fibrous scaffolds were characterized using scanning electron microscopy, energy dispersive X-Ray analysis and mechanical tensile testing. All the fabricated PCL-CTS electrospun scaffolds were composed of beadless and homogeneous nanofibers. On the other hand, PCL electrospun scaffolds presented a more heterogenous fiber diameter, but were still mainly constituted of beadless fibers in the nanometer range. This is due to the fact that the electrospinning parameters were optimized for PCL-CTS fibers, whose blend solutions are less viscous than PCL only solutions. The average fiber diameter of electrospun PCL fibers was 481 $\pm$ 310 nm, whilst the average of PCL-CTS fibers ranged between 106 and 137 nm. The presence of CTS in the fibers led to a significant decrease in the fiber diameter. The average fiber diameter of each experimental condition can be consulted in table 4.1. Crosslinking performed on PCL-CTS fibers did not alter their diameter. Histograms showing fiber diameter distribution are presented in annex (figure A.1).

Table 4.1: Average fiber diameter of PCL and PCL-CTS electrospun scaffolds, prepared with 1% (PC1), 2% (PC2), 3% (PC3), 4% (PC4) and 5% (PC5) CTS solutions, with (w/) and without (w/o) crosslinking (CL).

Scaffold	PCL	PC1 w/o CL	PC2 w/o CL	PC3 w/o CL	PC4 w/o CL	PC5 w/o CL
MFD (nm)	481 $\pm$ 310	109 $\pm$ 17	110 $\pm$ 21	123 $\pm$ 24	115 $\pm$ 24	137 $\pm$ 24
Scaffold		PC1 w/ CL	PC2 w/ CL	PC3 w/ CL	PC4 w/ CL	PC5 w/ CL
MFD (nm)		106 $\pm$ 17	110 $\pm$ 19	114 $\pm$ 23	118 $\pm$ 20	129 $\pm$ 26

EDX analysis of the 11 experimental conditions showed different carbon and oxygen percentages when comparing PCL fibers to PCL-CTS fibers. However there were no significant differences between the various PCL-CTS scaffolds. The only source of nitrogen present in the scaffolds is chitosan, however EDX analysis was only able to detect it in some scaffolds. This can be a result of the low amount of nitrogen present in the scaffolds, which can be under the detection limit. EDX spectra together with SEM micrographs of the 11 experimental conditions are presented in annex (figure A.2).

Finally, mechanical tensile testing was performed on specimens of the 11 experimental conditions. The PCL-CTS blends were prepared using CTS solutions with up to 5% CTS, taking into account the brittle nature of CTS. PCL-CTS scaffolds with and without crosslinking exhibited decreased elastic modulus, UTS and elongation compared to PCL scaffolds, as can be seen in figure 4.11. This result was expected considering the brittle behaviour of CTS. Furthermore, at first glance of the results in figure 4.11, crosslinking resulted in decreased elastic modulus, decreased UTS and increased elongation compared to the non-crosslinked counterparts. However the differences were not statistically significant.

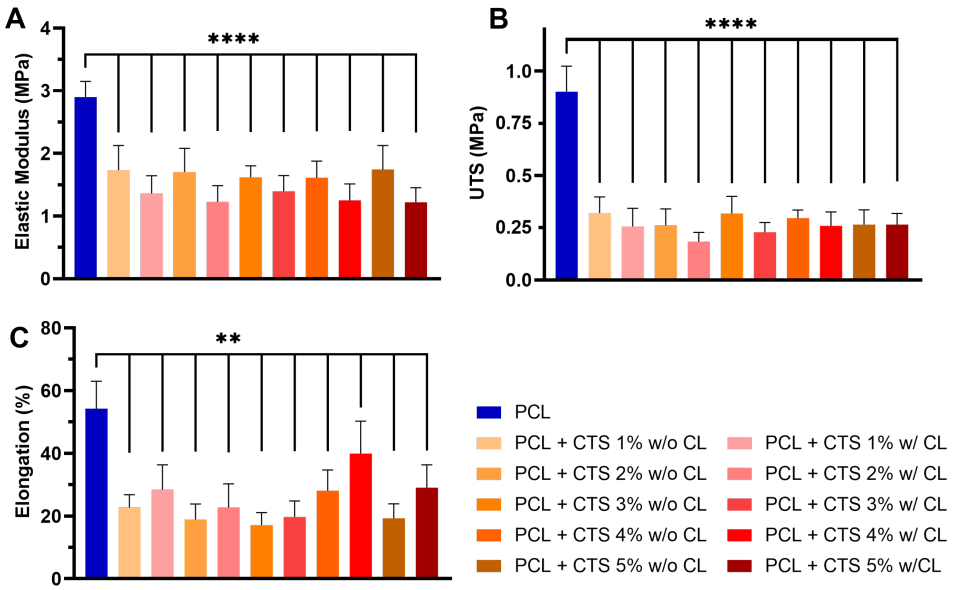

Figure 4.11: Mechanical properties of PCL and PCL-CTS electrospun scaffolds, prepared with 1%, 2%, 3%, 4% and 5% CTS solutions, with (w/) and without (w/o) crosslinking (CL): elastic modulus (A), ultimate tensile strength (UTS) (B), and ultimate elongation (C). Values are expressed as mean $\pm$ SD. For each experimental condition, seven different sample specimens (N=7) were used in the analysis; ** $p < 0.01$, **** $p < 0.0001$.

When analyzing only non-crosslinked or only crosslinked scaffolds, the mechanical properties of PCL-CTS scaffolds with different CTS concentrations were overall similar between them. Statistical tests did not find significant differences between non-crosslinked scaffolds with different CTS concentrations or between crosslinked scaffolds with different CTS concentrations. Representative stress-strain curves of the 11 experimental conditions can be found in annex (figures A.3 and A.4).

Considering that the average fiber diameter did not significantly change with increasing CTS concentration and that the mechanical properties of all PCL-CTS scaffolds were overall similar between them, the CTS concentration of 5% was selected, to maximize the amount of this natural polymer in the scaffolds and potentially to maximize the biological/antimicrobial features of the scaffolds. All PCL-CTS and PCL-CTS-ECM scaffolds characterized in the following sections were prepared with a 5% CTS solution.

4.2.2 Scanning Electron Microscopy and Energy Dispersive X-Ray Analysis

SEM micrographs (figure 4.12) showed that PCL-CTS and PCL-CTS-ECM electrospun scaffolds were composed of beadless and homogeneous nanofibers. However, PCL electrospun scaffolds were more heterogeneous, but were still mainly constituted of beadless fibers in the nanometer range, as previously observed in the initial scaffolds for optimization and selection of CTS concentration. All scaffolds were highly porous and showed high interconnectivity, which is characteristic of electrospun fibers. In PCL-CTS-ECM scaffolds, ECM particles were clearly detected on top of the fibers, as illustrated in figure 4.13.

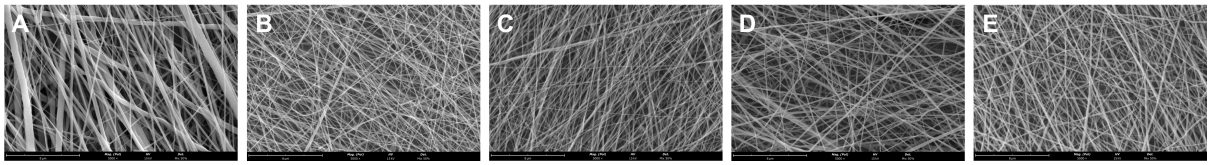

Figure 4.12: SEM images of PCL (A), PCL-CTS (B,C) and PCL-CTS-ECM (D,E) electrospun scaffolds prepared with 5% CTS solution, without (B,D) and with crosslinking (C,E). Scale bar 8 µm.

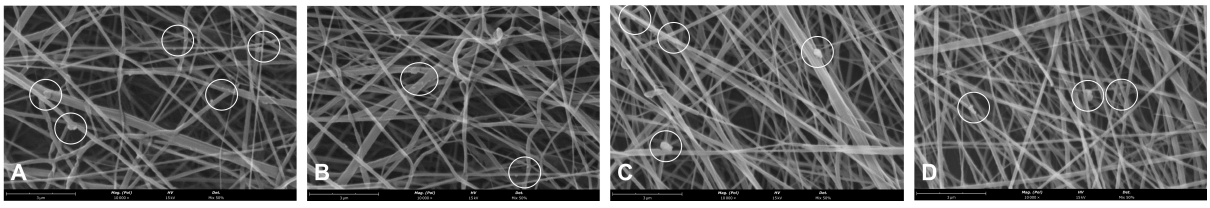

Figure 4.13: SEM images of dECM particles, identified with white circles, on PCL-CTS-ECM fibers with crosslinking (A,B) and without crosslinking (C,D). Scale bar 3 µm.

The average fiber diameter of electrospun PCL fibers was 284 $\pm$ 150 nm, whilst the average fiber diameter of PCL-CTS and PCL-CTS-ECM fibers ranged between 121 and 132 nm. The presence of

CTS in the fibers led to a significant decrease in the fiber diameter. The average fiber diameter of each experimental condition can be consulted in table 4.2. Crosslinking performed on PCL-CTS and PCL-CTS-ECM fibers did not significantly alter their diameter. All PCL-CTS and PCL-CTS-ECM fibers presented similar diameters at the nanoscale, which indicates that the incorporation of decellularized cell-derived ECM did not influence the electrospinning process or alter the average fiber diameter of scaffolds. Histograms showing fiber diameter distribution are presented in annex (figure A.5).

Table 4.2: Average fiber diameters of PCL, PCL-CTS and PCL-CTS-ECM electrospun scaffolds prepared with 5% CTS solution, with (w/) and without (w/o) crosslinking (CL).

Scaffold	PCL	PCL-CTS w/o CL	PCL-CTS w/ CL	PCL-CTS-ECM w/o CL	PCL-CTS-ECM w/ CL
MFD (nm)	284 ± 150	122 ± 21	121 ± 27	132 ± 32	127 ± 25

Elemental composition of electrospun scaffolds was obtained through two types of EDX analysis: a generic analysis (figure 4.14) of a large area covered with several fibers of each sample and a more specific analysis (figure 4.15) of a small area comprised of very few individual fibers of each sample.

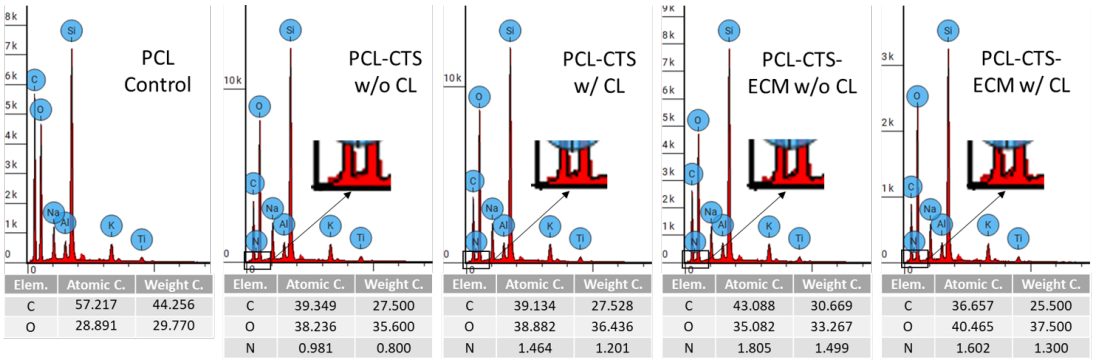

Elem.	Atomic C.	Weight C.
C	57.217	44.256
O	28.891	29.770

Elem.	Atomic C.	Weight C.
C	39.349	27.500
O	38.236	35.600
N	0.981	0.800

Elem.	Atomic C.	Weight C.
C	39.134	27.528
O	38.882	36.436
N	1.464	1.201

Elem.	Atomic C.	Weight C.
C	43.088	30.669
O	35.082	33.267
N	1.805	1.499

Elem.	Atomic C.	Weight C.
C	36.657	25.500
O	40.465	37.500
N	1.602	1.300

Figure 4.14: EDX spectra, atomic and weight percentages of carbon (C), oxygen (O) and nitrogen (N) in PCL, PCL-CTS and PCL-CTS-ECM electrospun scaffolds with (w/) and without (w/o) crosslinking (CL). EDX analysis was performed generically on a large area covered with several fibers of each sample.

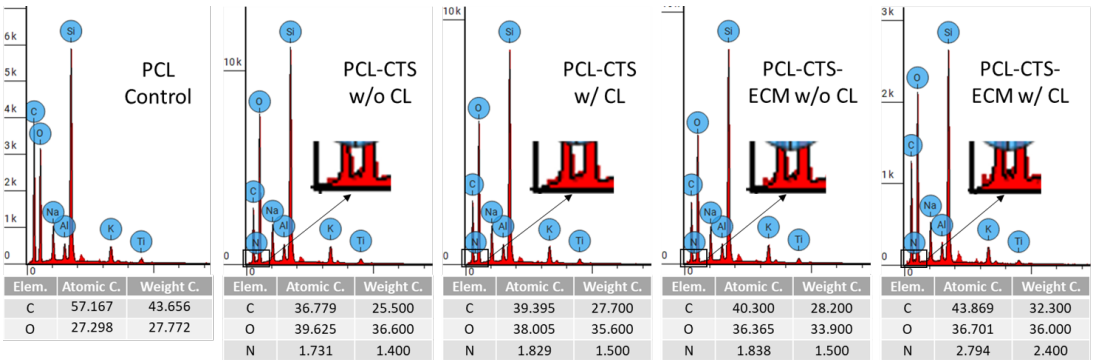

Elem.	Atomic C.	Weight C.
C	57.167	43.656
O	27.298	27.772

Elem.	Atomic C.	Weight C.
C	36.779	25.500
O	39.625	36.600
N	1.731	1.400

Elem.	Atomic C.	Weight C.
C	39.395	27.700
O	38.005	35.600
N	1.829	1.500

Elem.	Atomic C.	Weight C.
C	40.300	28.200
O	36.365	33.900
N	1.838	1.500

Elem.	Atomic C.	Weight C.
C	43.869	32.300
O	36.701	36.000
N	2.794	2.400

Figure 4.15: EDX spectra, atomic and weight percentages of carbon (C), oxygen (O) and nitrogen (N) in PCL, PCL-CTS and PCL-CTS-ECM scaffolds with (w/) and without (w/o) crosslinking (CL). EDX analysis was performed specifically on a small area comprised of very few individual fibers of each sample.

All the obtained EDX spectra showed visible peaks of carbon and oxygen, which are the main constituents of all electrospun scaffolds. PCL $(C_6H_{10}O_2)_n$ is composed of carbon and oxygen, while CTS ($C_{56}H_{103}N_9O_{39}$) is also composed of nitrogen. Nitrogen was only detected in scaffolds containing CTS, namely all PCL-CTS and PCL-CTS-ECM scaffolds. PCL scaffolds showed higher atomic and weight percentages of carbon and lower percentages of oxygen when comparing with the chitosan containing scaffolds. Carbon and oxygen percentages were similar in PCL-CTS and PCL-CTS-ECM scaffolds. Interestingly, atomic and weight percentages of nitrogen were slightly higher in PCL-CTS-ECM scaffolds, compared to PCL-CTS scaffolds. This difference can be due to the presence of dECM, which is composed of proteins, a known source of nitrogen. In all the obtained EDX spectra, there were silicon and sodium peaks stemming from the glass cover glasses, on top of which the fibers were analyzed. The small aluminum peak can be a consequence of the use of aluminum foil collectors.

4.2.3 Attenuated Total Reflectance Fourier Transform Infrared Spectroscopy

The ATR-FTIR spectra of PCL, PCL-CTS and PCL-CTS-ECM electrospun scaffolds and the used materials (PCL, CTS and ECM) are shown in figure 4.16.

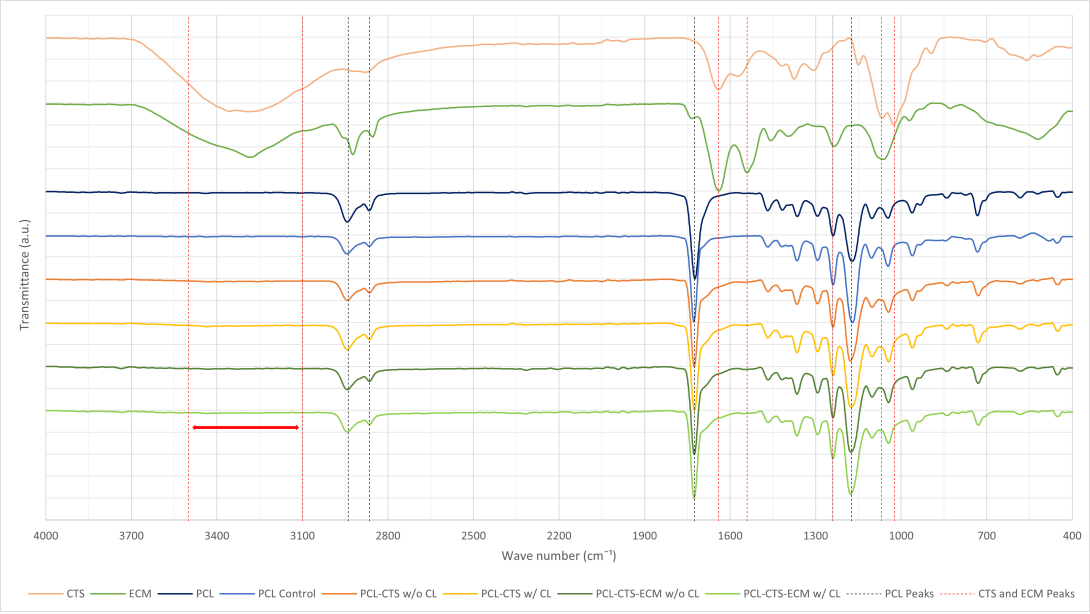

Figure 4.16: FTIR spectra of dECM, PCL and CTS polymers, PCL (PCL Control), PCL-CTS and PCL-CTS-ECM electrospun scaffolds with (w/) and without (w/o) crosslinking (CL).

It can easily be observed that the spectra of all electrospun scaffolds resemble the spectra of the PCL polymer. The spectra of PCL, PCL-CTS and PCL-CTS-ECM electrospun scaffolds showed all the major characteristic peaks of PCL: peaks at 2940 and 2865 cm^{-1} corresponding to asymmetric and symmetric C-H_2 stretching, respectively; the most pronounced peak at 1725 cm^{-1} that corresponds to

ester carbonyl bond stretching; and peaks at 1240 and 1175 cm^{-1} that correspond to asymmetric and symmetric C–O–C stretching, respectively. The FTIR spectra of CTS polymer and of ECM showed bands and peaks in similar regions. In both spectra it is observed a broad band between 3500 and 3100 cm^{-1} associated with O-H and N-H stretching and a peak at 1640 cm^{-1} related to C=O stretching of amide I. ECM spectrum showed peaks at 2925 and 2855 cm^{-1} corresponding to asymmetric and symmetric C-H_2 stretching, respectively, similar to PCL spectra, but slightly shifted. In addition, ECM spectrum showed an evident peak at 1540 cm^{-1} corresponding to N-H deformation of amide II, which was less visible in the CTS spectrum and possibly slightly shifted. In contrast to the PCL spectrum, the peak at 1240 cm^{-1} from the ECM spectrum corresponds to N-H bending of amide III. Finally, CTS spectrum presented peaks at 1070 and 1023 cm^{-1}, whilst ECM spectrum only showed one peak at 1070 cm^{-1}, all corresponding to C-O stretching vibrations. The peaks present in the spectra of the used materials (PCL, CTS and ECM) are displayed in table 4.3 along with the corresponding vibrations.

Table 4.3: FTIR transmittance peaks and bands present in the spectra of PCL and CTS polymers, and ECM, with corresponding functional groups and types of vibration.

Wave number [cm^{-1}]	Type of vibration	Material
3500-3100	O-H and N-H stretching	CTS; ECM
2940	asymmetric C-H_2 stretching	PCL
2925	asymmetric C-H_2 stretching	ECM
2865	symmetric C-H_2 stretching	PCL
2855	symmetric C-H_2 stretching	ECM
1725	C=O stretching (Carbonyl)	PCL
1640	C=O stretching of amide I	CTS; ECM
1540	N-H deformation of amide II	ECM
1240	asymmetric C–O–C stretching	PCL
1240	N-H bending of amide III	ECM
1175	symmetric C–O–C stretching	PCL
1070	C-O stretching	CTS; ECM
1023	C-O stretching	CTS

In an attempt to confirm the presence of CTS in PCL-CTS and PCL-CTS-ECM electrospun scaffolds, the FTIR spectra were closely analyzed (figure 4.17) to identify regions with differences in comparison to the spectrum of the PCL scaffold. The broad band between 3500 and 3100 cm^{-1} resulted in a slight deformation in that region in comparison to the PCL scaffold's spectrum, as can be seen in figure 4.17 A. The peak at 1640 cm^{-1} resulted in the most visible effect on the spectra, with a clear deformation around 1670 cm^{-1} right after the PCL peak at 1725 cm^{-1}, as can be observed in figure 4.17 B. The peak at 1540 cm^{-1} also resulted in a slight deformation in that region of the spectra compared to the flat line visible in the same region of the PCL scaffold's spectrum, as seen in figure 4.17 B. Furthermore, the peaks at 1070 and 1023 resulted in decreased transmittance values and slight deformations in comparison to the PCL scaffold's spectrum, as illustrated in figure 4.17 C. Since the ECM spectrum presented peaks and bands in the same regions as CTS, or peaks in similar regions as PCL, it was not possible to see

differences in the spectra resulting from ECM incorporation. It is also important to note that a low amount of ECM was present in the PCL-CTS-ECM scaffolds compared to the amounts of PCL and CTS.

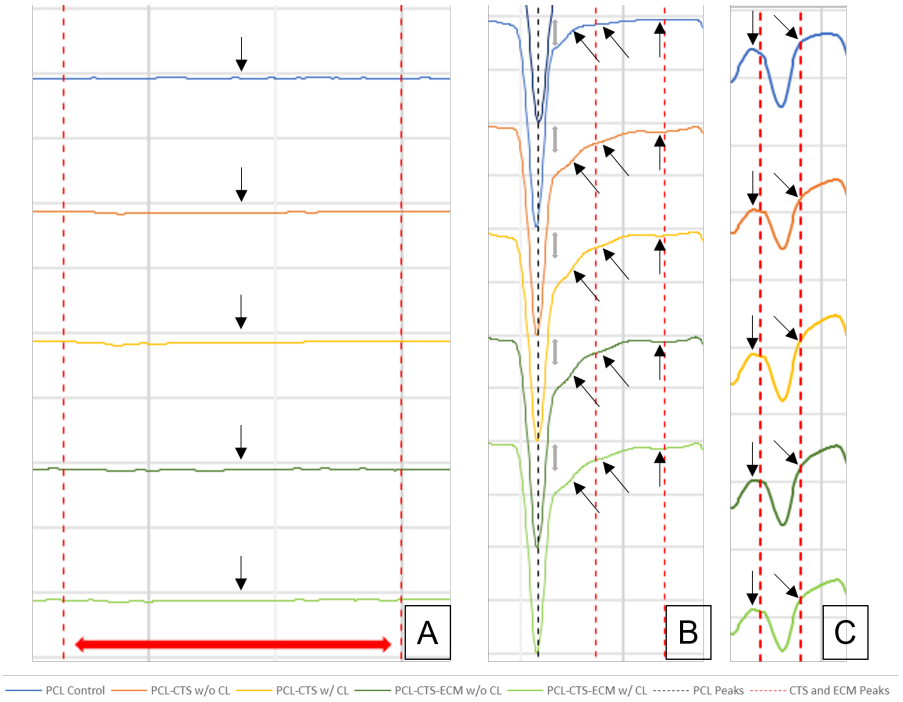

Figure 4.17: Enlarged images from the FTIR spectra of PCL (PCL Control), PCL-CTS and PCL-CTS-ECM electrospun scaffolds with (w/) and without (w/o) crosslinking (CL), on regions with CTS and ECM peaks or bands: band between 3500 and 3100 cm^{-1} (A); peaks at 1640 and 1540 cm^{-1} after the PCL peak at 1725 cm^{-1} (B); peaks at 1070 and 1023 cm^{-1} (C). Black arrows point to zones with visible differences.

4.2.4 Thermal Properties

DSC thermograms of the electrospun scaffolds and the pristine polymers are shown in figure 4.18.

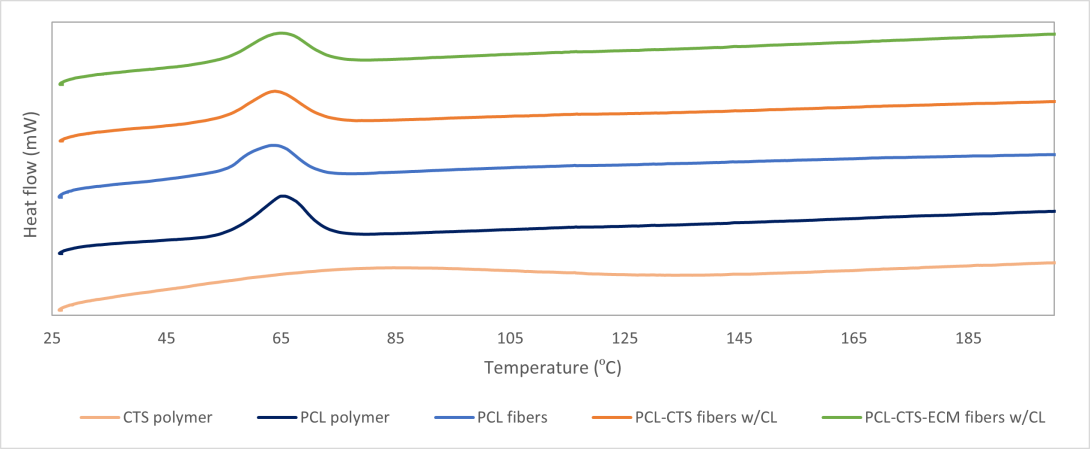

Figure 4.18: DSC heating thermograms of PCL and CTS polymers, PCL, PCL-CTS and PCL-CTS-ECM electrospun scaffolds with (w/) crosslinking (CL).

PCL, PCL-CTS and PCL-CTS-ECM electrospun scaffolds showed characteristic endothermic (melting) transformation points at 64.84 $\pm$ 1.13 ℃, 64.29 $\pm$ 0.29 ℃ and 64.44 $\pm$ 0.50 ℃, respectively. The melting temperatures (T_m) were similar to the one from the PCL polymer, 65.42 $\pm$ 0.50 ℃ (figure 4.18). CTS exhibited a melting temperature of 84.54 $\pm$ 1.31 ℃.

TGA thermograms of the PCL, PCL-CTS and PCL-CTS-ECM electrospun scaffolds and the used polymers are shown in figure 4.19. The first derivative of the mass loss curves (DTGA) was computed and plotted (figure 4.20). The PCL electrospun scaffold had a degradation temperature (T_d) of 391 ℃, which was lower than the value obtained for PCL polymer (410 ℃). PCL-CTS and PCL-CTS-ECM scaffolds had degradation temperatures of 406 ℃ and 408 ℃, respectively. Interestingly, these values were higher than the PCL scaffold and the difference was statistically significant (one way ANOVA, * $p < 0.05$). CTS showed two degradation steps: a slight degradation at the beginning of the analysis, as can be easily observed in figure 4.20, and a clear degradation at 298 ℃. The percentage of weight loss was also determined for the electrospun scaffolds and the polymers. The presence of dECM has no significant effect on the thermal properties of the scaffolds. The thermal properties of the PCL, PCL-CTS and PCL-CTS-ECM electrospun scaffolds and the used polymers are displayed in table 4.4.

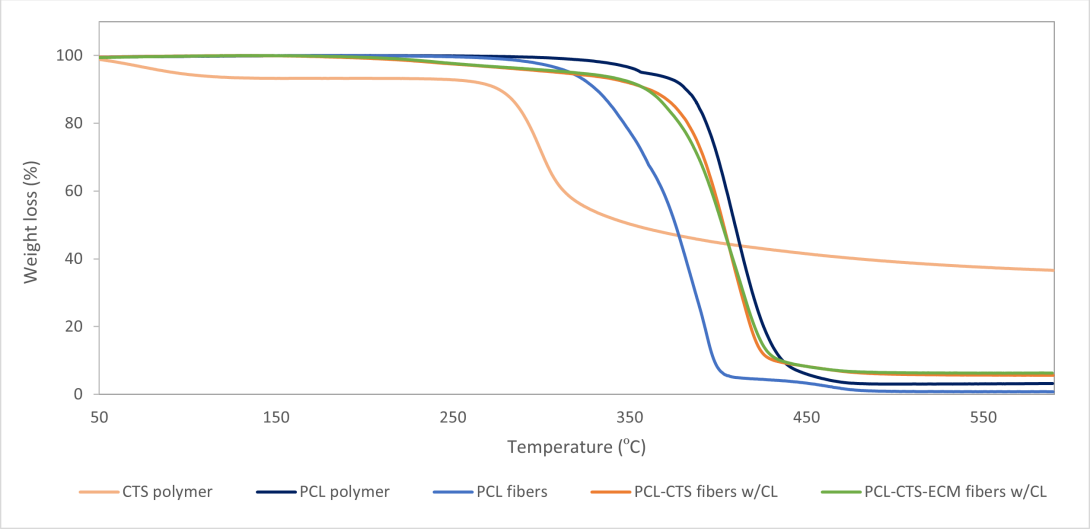

Figure 4.19: Mass loss curves (TGA) of PCL and CTS polymers, PCL, PCL-CTS and PCL-CTS-ECM electrospun scaffolds with (w/) crosslinking (CL).

Table 4.4: Thermal properties of PCL and CTS polymers, PCL, PCL-CTS and PCL-CTS-ECM scaffolds. Values are expressed as mean $\pm$ SD. For each condition, three different samples were used (N=3).

	PCL polymer	CTS polymer	PCL fibers	PCL-CTS fibers w/ CL	PCL-CTS-ECM fibers w/ CL
T_m (℃)	65.42 $\pm$ 0.50	84.54 $\pm$ 1.31	64.84 $\pm$ 1.13	64.29 $\pm$ 0.29	64.44 $\pm$ 0.50
Weight loss (%)	96.70 $\pm$ 0.65	61.53 $\pm$ 0.77	99.83 $\pm$ 0.24	95.92 $\pm$ 2.89	93.69 $\pm$ 0.45
T_d (℃)	410.27 $\pm$ 0.33	298.30 $\pm$ 0.22	390.88 $\pm$ 5.20	406.48 $\pm$ 2.52	408.10 $\pm$ 0.93

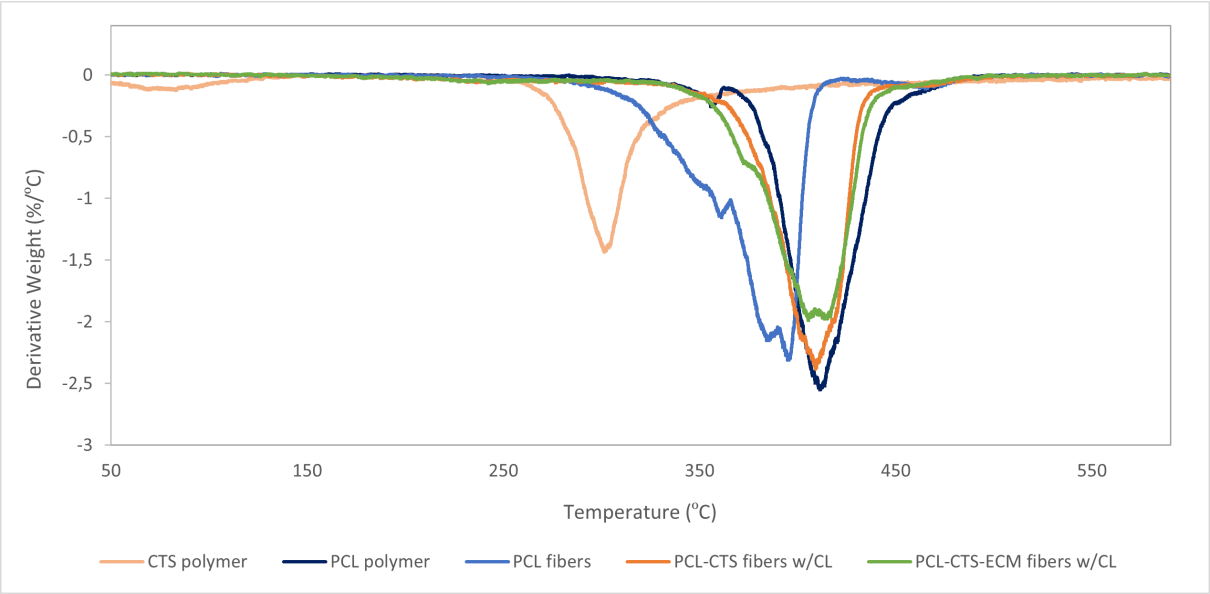

Figure 4.20: First derivative of the mass loss curves (DTGA) from PCL and CTS polymers, PCL, PCL-CTS and PCL-CTS-ECM electrospun scaffolds with (w/) crosslinking (CL).

4.2.5 Contact Angle

Contact angle measurement was used to assess the hydrophobicity or hydrophilicity of the electrospun scaffolds. PCL scaffolds were hydrophobic, since they presented an average contact angle of 109 ± 4°. PCL-CTS and PCL-CTS-ECM scaffolds without crosslinking presented average contact angle values of 69 ± 4°and 65 ± 11°, respectively, whilst with crosslinking the values were 47 ± 2°and 44 ± 3°, respectively. The average contact angle values of the electrospun scaffolds are displayed in table 4.5. In PCL-CTS and PCL-CTS-ECM scaffolds, it was observed that the droplet continued to spread after its placement on the scaffolds, resulting in a decreasing contact angle across time (figure 4.21 A). In contrast, PCL presented the same contact angle value across time. The addition of CTS to the scaffolds resulted in a statistically significant decrease of the contact angle in comparison to the PCL scaffold (figure 4.21 B). Interestingly, crosslinked scaffolds showed lower contact angle values than non-crosslinked scaffolds. This increased hydrophilicity of crosslinked scaffolds was also statistically significant (figure 4.21 B). Images taken upon droplet placement on the scaffolds illustrate the difference between the hydrophobic PCL scaffold and the hydrophilic CTS-containing scaffolds (figure 4.21 C-G).

Table 4.5: Contact angle (CA) values, registered at droplet placement, of PCL, PCL-CTS and PCL-CTS-ECM electrospun scaffolds with (w/) and without (w/o) crosslinking (CL). Values are expressed as mean ± SD. For each condition, three different samples were used (N=3).

Scaffold	PCL	PCL-CTS w/o CL	PCL-CTS w/ CL	PCL-CTS-ECM w/o CL	PCL-CTS-ECM w/ CL
CA (°)	109.2 ± 4.1	68.93 ± 4.31	46.87 ± 1.63	64.9 ± 10.81	43.80 ± 2.71

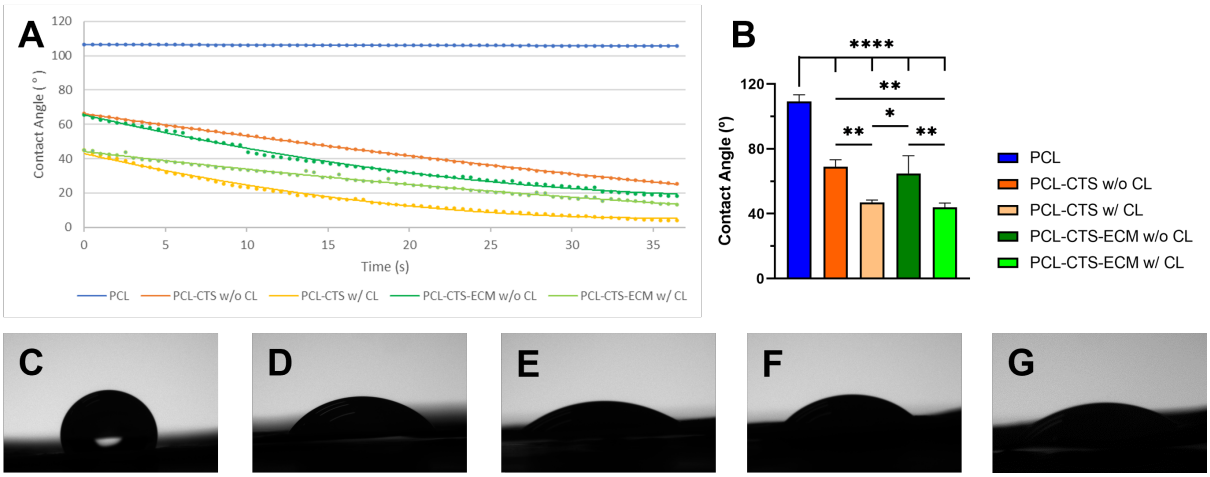

Figure 4.21: Contact angle results of PCL, PCL-CTS and PCL-CTS-ECM electrospun scaffolds with (w/) and without (w/o) crosslinking (CL). (A) Contact angle measurements across time after droplet placement on electrospun scaffolds. (B) Contact angle mean values. Three different samples (N=3) were used in the analysis; * $p < 0.05$, ** $p < 0.01$, **** $p < 0.0001$. Images at droplet placement on PCL (C), PCL-CTS w/o CL (D), PCL-CTS w/ CL (E), PCL-CTS-ECM w/o CL (F) and PCL-CTS-ECM w/ CL (G) scaffolds.

4.2.6 Mechanical Tensile Testing

Results of mechanical tensile testing showed that PCL-CTS and PCL-CTS-ECM scaffolds with and without crosslinking exhibited decreased elastic modulus, UTS and elongation compared to PCL scaffolds, as can be seen in figure 4.22. This trend was also observed in the testing of the initial optimization scaffolds and it is due to the brittle behaviour of CTS. Crosslinking seems to result in decreased UTS and increased elongation compared to the non-crosslinked counterparts. However, only the increased elongation of PCL-CTS scaffolds with crosslinking was statistically significant in comparison to PCL-CTS without crosslinking. The incorporation of ECM did not greatly affect the mechanical properties of the electrospun scaffolds, as can be observed in figure 4.22.

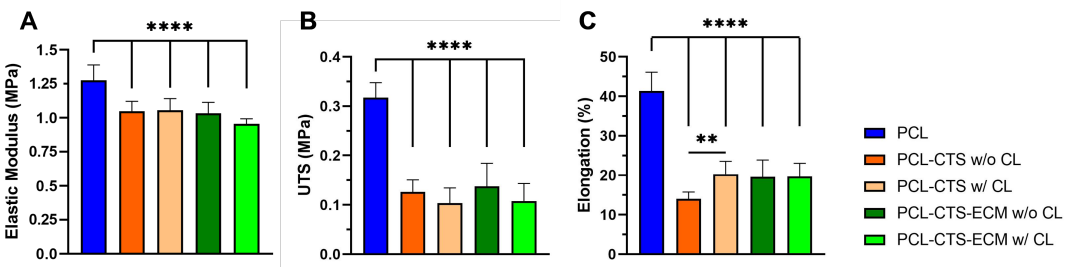

Figure 4.22: Mechanical properties of PCL, PCL-CTS and PCL-CTS-ECM electrospun scaffolds with (w/) and without (w/o) crosslinking (CL) obtained after mechanical tensile testing: elastic modulus (A), ultimate tensile strength (UTS) (B), and ultimate elongation (C). Values are expressed as mean ± SD. Ten different samples (N=10) were used in the analysis; ** $p < 0.01$, **** $p < 0.0001$.

4.3 *In Vitro* Cell Culture on Electrospun Scaffolds

4.3.1 PDLSC Proliferation on Scaffolds

The average number of viable PDLSCs per scaffold on days 1, 7, 14 and 21 is represented in figure 4.23A. On days 1 and 7, PCL scaffolds showed higher numbers of cells compared to PCL-CTS and PCL-CTS-ECM scaffolds. However, it is important to note that PCL-CTS and PCL-CTS-ECM scaffolds showed a higher fold increase in the number of cells at day 7 (figure 4.23B) and at day 21 (figure 4.23C), compared to PCL scaffolds. On days 14 and 21, PCL-CTS and PCL-CTS-ECM scaffolds showed higher number of cells than PCL scaffolds. On days 7, 14 and 21 days, there was a statistically significant increase in cell numbers on PCL-CTS-ECM scaffolds in comparison to PCL-CTS scaffolds. Moreover, PCL-CTS-ECM scaffolds showed significantly higher fold increases, which suggests an enhanced PDLSC proliferation due to the presence of ECM in the nanofibers.

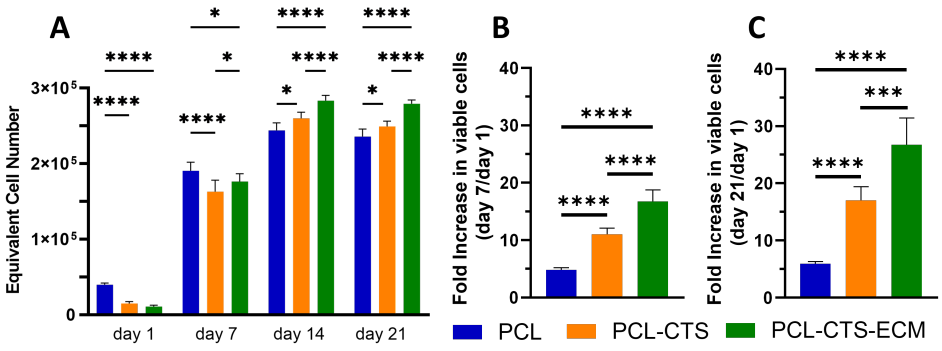

Figure 4.23: PDLSC proliferation assay (A) and fold increase in viable cells at day 7 (B) and day 21 (C) compared to day 1 on PCL, PCL-CTS and PCL-CTS-ECM electrospun scaffolds. For each condition, six different samples (N=6) were used in the analysis; * $p < 0.05$, *** $p < 0.001$, **** $p < 0.0001$.

4.3.2 Immunocytochemistry Analysis and Cell Morphology

The morphology of PDLSCs on electrospun scaffolds after 21 days of culture is shown in figure 4.24.

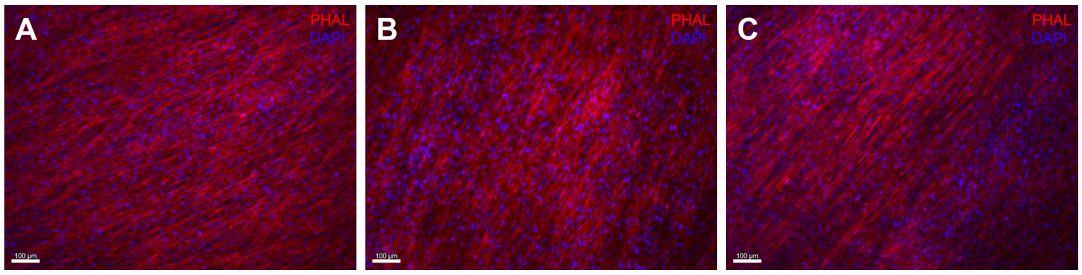

Figure 4.24: Cell morphology assessment by DAPI-Phalloidin staining on PCL (A), PCL-CTS (B) and PCL-CTS-ECM (C) electrospun scaffolds. The cytoskeleton actin filaments were stained with phalloidin (PHAL, red) and nuclei stained with DAPI (blue). Scale bar 100 µm.

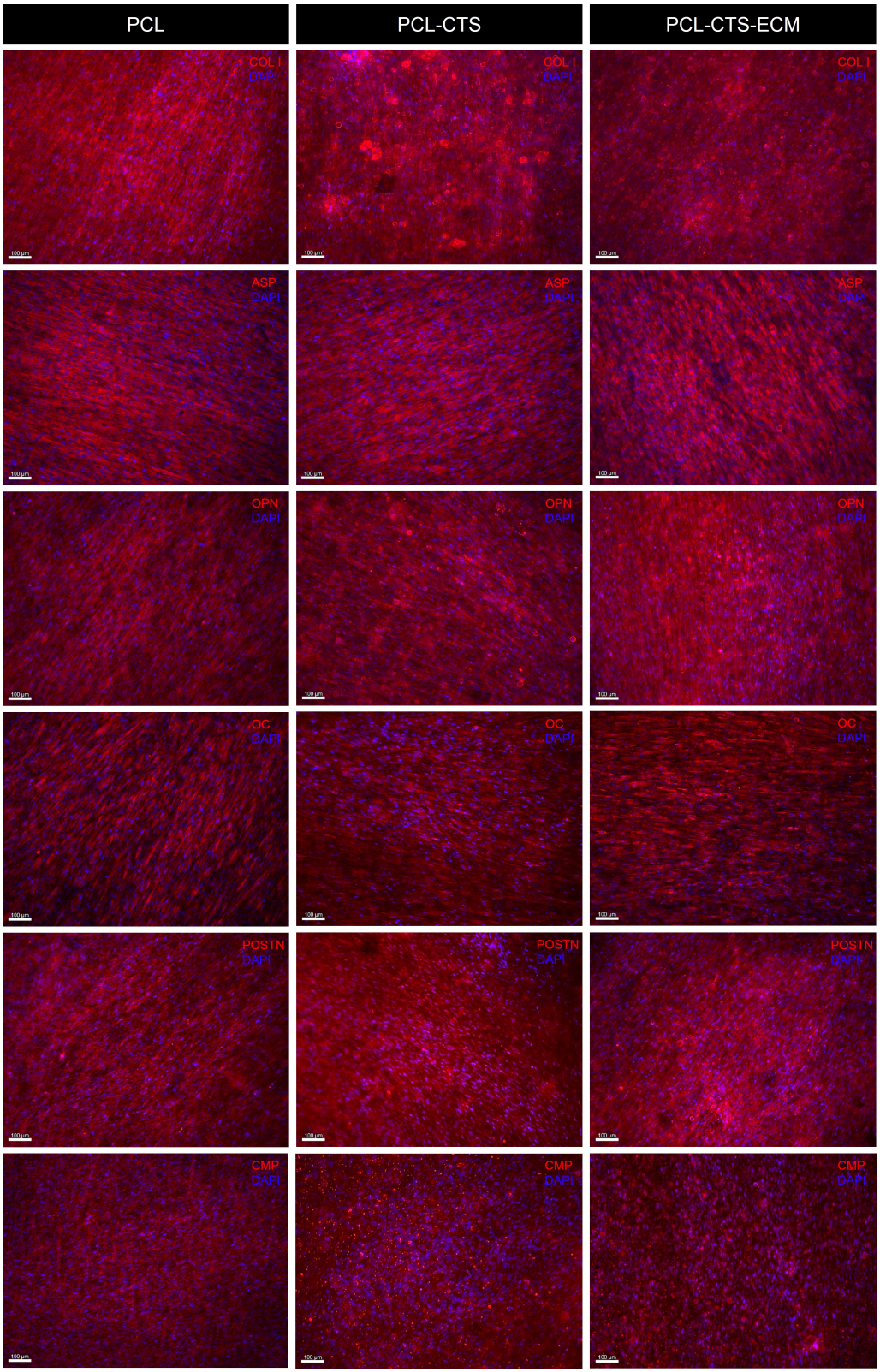

Figure 4.25: Characterization of PDLSCs on PCL, PCL-CTS and PCL-CTS-ECM electrospun scaffolds by immunocytochemistry analysis. Immunofluorescent staining images of collagen I (COL I, red), asporin (ASP, red), osteopontin (OPN, red), osteocalcin (OC, red), periostin (POSTN, red) and cementum protein (CMP, red). Nuclei were counterstained with DAPI (blue). Scale bar 100 µm.

After 21 days of osteogenic differentiation, PDLSCs seeded on all electrospun scaffolds presented similar morphology, as seen in figure 4.24. PDLSCs densely populated and seemed similarly distributed across on all electrospun scaffolds. The expression of various proteins by PDLSCs on PCL, PCL-CTS and PCL-CTS-ECM electrospun scaffolds after 21 days of osteogenic differentiation is illustrated in figure 4.25. Overall, PDLSCs seeded on all electrospun scaffolds showed a positive expression of collagen I, asporin, osteopontin, osteocalcin, periostin and cementum protein. PDLSCs showed a more visible expression of POSTN than CMP1. No significant differences with regards to the immunofluorescent staining images were observed between the different types of scaffolds.

4.3.3 ALP Activity Assay

After 21 days of osteogenic differentiation, PDLSCs cultured on PCL-CTS-ECM scaffolds presented statistically significant higher ALP activity values compared to PCL and PCL-CTS scaffolds, as can be observed in figure 4.26.

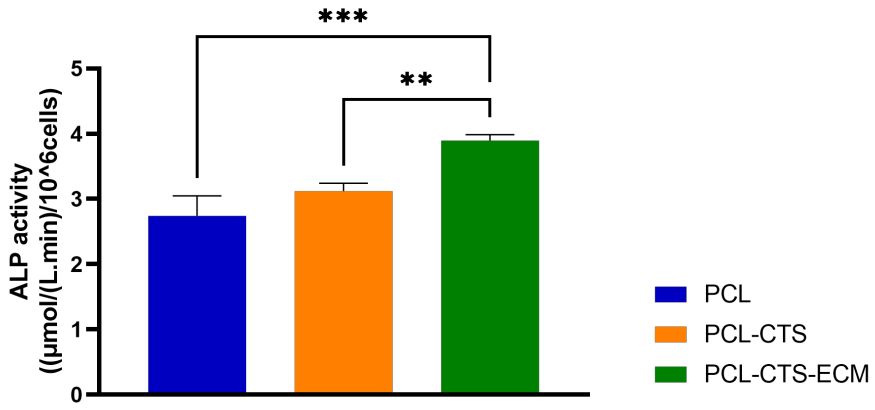

Figure 4.26: ALP activity normalized to the number of cells present on PCL, PCL-CTS and PCL-CTS-ECM electrospun scaffolds. Values are expressed as mean ± SD. For each experimental group, three different samples (N=3) were used in the analysis; ** $p < 0.01$, *** $p < 0.001$.

4.3.4 ALP/Von Kossa Stainings

ALP stainings demonstrated ALP activity of PDLSCs more evidently on PCL-CTS and PCL-CTS-ECM scaffolds, with a more reddish tone in comparison to the PCL scaffolds. (figure 4.27 A-C) This observation lays in agreement with the higher ALP activity values on PCL-CTS and PCL-CTS-ECM scaffolds, obtained with the ALP activity quantification assay in the previous section. The presence of mineralized deposits was identified through black precipitates resulting from the Von Kossa staining, which was performed after the ALP staining. PCL-CTS and PCL-CTS-ECM scaffolds showed more abundant presence of black mineralized deposits than PCL scaffolds, as can be observed in figure 4.27 D-F.

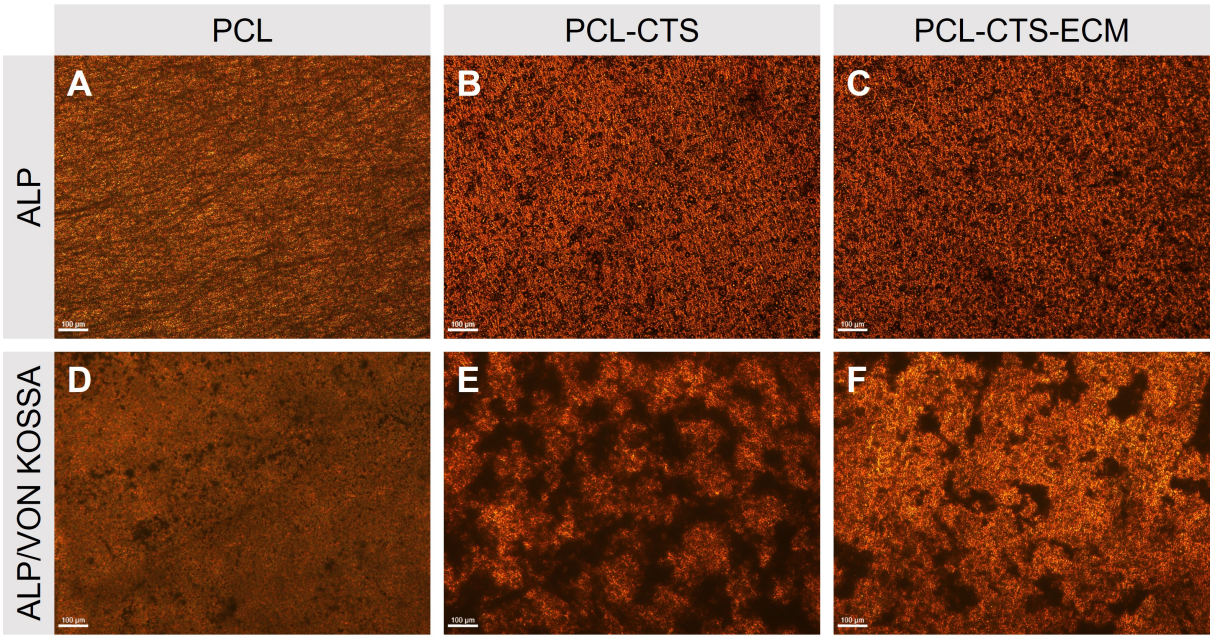

Figure 4.27: ALP and ALP/Von Kossa staining images of differentiated PDLSCs on PCL (A and D), PCL-CTS (B and E) and PCL-CTS-ECM (C and F) scaffolds. Scale bar 100 µm.

4.3.5 Alizarin Red Staining and Quantification

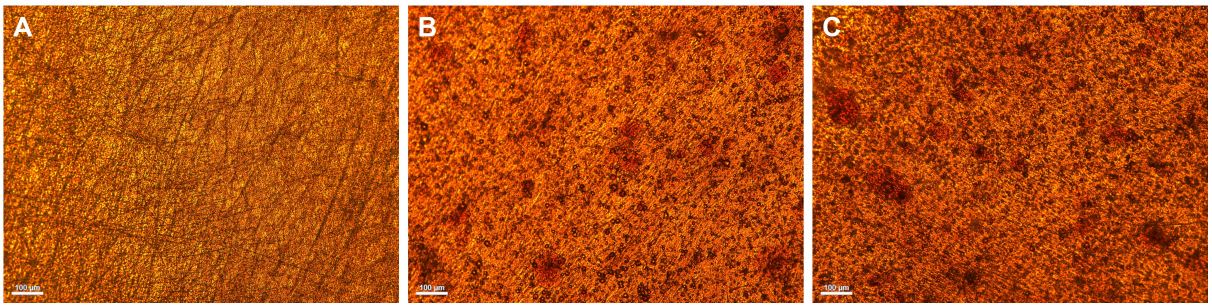

Figure 4.28: Alizarin Red staining of differentiated PDLSCs on PCL (A), PCL-CTS (B) and PCL-CTS-ECM (C) scaffolds. Alizarin Red allows the visualization of calcium deposits in red. Scale bars 100 µm.

Alizarin Red staining confirmed calcium deposition (in red) on PCL, PCL-CTS and PCL-CTS-ECM electrospun scaffolds (figure 4.28). On PCL-CTS and PCL-CTS-ECM scaffolds large calcium deposits were clearly visible, which were not present on PCL scaffolds. Alizarin Red quantification confirmed an increase in calcium deposition on PCL-CTS and PCL-CTS-ECM in comparison to PCL scaffolds. (figure 4.29) There was a small difference between PCL-CTS and PCL-CTS-ECM scaffolds.

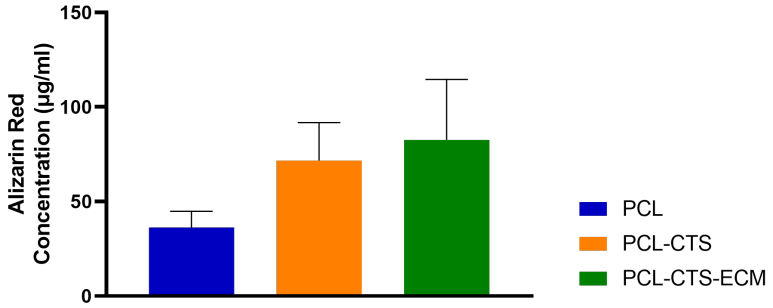

Figure 4.29: Quantification of Alizarin Red staining bound to PCL, PCL-CTS and PCL-CTS-ECM scaffolds. Values are expressed as mean ± SD. Three different samples (N=3) were used in the analysis.

4.3.6 Biomineralization Assay

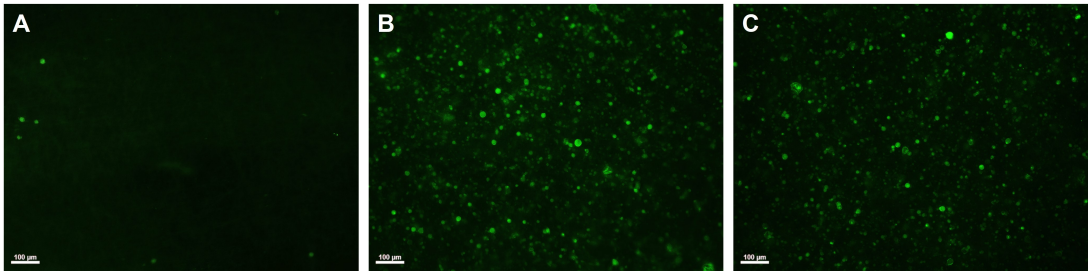

Figure 4.30: Fluorescent staining of cell mineralization on PCL (A), PCL-CTS (B) and PCL-CTS-ECM (C) scaffolds. Hydroxyapatite portion of bone-like nodules deposited by cells stained in green. Scale bar 100 µm.

Fluorescent staining images confirm higher cell mineralization on PCL-CTS and PCL-CTS-ECM scaffolds, showing more intense fluorescence in comparison to PCL scaffolds, as can be observed in figure 4.30. The quantification of the fluorescent staining confirmed higher levels of cell mineralization on PCL-CTS and PCL-CTS-ECM scaffolds in comparison to PCL scaffolds. (figure 4.31) There was an increase in fluorescence in PCL-CTS-ECM scaffolds in comparison to PCL-CTS scaffolds (figure 4.31).

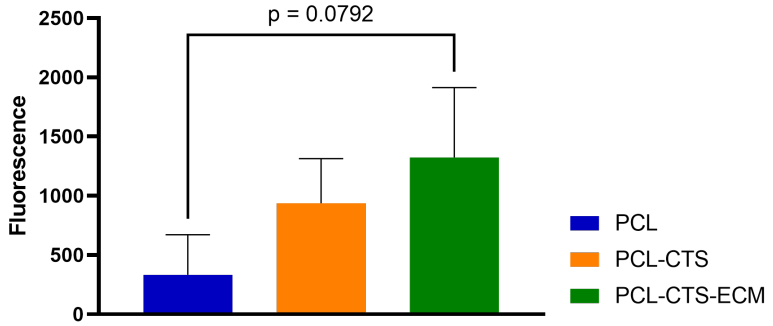

Figure 4.31: Quantification of cell mineralization on PCL, PCL-CTS and PCL-CTS-ECM electrospun scaffolds. Values are expressed as mean ± SD. Three different samples (N=3) were used in the analysis.

4.3.7 Scanning Electron Microscopy and Energy Dispersive X-Ray Analysis

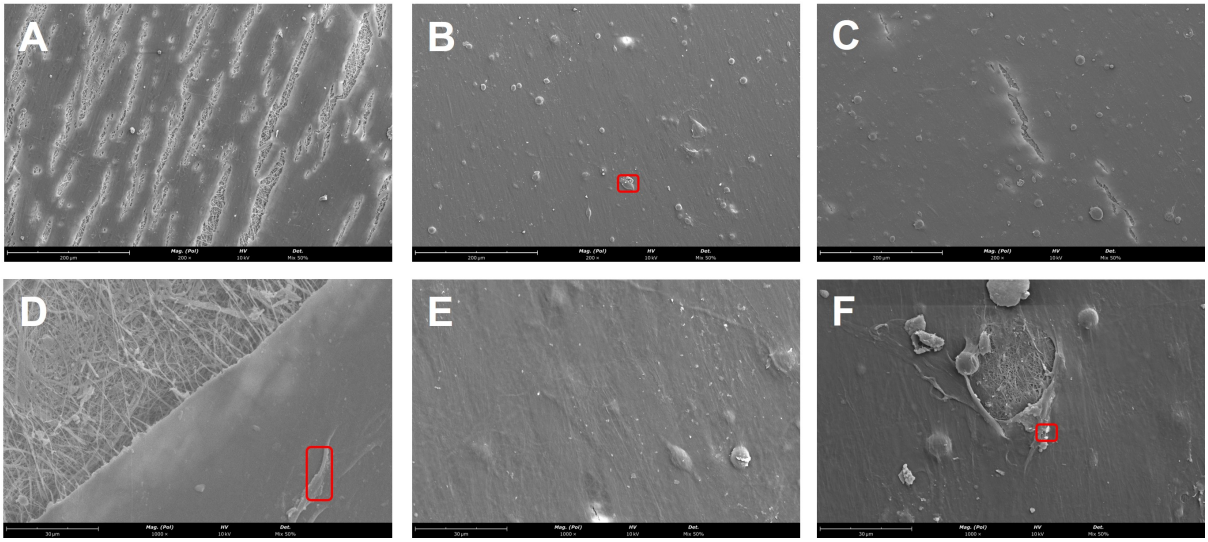

Figure 4.32: SEM images of PDLSCs on PCL (A,D), PCL-CTS (B,E) and PCL-CTS-ECM (C,F) electrospun scaffolds, after osteogenic differentiation. Spots where EDX analysis was performed outlined in red. Scale bars 200 µm (A,B,C) and 30 µm (D,E,F).

As can be observed in figure 4.32, after 21 days of osteogenic differentiation, PDLSCs are densely covering the surface of all electrospun scaffolds, which is illustrated by dark grey stains on top of the fibers. In some regions of the images, the fibers can be seen underneath the seeded cells.

EDX analysis was performed on certain spots of the electrospun scaffolds that presented deposit-like dots, to ascertain if these were calcium deposits resulting from cell mineralization. The results of the EDX analysis on the spots outlined red observed in figure 4.32 are displayed in table 4.6. The obtained EDX spectra are presented in annex (figure A.6). The detection of calcium and phosphorous confirms the presence of mineralization after 21 days of PDLSCs osteogenic differentiation.

Table 4.6: Atomic (AC) and weight (WC) concentrations of carbon (C), oxygen (O), nitrogen (N), phosphorus (P) and calcium (Ca) obtained through EDX analysis on the spots are outlined red in fig. 4.32 of PCL, PCL-CTS and PCL-CTS-ECM electrospun scaffolds after 21 days of osteogenic differentiation.

	C (%)		O (%)		N (%)		P (%)		Ca (%)	
Scaffold	AC	WC	AC	WC	AC	WC	AC	WC	AC	WC
PCL	46.402	40.260	23.249	26.873	28.723	29.071	0.670	1.499	0.414	1.199
PCL-CTS	53.288	42.700	20.890	22.300	23.215	21.700	0.484	1.000	0.860	2.300
PCL-CTS-ECM	45.557	30.631	25.368	22.723	16.336	12.813	2.020	3.504	4.550	10.210

4.3.8 Gene expression analysis

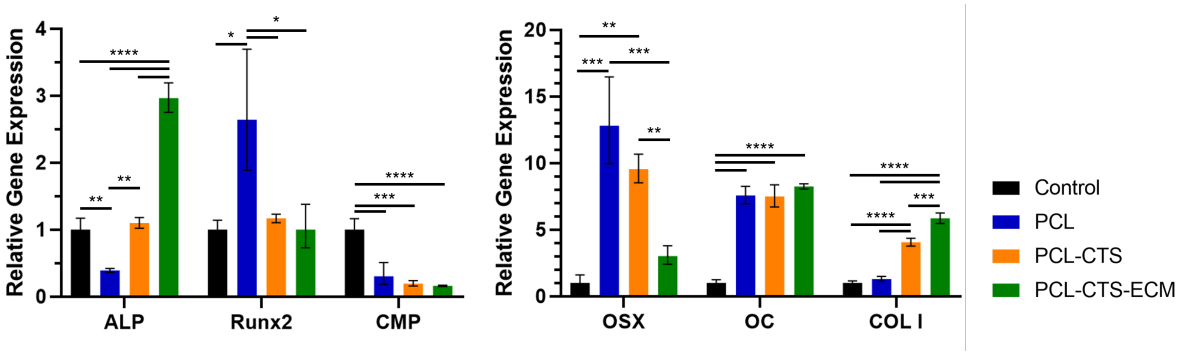

Figure 4.33: Effects of electrospun scaffolds on ALP, RUNX2, CMP1, OSX, OC and Col I gene expression by PDLSCs after 21 days of osteogenic differentiation. Results normalized to the GAPDH gene and presented as fold change expression relative to undifferentiated PDLSCs at day 0 (Control). Values are expressed as mean ± SD (N=3). * $p < 0.05$, ** $p < 0.01$, *** $p < 0.001$, **** $p < 0.0001$.

Results obtained from gene expression analysis are represented in figure 4.33. Different osteogenic marker genes were analyzed (ALP, RUNX2, OSX, OC and COLI), as well as CMP1, which is frequently expressed in periodontal tissues. In agreement with the results obtained in ALP activity assay, ALP gene expression was higher in PCL-CTS-ECM scaffolds than PCL-CTS and PCL scaffolds. Compared to the control (undifferentiated PDLSCs at day 0), PCL-CTS-ECM scaffolds significantly upregulated, PCL-CTS scaffolds sustained and PCL scaffolds notably downregulated ALP gene expression. RUNX2 and OSX are key transcription factors for osteogenic differentiation. PCL scaffolds showed a significant upregulation in RUNX2 and OSX expression compared to the control. In PCL-CTS and PCL-CTS-ECM scaffolds RUNX2 expression was sustained in relation to the control and OSX was increased, more significantly in PCL-CTS scaffolds than in PCL-CTS-ECM ones. Interestingly, all scaffolds very similarly showed downregulated expression of CMP1 and upregulated OC expression (no statistically significant differences in gene expression between different scaffolds). Furthermore, the expression of collagen I was significantly upregulated in PCL-CTS and PCL-CTS-ECM scaffolds, whilst in PCL scaffolds it was maintained in relation to the control. PCL-CTS-ECM scaffolds showed significantly increased upregulation in comparison to PCL-CTS scaffolds.

5

Discussion

Contents

5.1 PDLSCs and Decellularized cell-derived ECM

PDLSCs were characterized using various techniques. PDLSCs were successfully differentiated towards the adipogenic, chondrogenic and osteogenic lineages. This multilineage differentiation capacity is one of the criteria of MSC identification [14]. The multilineage differentiation was confirmed with appropriate stainings and the results are shown in figure 4.1. These results are in agreement with previous PDLSC characterization studies reported in the literature [21, 110–112]. The immunophenotype of PDLSCs was analysed using flow cytometry. PDLSCs showed positive expression of MSC-related surface markers, namely CD73, CD90, and CD105 [14, 110, 111]. The CD106 marker was negatively expressed in PDLSCs, whilst it has been shown to be expressed in MSCs [113]. Similar to MSCs, PDLSCs did not express hematopoietic stem cell surface markers CD34 and CD45 [14, 110, 111]. CD146 is an endothelial surface marker, also known as melanoma cell adhesion molecule (MCAM), and was positively expressed by PDLSCs, as it was already reported in the literature [21, 106, 114].

PDLSCs and decellularized PDLSC-derived ECM were characterized with regards to morphology and expression of certain proteins. PDLSCs presented a fibroblast-like morphology similar to MSCs, whilst ECM showed a fibrillary structure, similar to other cell-derived ECMs in the literature [31, 101, 105]. Regarding immunocytochemistry analysis, PDLSCs that were expanded and not differentiated (DMEM + 10% FBS + 1% A/A) expressed collagen I, fibronectin, laminin, asporin, osteopontin and osteocalcin. The expression of these proteins was sustained after the decellularization process, which is in accordance with previous studies [102, 103]. Type I collagen and fibronectin are two of the predominant proteins present in the native periodontal ligament tissue [5]. Collagen I, fibronectin and laminin are three main ECM proteins present in cell-derived ECM from various sources (e.g. MSC- and HUVEC-derived ECM) [31, 33]. Therefore, the expression of these three main ECM proteins by PDLSCs and PDLSC derived ECM was expected and lays in agreement with the literature [31, 101, 105]. Asporin is an ECM protein, also known as periodontal ligament-associated protein 1 (PLAP1) and is predominantly expressed in the PDL, thus its positive expression by PDLSCs is understandable [106, 107]. Interestingly, PDLSCs expressed proteins typically present in bone. Osteocalcin and osteopontin are present in the cementum and the alveolar bone [5]. Both proteins are osteogenic markers and showed positive expression by PDLSCs, even though they were not cultured under osteogenic differentiation conditions. The positive expression demonstrated the intrinsic osteogenic potential of PDLSCs, which *in vivo* serve as a source for renewable progenitor cells, which differentiate into osteoblasts.

Furthermore, the effect of decellularization on DNA, GAGs and collagen content was assessed. The DNA content was almost completely diminished. Decellularization resulted in the removal of over 95% of the DNA, which confirms the success of the decellularization process. The results are in agreement with the existing literature [103, 109]. GAG and collagen content was retained after decellularization, which shows that the decellularization process does not greatly affect the ECM and its components.

This retention has been reported in the literature not only for GAGs and collagen [103, 105, 109], but also for growth factors [103].

5.2 Electrospun nanofibrous scaffolds

Electrospun scaffolds were composed of nanofibers, thus mimicking in scale the fibers of the PDL [1]. PCL scaffolds had an average fiber diameter of 284 nm, whilst PCL-CTS and PCL-CTS-ECM had average fiber diameters ranging between 121 and 132 nm. The presence of CTS in the fibers led to a significant decrease in the fiber diameter, as it has been previously reported in the literature [77, 80, 83, 90, 91]. Crosslinking performed on PCL-CTS fibers did not alter their diameter, since this process was performed after electrospinning and glutaraldehyde only bonds with free amino groups of CTS that is present in the formed fibers. The incorporation of decellularized cell-derived ECM was confirmed with SEM images and did not influence the electrospinning process or alter the average fiber diameter of scaffolds, which is in accordance with previous studies [65]. Nitrogen content detected by EDX analysis confirmed the presence of CTS in PCL-CTS and PCL-CTS-ECM. Nitrogen content was slightly higher in PCL-CTS-ECM scaffolds, compared to PCL-CTS scaffolds. This difference can be due to the presence of dECM, which is composed of proteins, a known source of nitrogen.

ATR-FTIR spectra of all electrospun scaffolds resembled the spectra of the PCL polymer, confirming PCL presence in the scaffolds. The spectra of PCL, PCL-CTS and PCL-CTS-ECM electrospun scaffolds showed all the major characteristic peaks of PCL, which have been extensively reported in the literature [76–78, 80, 83]. The presence of CTS in PCL-CTS and PCL-CTS-ECM scaffolds was suggested through deformations of certain regions in comparison to the PCL scaffold spectra. The broad band between 3500 and 3100 cm^{-1} resulted in a slight deformation in that region of the spectra and the peak at 1640 cm^{-1} resulted in a clear deformation, in the form of a shoulder, around 1670 cm^{-1}. These effects due to CTS presence in the scaffolds have been reported in the literature [78, 80, 81, 83, 91, 99]. The spectra of lyophilized PDLSC-derived ECM showed some similarities with other spectras from ECM derived from other sources [33, 65]. The presence of ECM in PCL-CTS-ECM could not be confirmed with ATR-FTIR analysis due to the overlap of the ECM's peaks and bands with those from CTS and PCL. It is also important to note that a low amount of ECM was present in the PCL-CTS-ECM scaffolds compared to the large amounts of PCL and CTS, therefore no visible differences resulting from the ECM incorporation could be observed, as reported in a previous study from our group [65]

Electrospun scaffolds showed characteristic endothermic transformation points at temperatures identical to the PCL polymer, which lays in agreement with the existing literature [77, 83, 91]. PCL fibers had a degradation temperature, which was lower than the value obtained for PCL polymer. This result has been reported in the literature and may be due to the effect of the solvent used for electrospinning [77, 83]. Interestingly, PCL-CTS and PCL-CTS-ECM scaffolds showed higher degradation temperatures than the

PCL scaffold, which contrast the existing literature. The addition of CTS has been shown to result in a decrease of the degradation temperature in comparison to PCL scaffolds [81,83]. The presence of ECM has no significant effect on the thermal properties of the scaffolds, which is in accordance with previous studies from our group [65].

Contact angle measurements demonstrated that PCL scaffolds were hydrophobic, due to the high contact angle value, similar to what is reported in the literature [76,83,91]. The addition of CTS resulted in a decrease of the contact angle, thus enhancing the hydrophilicity of the scaffolds which might be favorable for cell adhesion and proliferation. The contact angle values of PCL-CTS and PCL-CTS-ECM were similar to those found in the literature [76, 91]. The incorporation of ECM did not affect the hydrophilicity of the electrospun scaffolds. Interestingly, crosslinked scaffolds showed lower contact angle values than non-crosslinked scaffolds, opposite to what Zhu *et al.* observed after performing glutaraldehyde crosslinking on PCL-CTS scaffolds [76].

Taking into account that pure CTS fibers have poor mechanical properties, rapid degradation and tend to absorb moisture [70], mechanical tensile testing revealed decreased mechanical properties of PCL-CTS and PCL-CTS-ECM scaffolds in comparison to PCL scaffolds, as reported in the literature [76,77,80]. It has been shown when increasing the amount of CS, nanofibers tend to become more brittle [80]. Nevertheless, PCL-CTS and PCL-CTS-ECM scaffolds showed elastic modulus of around 1 MPa, comparable to the modulus of the PDL that ranges between 0.607 and 4.274 MPa under loads between 1 and 5 N [7]. Crosslinking with glutaraldehyde results in the formation of stable imine bonds between the aldehydic groups of the glutaraldehyde with free amino groups of CTS, possibly interconnecting different CTS polymer chains, thus improving the stability of the CTS containing electrospun fibers [69,70]. More restrained movements of the CTS polymer molecules due to crosslinking, can possibly explain the early break of the fibrous scaffold with a decreased ultimate strength, which has been previously reported in PCL-CTS fibers [76] and pure CTS fibers [115]. The incorporation of dECM did not greatly affect the mechanical properties of the PCL-CTS electrospun scaffolds, as it has been previously reported [65].

5.3 Osteogenic differentiation on electrospun scaffolds

PDLSCs cultured on scaffolds initially adhered more to PCL scaffolds compared to PCL-CTS and PCL-CTS-ECM scaffolds. However, during the 21 days of culture PDLSCs proliferated more on PCL-CTS and PCL-CTS-ECM scaffolds, in comparison to PCL scaffolds, as confirmed by higher fold increases in the number of viable cells. PCL-CTS scaffolds have been reported to show increased cell viability compared to PCL scaffolds [68, 83, 91, 116]. PCL-CTS-ECM scaffolds showed increased cell viability compared to the other scaffolds. Enhanced cell proliferation and viability due to the presence of ECM in the scaffold has been previously reported in the literature [65, 117–119].

Expanded and undifferentiated PDLSCs already expressed collagen I, asporin, osteopontin and os-

teocalcin. After 21 days of osteogenic differentiation, PDLSCs cultured on scaffolds showed positive expression of collagen I, asporin, osteopontin, osteocalcin, periostin and cementum protein. Periostin is a matricellular protein expressed in collagen-rich fibrous connective tissues that are subjected to constant mechanical strains such as the PDL [120]. This protein plays a role in osteoblast differentiation and survival, therefore positive expression of periostin was expected to be observed in PDLSCs cultured under osteogenic differentiation conditions. Cementum protein is a cementum component, whose presence seems limited to cementoblasts and their progenitors [121]. PDLSCs showed a more visible expression of periostin than cementum protein, probably due to osteoblast commitment of PDLSCs after osteogenic differentiation. Reduced expression of CMP1 has been reported when PDLSCs were differentiated to osteoblasts *in vitro* [121]. The positive expression of osteopontin, osteocalcin and periostin confirm successful osteogenic differentiation of PDLSCs on all electrospun scaffolds.

ALP activity is a byproduct of osteoblast activity. After 21 days of osteogenic differentiation, PDLSCs cultured on PCL-CTS-ECM scaffolds showed higher ALP activity values compared to PCL and PCL-CTS scaffolds. An increase in ALP activity has been reported in the literature in scaffolds with ECM incorporated [65, 117–119]. There was also an increase in ALP activity in PCL-CTS scaffolds compared to PCL scaffolds, which has been also previously shown in the literature [68].

Alizarin Red staining and its quantification confirmed increased calcium deposition on PCL-CTS and PCL-CTS-ECM in comparison to PCL scaffolds, which lays in agreement with the literature [68, 117]. A more abundant presence of calcium phosphate deposits was observed on PCL-CTS and PCL-CTS-ECM in comparison to PCL scaffolds, through the visualization of black precipitates resulting from the Von Kossa staining. The presence of calcium and phosphorous after 21 days of PDLSCs osteogenic differentiation on electrospun scaffolds was further confirmed through elemental analysis with EDX.

Cell mineralization, specifically the hydroxyapatite portion of bone-like nodules deposited by cells, was visualized and quantified after 21 days of osteogenic differentiation. PCL-CTS and PCL-CTS-ECM scaffolds showed higher levels of cell mineralization in comparison to PCL scaffolds.

Gene expression analysis confirmed the results obtained in the ALP activity assay and ALP staining. Undifferentiated PDLSCs already show ALP activity, as it was assessed in the multilineage differentiation assay. ALP activity seemed to decrease after osteogenic differentiation of PDLSCs on tissue culture plates. Interestingly, qRT-PCR analyses showed a decreased ALP gene expression by PDLSCs after 21 days of osteogenic differentiation on PCL scaffolds in comparison to the control (undifferentiated PDLSCs at day 0). In contrast, ALP expression was sustained in PCL-CTS scaffolds and significantly upregulated in PCL-CTS-ECM scaffolds. All scaffolds showed upregulated expression of RUNX2 and OSX, which are essential genes involved in osteogenic differentiation. Although, PCL scaffolds showed increased upregulation of RUNX2 and OSX expression, the associated standard error was elevated. All electrospun scaffolds similarly upregulated OC, which lays in agreement with the immunofluorescent

staining. All scaffolds also very similarly presented downregulated expression of CMP1, in accordance to what was visualized in the immunofluorescent stainings. The reduced expression of CMP1 is associated with the commitment of PDLSCs to osteoblasts instead of cementoblasts, resulting from the *in vitro* osteogenic differentiation [121]. Undifferentiated PDLSCs, therefore show an increased expression of CMP1 and capacity to differentiate into cementoblasts in comparison to PDLSCs that underwent osteogenic differentiation on electrospun scaffolds. The expression of collagen I was significantly upregulated in PCL-CTS and even more in PCL-CTS-ECM scaffolds, whilst in PCL scaffolds it was only maintained. The upregulated expression of RUNX2, OSX and OC, in addition to the positive expression of osteopontin, osteocalcin and periostin visualized with immunofluorescence, confirmed successful osteogenic differentiation of PDLSCs on all electrospun scaffolds. Nevertheless, PCL-CTS-ECM scaffolds stand out for the 3-fold increase in ALP and 5-fold increase in COL I expression, in combination with the multiple results showing increased mineralization compared with the other scaffolds.

Both CTS and ECM have osteogenic properties and the effects are visible when comparing ALP activity, calcium deposition and cell mineralization against pure PCL scaffolds. The addition of CTS in PCL fibers has been shown to increase calcium deposition, ALP activity, and the expression of osteopontin in murine pre-osteoblast cells compared to pure PCL fibers [116]. The use of PDLSC-derived ECM is associated with enhanced osteogenic differentiation, shown by increased calcium deposition, ALP activity and expression of osteogenic markers (osteocalcin, osteopontin, bone sialoprotein and bone morphogenetic protein 2), as previously reported in the literature [101,104]. Decellularized PDLSC-derived ECM has the advantage of mimicking the specific *in vivo* microenvironment, including its complex bioactivity, and promoting periodontal regeneration without the potentially immunogenic effects of cellular material. Instead of seeding cells on top of electrospun scaffolds, allowing the cells to secrete ECM to decorate the scaffolds and finally decellularizing the constructs, the ECM can be produced in culture plates *in vitro*, collected, lyophilized and stored in a dry storage place. This facilitates and expedites the use of the decellularized ECM which can be easily incorporated upon fabricating the electrospun scaffolds.

By combining PCL, CTS and ECM, electrospun scaffolds were developed with desirable mechanical properties, enhanced bioactivity and superior osteogenic potential. PCL was responsible for providing the mechanical and structural backbone of the electrospun scaffolds. CTS increased the hydrophilicity, enhanced the biological effects and promoted osteogenesis, at the cost of slightly reducing the mechanical properties. PDLSC-derived ECM increased the bioactivity and further promoted osteogenesis, without altering the scaffold's properties. In addition, ECM ensured that the electrospun scaffolds mimicked more closely the composition of native ECM. PCL-CTS-ECM scaffolds were successfully developed with the aim of mimicking the structure, architecture, mechanical properties and composition of native periodontal niche.

6

Conclusions and Future Work

In this work, PDLSCs and PDLSC-derived ECM were characterized and studied. PDLSCs showed multilineage differentiation capacity and positive expression of MSC-related surface markers. PDLSCs possess characteristics similar to MSCs, including a fibroblast-like morphology. This work's findings revealed maintained expression of proteins present in PDLSCs after decellularization process, namely collagen I, fibronectin, laminin, asporin, osteopontin and osteocalcin. ECM showed a fibrillary structure and retained GAG and collagen content present before the decellularization process. Successful decellularization was confirmed with residual DAPI staining in ECM and residual DNA content.

The obtained results demonstrate that PCL-CTS-ECM electrospun scaffolds maintained similar physical and mechanical properties of PCL-CTS scaffolds. The incorporation of ECM did not greatly alter the scaffolds characteristics. The presence of CTS in PCL-CTS and PCL-CTS-ECM electrospun scaffolds resulted in differences in comparison to PCL scaffolds, with regards to fiber diameter, thermal degradation, hydrophilicity and mechanical properties.

Regarding the *in vitro* cell culture, PCL-CTS-ECM electrospun scaffolds significantly promoted cell proliferation compared to PCL and PCL-CTS scaffolds, which results from the presence of ECM. After 21 days of osteogenic differentiation, PDLSCs populated densely and showed a positive expression of COL I, ASP, OPN, OC and POSTN on all electrospun scaffolds. Decreased expression of CMP1 suggests the commitment of PDLSCs to osteoblasts instead of cementoblasts. The positive expression of RUNX2, OSX, OPN, OC and POSTN confirmed successful osteogenic differentiation of PDLSCs on all electrospun scaffolds. PCL-CTS-ECM electrospun scaffolds enhanced osteogenic differentiation of PDLSCs, which was confirmed by increased levels of ALP activity, calcium deposition and cell mineralization. PCL-CTS scaffolds showed higher levels of calcium deposition and cell mineralization than PCL scaffolds. Overall, results show that CTS provided osteogenic properties to the scaffolds and cell-derived ECM further enhanced the proliferation and osteogenic differentiation of PDLSCs.

Electrospun scaffolds with cell-derived ECM were developed with the aim to mimic the structure, architecture and, very importantly, the composition of native ECM. Cell-derived ECM creates a biomimetic microenvironment, that enhances cell proliferation and osteogenic differentiation, which was combined with electrospun scaffolds with the desired properties for periodontal regeneration. This work describes the first use of lyophilized cell-derived ECM loaded electrospun scaffolds for periodontal tissue engineering applications and highlights its potential as a promising therapeutic strategy for periodontitis. For future research, these scaffolds can be part of a biphasic construct that can be inserted into periodontal defect sites and promote regeneration of all tissues. The developed electrospun scaffolds can be used as a novel bioactive GTR membrane or as an interface between root cementum and a bone graft, to tackle their limitation of absent periodontal ligament regeneration. Future studies on the ECM loaded electrospun scaffolds still need to be conducted to assess their antibacterial properties and optimize ECM amounts for improved periodontal tissue differentiation and maturation.

Bibliography

[1] O. M. Goudouri, E. Kontonasaki, and A. R. Boccaccini, *Layered scaffolds for periodontal regeneration*. Elsevier Inc., 8 2017, pp. 279–295.

[2] D. F. Kinane, P. G. Stathopoulou, and P. N. Papapanou, "Periodontal diseases," *Nature Reviews Disease Primers*, vol. 3, 6 2017.

[3] Y. Zhuang, K. Lin, and H. Yu, "Advance of nano-composite electrospun fibers in periodontal regeneration," *Frontiers in Chemistry*, vol. 7, 7 2019.

[4] W. B. Swanson, Y. Yao, and Y. Mishina, "Novel approaches for periodontal tissue engineering," *genesis*, vol. 60, no. 8-9, p. e23499, 2022.

[5] A. Nanci and D. D. Bosshardt, "Structure of periodontal tissues in health and disease," *Periodontology 2000*, vol. 40, pp. 11–28, 2 2006.

[6] T. de Jong, A. D. Bakker, V. Everts, and T. H. Smit, "The intricate anatomy of the periodontal ligament and its development: Lessons for periodontal regeneration," *Journal of Periodontal Research*, vol. 52, pp. 965–974, 12 2017.

[7] B. Wu, Y. Fu, H. Shi, B. Yan, R. Lu, S. Ma, and B. Markert, "Tensile testing of the mechanical behavior of the human periodontal ligament," *BioMedical Engineering Online*, vol. 17, 11 2018.

[8] N. M. A., "Prevalence of periodontal disease, its association with systemic diseases and prevention," *International journal of health sciences*, vol. 11, pp. 72–80, 2017.

[9] P. M. Preshaw, R. A. Seymour, and P. A. Heasman, "Current concepts in periodontal pathogenesis," *Dental Update*, vol. 31, no. 10, pp. 570–578, Dec. 2004.

[10] M. Sanz, F. D'aiuto, J. Deanfield, and F. Fernandez-Avilés, "European workshop in periodontal health and cardiovascular disease - scientific evidence on the association between periodontal and cardiovascular diseases: A review of the literature," *European Heart Journal, Supplement*, vol. 12, 4 2010.

[11] P. Zhao, W. Chen, Z. Feng, Y. Liu, P. Liu, Y. Xie, and D. G. Yu, "Electrospun nanofibers for periodontal treatment: A recent progress," *International Journal of Nanomedicine*, vol. 17, pp. 4137–4162, 2022.

[12] X. Xu, S. Ren, L. Li, Y. Zhou, W. Peng, and Y. Xu, "Biodegradable engineered fiber scaffolds fabricated by electrospinning for periodontal tissue regeneration," *Journal of Biomaterials Applications*, vol. 36, pp. 55–75, 7 2021.

[13] R. Zhao, R. Yang, P. R. Cooper, Z. Khurshid, A. Shavandi, and J. Ratnayake, "Bone grafts and substitutes in dentistry: A review of current trends and developments," *Molecules*, vol. 26, 2021.

[14] M. Dominici, K. Le Blanc, I. Mueller, I. Slaper-Cortenbach, F. Marini, D. Krause, R. Deans, A. Keating, D. Prockop, and E. Horwitz, "Minimal criteria for defining multipotent mesenchymal stromal cells. the international society for cellular therapy position statement," *Cytotherapy*, vol. 8, no. 4, pp. 315–317, 2006.

[15] N. G. Singer and A. I. Caplan, "Mesenchymal stem cells: Mechanisms of inflammation," *Annual Review of Pathology: Mechanisms of Disease*, vol. 6, pp. 457–478, 2 2011.

[16] A. Markov, L. Thangavelu, S. Aravindhan, A. O. Zekiy, M. Jarahian, M. S. Chartrand, Y. Pathak, F. Marofi, S. Shamlou, and A. Hassanzadeh, "Mesenchymal stem/stromal cells as a valuable source for the treatment of immune-mediated disorders," *Stem Cell Research and Therapy*, vol. 12, 12 2021.

[17] X.-Y. Xu, X. Li, J. Wang, X.-T. He, H.-H. Sun, and F.-M. Chen, "Concise Review: Periodontal Tissue Regeneration Using Stem Cells: Strategies and Translational Considerations," *Stem Cells Translational Medicine*, vol. 8, no. 4, pp. 392–403, 12 2018.

[18] W. Y. Zeng, Y. Ning, and X. Huang, "Advanced technologies in periodontal tissue regeneration based on stem cells: Current status and future perspectives," *Journal of Dental Sciences*, vol. 16, pp. 501–507, 1 2021.

[19] M. Takewaki, M. Kajiya, K. Takeda, S. Sasaki, S. Motoike, N. Komatsu, S. Matsuda, K. Ouhara, N. Mizuno, T. Fujita, and H. Kurihara, "Msc/ecm cellular complexes induce periodontal tissue regeneration," *Journal of Dental Research*, vol. 96, no. 9, pp. 984–991, 2017, pMID: 28521114.

[20] T. Zhou, J. Pan, P. Wu, R. Huang, W. Du, Y. Zhou, M. Wan, Y. Fan, X. Xu, X. Zhou, L. Zheng, and X. Zhou, "Dental follicle cells: Roles in development and beyond," *Stem Cells International*, vol. 2019, 2019.

[21] B. M. Seo, M. Miura, S. Gronthos, P. M. Bartold, S. Batouli, J. Brahim, M. Young, P. G. Robey, C. Y. Wang, and S. Shi, "Investigation of multipotent postnatal stem cells from human periodontal ligament," *Lancet*, vol. 364, pp. 149–155, 7 2004.

[22] J. Qiu, X. Wang, H. Zhou, C. Zhang, Y. Wang, J. Huang, M. Liu, P. Yang, and A. Song, "Enhancement of periodontal tissue regeneration by conditioned media from gingiva-derived or periodontal ligament-derived mesenchymal stem cells: A comparative study in rats," *Stem Cell Research and Therapy*, vol. 11, 2 2020.

[23] M. G. Flores, R. Yashiro, K. Washio, M. Yamato, T. Okano, and I. Ishikawa, "Periodontal ligament cell sheet promotes periodontal regeneration in athymic rats," *Journal of Clinical Periodontology*, vol. 35, pp. 1066–1072, 12 2008.

[24] Y. Liu, Y. Zheng, G. Ding, D. Fang, C. Zhang, P. M. Bartold, S. Gronthos, S. Shi, and S. Wang, "Periodontal ligament stem cell-mediated treatment for periodontitis in miniature swine," *Stem Cells*, vol. 26, pp. 1065–1073, 4 2008.

[25] J. Hu, Y. Cao, Y. Xie, H. Wang, Z. Fan, J. Wang, C. Zhang, J. Wang, C. T. Wu, and S. Wang, "Periodontal regeneration in swine after cell injection and cell sheet transplantation of human dental pulp stem cells following good manufacturing practice," *Stem Cell Research and Therapy*, vol. 7, 9 2016.

[26] J. K. Mouw, G. Ou, and V. M. Weaver, "Extracellular matrix assembly: A multiscale deconstruction," *Nature Reviews Molecular Cell Biology*, vol. 15, pp. 771–785, 12 2014.

[27] K. C. Clause and T. H. Barker, "Extracellular matrix signaling in morphogenesis and repair," *Current Opinion in Biotechnology*, vol. 24, no. 5, pp. 830–833, 2013, tissue, cell and engineering.

[28] M. Assunção, D. Dehghan-Baniani, C. H. K. Yiu, T. Später, S. Beyer, and A. Blocki, "Cell-derived extracellular matrix for tissue engineering and regenerative medicine," *Frontiers in Bioengineering and Biotechnology*, vol. 8, 2020.

[29] Y. Guan, B. Yang, W. Xu, D. Li, S. Wang, Z. Ren, J. Zhang, T. Zhang, X. Liu, J. Li, C. Li, F. Meng, F. Han, T. Wu, Y. Wang, and J. Peng, "Cell-derived extracellular matrix materials for tissue engineering," *Tissue Engineering Part B: Reviews*, vol. 28, no. 5, pp. 1007–1021, 2022.

[30] H. Xing, H. Lee, L. Luo, and T. R. Kyriakides, "Extracellular matrix-derived biomaterials in engineering cell function," *Biotechnology Advances*, vol. 42, p. 107421, 2020.

[31] M. S. Carvalho, J. C. Silva, J. M. Cabral, C. L. da Silva, and D. Vashishth, "Cultured cell-derived extracellular matrices to enhance the osteogenic differentiation and angiogenic properties of hu-

man mesenchymal stem/stromal cells," *Journal of Tissue Engineering and Regenerative Medicine*, vol. 13, pp. 1544–1558, 9 2019.

[32] Y. Yang, H. Lin, H. Shen, B. Wang, G. Lei, and R. S. Tuan, "Mesenchymal stem cell-derived extracellular matrix enhances chondrogenic phenotype of and cartilage formation by encapsulated chondrocytes in vitro and in vivo," *Acta Biomaterialia*, vol. 69, pp. 71–82, 3 2018.

[33] Y. Kang, S. Kim, J. Bishop, A. Khademhosseini, and Y. Yang, "The osteogenic differentiation of human bone marrow mscs on huvec-derived ecm and β-tcp scaffold," *Biomaterials*, vol. 33, pp. 6998–7007, 10 2012.

[34] S. B. Qasim, S. Najeeb, R. M. Delaine-Smith, A. Rawlinson, and I. U. Rehman, "Potential of electrospun chitosan fibers as a surface layer in functionally graded gtr membrane for periodontal regeneration," *Dental Materials*, vol. 33, pp. 71–83, 1 2017.

[35] I. N. Safi, A. M. Al-Shammari, M. A. Ul-Jabbar, and B. M. Hussein, "Preparing polycaprolactone scaffolds using electrospinning technique for construction of artificial periodontal ligament tissue," *Journal of Taibah University Medical Sciences*, vol. 15, pp. 363–373, 10 2020.

[36] M. N. Sundaram, S. Sowmya, S. Deepthi, J. D. Bumgardener, and R. Jayakumar, "Bilayered construct for simultaneous regeneration of alveolar bone and periodontal ligament," *Journal of Biomedical Materials Research - Part B Applied Biomaterials*, vol. 104, pp. 761–770, 5 2016.

[37] L. R. W. Lam, K. Schilling, S. Romas, R. Misra, Z. Zhou, J. G. Caton, and X. Zhang, "Electrospun core-shell nanofibers with encapsulated enamel matrix derivative for guided periodontal tissue regeneration," *Dental Materials Journal*, vol. 40, pp. 1208–1216, 2021.

[38] Z. Ye, W. Xu, R. Shen, and Y. Yan, "Emulsion electrospun pla/calcium alginate nanofibers for periodontal tissue engineering," *Journal of Biomaterials Applications*, vol. 34, pp. 763–777, 1 2020.

[39] S. Ren, Y. Yao, H. Zhang, R. Fan, Y. Yu, J. Yang, R. Zhang, C. Liu, W. Sun, and L. Miao, "Aligned fibers fabricated by near-field electrospinning influence the orientation and differentiation of hpdlscs for periodontal regeneration," *Journal of Biomedical Nanotechnology*, vol. 13, pp. 1725–1734, 12 2017.

[40] S. Guo, L. He, R. Yang, B. Chen, X. Xie, B. Jiang, T. Weidong, and Y. Ding, "Enhanced effects of electrospun collagen-chitosan nanofiber membranes on guided bone regeneration," *Journal of Biomaterials Science, Polymer Edition*, vol. 31, pp. 155–168, 1 2020.

[41] F. B. D. Sousa, H. S. Barud, A. Delgado, M. P. Dieterle, T. Steinberg, P. Tomakidi, J. Nohava, K. Vach, S. D. Schulz, E. Hellwig, and S. Proksch, "Novel in situ-cross-linked electrospun gelat-

in/hydroxyapatite nonwoven scaffolds prove suitable for periodontal tissue engineering," *Pharmaceutics*, 2022.

[42] M. Yang, X. Gao, Z. Shen, X. Shi, and Z. Lin, "Gelatin-assisted conglutination of aligned polycaprolactone nanofilms into a multilayered fibre-guiding scaffold for periodontal ligament regeneration," *RSC Advances*, vol. 9, pp. 507–518, 2019.

[43] X. Xu, Y. Zhou, K. Zheng, X. Li, L. Li, and Y. Xu, "3d polycaprolactone/gelatin-oriented electrospun scaffolds promote periodontal regeneration," *ACS Applied Materials and Interfaces*, 10 2022.

[44] W. Peng, S. Ren, Y. Zhang, R. Fan, Y. Zhou, L. Li, X. Xu, and Y. Xu, "Mgo nanoparticles-incorporated pcl/gelatin-derived coaxial electrospinning nanocellulose membranes for periodontal tissue regeneration," *Frontiers in Bioengineering and Biotechnology*, vol. 9, 3 2021.

[45] S. Ren, Y. Zhou, K. Zheng, X. Xu, J. Yang, X. Wang, L. Miao, H. Wei, and Y. Xu, "Cerium oxide nanoparticles loaded nanofibrous membranes promote bone regeneration for periodontal tissue engineering," *Bioactive Materials*, vol. 7, pp. 242–253, 1 2022.

[46] T. Y. Huang, M. Shahrousvand, Y. T. Hsu, and W. T. Su, "Polycaprolactone/polyethylene glycol blended with dipsacus asper wall extract nanofibers promote osteogenic differentiation of periodontal ligament stem cells," *Polymers*, vol. 13, 7 2021.

[47] F. Tondnevis, M. A. Ketabi, R. Fekrazad, A. Sadeghi, H. Keshvari, and M. M. Abolhasani, "In vitro characterization of polyurethane-carbon nanotube drug eluting composite scaffold for dental tissue engineering application," *Journal of Biomimetics, Biomaterials and Biomedical Engineering*, vol. 47, pp. 13–24, 2020.

[48] L. Jiang, Z. Ding, S. Xia, Y. Liu, S. Lei, M. Zhong, and X. Chen, "Poly lactic-co-glycolic acid scaffold loaded with plasmid dna encoding fibroblast growth factor-2 promotes periodontal ligament regeneration of replanted teeth," *Journal of Periodontal Research*, vol. 55, pp. 488–495, 8 2020.

[49] J. Chen, W. Li, Q. Li, Y. Wang, B. Zhao, X. Han, J. Deng, and Y. Liu, "The composite sandwich structure of dncps polyelectrolyte multilayers induced the osteogenic differentiation of pdlscs in vitro," *Journal of Applied Biomaterials and Functional Materials*, vol. 18, 2020.

[50] Q. Ou, Y. Miao, F. Yang, X. Lin, L. M. Zhang, and Y. Wang, "Zein/gelatin/nanohydroxyapatite nanofibrous scaffolds are biocompatible and promote osteogenic differentiation of human periodontal ligament stem cells," *Biomaterials Science*, vol. 7, pp. 1973–1983, 5 2019.

[51] B. Zhao, J. Chen, L. Zhao, J. Deng, and Q. Li, "A simvastatin-releasing scaffold with periodontal ligament stem cell sheets for periodontal regeneration," *Journal of Applied Biomaterials and Functional Materials*, vol. 18, 2020.

[52] L. Shang, Z. Liu, B. Ma, J. Shao, B. Wang, C. Ma, and S. Ge, "Dimethyloxallyl glycine/nanosilicates-loaded osteogenic/angiogenic difunctional fibrous structure for functional periodontal tissue regeneration," *Bioactive Materials*, vol. 6, pp. 1175–1188, 4 2021.

[53] H. Lyu, X. Zhou, Y. Qian, X. Liu, G. Gopinathan, M. Pandya, C. Qin, X. Luan, and T. G. Diekwisch, "Long-acting pfi-2 small molecule release and multilayer scaffold design achieve extensive new formation of complex periodontal tissues with unprecedented fidelity," *Biomaterials*, p. 121819, 11 2022.

[54] R. Serôdio, S. L. Schickert, A. R. Costa-Pinto, J. R. Dias, P. L. Granja, F. Yang, and A. L. Oliveira, "Ultrasound sonication prior to electrospinning tailors silk fibroin/peo membranes for periodontal regeneration," *Materials Science and Engineering C*, vol. 98, pp. 969–981, 5 2019.

[55] H. Zhang, H. Ma, R. Zhang, K. Wang, and J. Liu, "Construction and characterization of antibacterial plga/wool keratin/ornidazole composite membranes for periodontal guided tissue regeneration," *Journal of Biomaterials Applications*, vol. 34, pp. 1267–1281, 4 2020.

[56] H. Zhang, K. Wang, T. Gao, R. Zhang, Z. Cai, J. Liu, H. Ma, and W. Zhang, "Controlled release of bfgf loaded into electrospun core-shell fibrous membranes for use in guided tissue regeneration," *Biomedical Materials (Bristol)*, vol. 15, 5 2020.

[57] E. A. Münchow, M. T. P. Albuquerque, B. Zero, K. Kamocki, E. Piva, R. L. Gregory, and M. C. Bottino, "Development and characterization of novel zno-loaded electrospun membranes for periodontal regeneration," *Dental Materials*, vol. 31, pp. 1038–1051, 9 2015.

[58] A. Nasajpour, S. Ansari, C. Rinoldi, A. S. Rad, T. Aghaloo, S. R. Shin, Y. K. Mishra, R. Adelung, W. Swieszkowski, N. Annabi, A. Khademhosseini, A. Moshaverinia, and A. Tamayol, "A multifunctional polymeric periodontal membrane with osteogenic and antibacterial characteristics," *Advanced Functional Materials*, vol. 28, 1 2018.

[59] R. Shen, W. Xu, Y. Xue, L. Chen, H. Ye, E. Zhong, Z. Ye, J. Gao, and Y. Yan, "The use of chitosan/pla nano-fibers by emulsion eletrospinning for periodontal tissue engineering," *Artificial Cells, Nanomedicine and Biotechnology*, vol. 46, pp. 419–430, 11 2018.

[60] F. Yang, Y. Miao, Y. Wang, L. M. Zhang, and X. Lin, "Electrospun zein/gelatin scaffold-enhanced cell attachment and growth of human periodontal ligament stem cells," *Materials*, vol. 10, 10 2017.

[61] T. Zhou, X. Liu, B. Sui, C. Liu, X. Mo, and J. Sun, "Development of fish collagen/bioactive glass/chitosan composite nanofibers as a gtr/gbr membrane for inducing periodontal tissue regeneration," *Biomedical Materials (Bristol)*, vol. 12, 9 2017.

[62] J. Song, A. Klymov, J. Shao, Y. Zhang, W. Ji, E. Kolwijck, J. A. Jansen, S. C. Leeuwenburgh, and F. Yang, "Electrospun nanofibrous silk fibroin membranes containing gelatin nanospheres for controlled delivery of biomolecules," *Advanced Healthcare Materials*, vol. 6, 7 2017.

[63] L. N. Jia, X. Zhang, H. Y. Xu, F. Hua, X. G. Hu, Q. Xie, W. Wang, and J. Jia, "Development of a doxycycline hydrochloride-loaded electrospun nanofibrous membrane for gtr/gbr applications," *Journal of Nanomaterials*, vol. 2016, 2016.

[64] X. Chen, Y. Liu, L. Miao, Y. Wang, S. Ren, X. Yang, Y. Hu, and W. Sun, "Controlled release of recombinant human cementum protein 1 from electrospun multiphasic scaffold for cementum regeneration," *International Journal of Nanomedicine*, vol. 11, pp. 3145–3158, 7 2016.

[65] M. S. Carvalho, J. C. Silva, R. N. Udangawa, J. M. Cabral, F. C. Ferreira, C. L. da Silva, R. J. Linhardt, and D. Vashishth, "Co-culture cell-derived extracellular matrix loaded electrospun microfibrous scaffolds for bone tissue engineering," *Materials Science and Engineering C*, vol. 99, pp. 479–490, 6 2019.

[66] R. Xue, Y. Qian, L. Li, G. Yao, L. Yang, and Y. Sun, "Polycaprolactone nanofiber scaffold enhances the osteogenic differentiation potency of various human tissue-derived mesenchymal stem cells," *Stem Cell Research and Therapy*, vol. 8, 6 2017.

[67] J. Li and S. Zhuang, "Antibacterial activity of chitosan and its derivatives and their interaction mechanism with bacteria: Current state and perspectives," *European Polymer Journal*, vol. 138, 9 2020.

[68] Y. He, W. Wang, X. Tang, and X. Liu, "Osteogenic induction of bone marrow mesenchymal cells on electrospun polycaprolactone/chitosan nanofibrous membrane," *Dental Materials Journal*, vol. 36, pp. 325–332, 2017.

[69] S. B. Qasim, M. S. Zafar, S. Najeeb, Z. Khurshid, A. H. Shah, S. Husain, and I. U. Rehman, "Electrospinning of chitosan-based solutions for tissue engineering and regenerative medicine," *International Journal of Molecular Sciences*, vol. 19, 2 2018.

[70] C. Cui, S. Sun, S. Wu, S. Chen, J. Ma, and F. Zhou, "Electrospun chitosan nanofibers for wound healing application," *Engineered Regeneration*, vol. 2, pp. 82–90, 2021.

[71] M. H. Mirmusavi, M. Ahmadian, and S. Karbasi, "Polycaprolactone-chitosan/multi-walled carbon nanotube: A highly strengthened electrospun nanocomposite scaffold for cartilage tissue engineering," *International Journal of Biological Macromolecules*, vol. 209, pp. 1801–1814, 6 2022.

[72] M. S. Karizmeh, S. A. Poursamar, A. Kefayat, Z. Farahbakhsh, and M. Rafienia, “An in vitro and in vivo study of pcl/chitosan electrospun mat on polyurethane/propolis foam as a bilayer wound dressing,” *Materials Science and Engineering: C*, p. 112667, 4 2022.

[73] O. K. Topsoy, F. Muhammad, S. Kolak, A. Ulu, Öznur Güngör, M. Şimşek, S. Köytepe, and B. Ateş, “Fabrication of electrospun polycaprolactone/chitosan nanofiber-modified screen-printed electrode for highly sensitive detection of diazinon in food analysis,” *Measurement: Journal of the International Measurement Confederation*, vol. 187, 1 2022.

[74] E. Saatcioglu, S. Ulag, A. Sahin, B. K. Yilmaz, N. Ekren, A. T. Inan, Y. Palaci, C. B. Ustundag, and O. Gunduz, “Design and fabrication of electrospun polycaprolactone/chitosan scaffolds for ligament regeneration,” *European Polymer Journal*, vol. 148, 4 2021.

[75] M. Oviedo, Y. Montoya, W. Agudelo, A. García-García, and J. Bustamante, “Effect of molecular weight and nanoarchitecture of chitosan and polycaprolactone electrospun membranes on physicochemical and hemocompatible properties for possible wound dressing,” *Polymers*, vol. 13, 12 2021.

[76] J. Zhu, H. Ye, D. Deng, J. Li, and Y. Wu, “Electrospun metformin-loaded polycaprolactone/chitosan nanofibrous membranes as promoting guided bone regeneration membranes: Preparation and characterization of fibers, drug release, and osteogenic activity in vitro,” *Journal of Biomaterials Applications*, vol. 34, pp. 1282–1293, 4 2020.

[77] Y. Zou, C. Zhang, P. Wang, Y. Zhang, and H. Zhang, “Electrospun chitosan/polycaprolactone nanofibers containing chlorogenic acid-loaded halloysite nanotube for active food packaging,” *Carbohydrate Polymers*, vol. 247, 11 2020.

[78] H. Ye, J. Zhu, D. Deng, S. Jin, J. Li, and Y. Man, “Enhanced osteogenesis and angiogenesis by pcl/chitosan/sr-doped calcium phosphate electrospun nanocomposite membrane for guided bone regeneration,” *Journal of Biomaterials Science, Polymer Edition*, vol. 30, pp. 1505–1522, 11 2019.

[79] F. Sharifi, S. M. Atyabi, D. Norouzian, M. Zandi, S. Irani, and H. Bakhshi, “Polycaprolactone/carboxymethyl chitosan nanofibrous scaffolds for bone tissue engineering application,” *International Journal of Biological Macromolecules*, vol. 115, pp. 243–248, 8 2018.

[80] M. Hadjianfar, D. Semnani, and J. Varshosaz, “Polycaprolactone/chitosan blend nanofibers loaded by 5-fluorouracil: An approach to anticancer drug delivery system,” *Polymers for Advanced Technologies*, vol. 29, pp. 2972–2981, 12 2018.

[81] L. Liverani, J. Lacina, J. A. Roether, E. Boccardi, M. S. Killian, P. Schmuki, D. W. Schubert, and A. R. Boccaccini, "Incorporation of bioactive glass nanoparticles in electrospun pcl/chitosan fibers by using benign solvents," *Bioactive Materials*, vol. 3, pp. 55–63, 3 2018.

[82] N. Saderi, M. Rajabi, B. Akbari, M. Firouzi, and Z. Hassannejad, "Fabrication and characterization of gold nanoparticle-doped electrospun pcl/chitosan nanofibrous scaffolds for nerve tissue engineering," *Journal of Materials Science: Materials in Medicine*, vol. 29, 9 2018.

[83] E. Bolaina-Lorenzo, C. Martinez-Ramos, M. Monleón-Pradas, W. Herrera-Kao, J. V. Cauich-Rodriguez, and J. M. Cervantes-Uc, "Electrospun polycaprolactone/chitosan scaffolds for nerve tissue engineering: Physicochemical characterization and schwann cell biocompatibility," *Biomedical Materials (Bristol)*, vol. 12, 2 2017.

[84] S. Gomes, G. Rodrigues, G. Martins, C. Henriques, and J. C. Silva, "Evaluation of nanofibrous scaffolds obtained from blends of chitosan, gelatin and polycaprolactone for skin tissue engineering," *International Journal of Biological Macromolecules*, vol. 102, pp. 1174–1185, 9 2017.

[85] O. Urbanek, P. Sajkiewicz, and F. Pierini, "The effect of polarity in the electrospinning process on pcl/chitosan nanofibres' structure, properties and efficiency of surface modification," *Polymer*, vol. 124, pp. 168–175, 8 2017.

[86] D. Semnani, E. Naghashzargar, M. Hadjianfar, F. D. Manshadi, S. Mohammadi, S. Karbasi, and F. Effaty, "Evaluation of pcl/chitosan electrospun nanofibers for liver tissue engineering," *International Journal of Polymeric Materials and Polymeric Biomaterials*, vol. 66, pp. 149–157, 2 2017.

[87] T. Fukunishi, C. A. Best, T. Sugiura, T. Shoji, T. Yi, B. Udelsman, D. Ohst, C. S. Ong, H. Zhang, T. Shinoka, C. K. Breuer, J. Johnson, and N. Hibino, "Tissue-engineered small diameter arterial vascular grafts from cell-free nanofiber pcl/chitosan scaffolds in a sheep model," *PLoS ONE*, vol. 11, 7 2016.

[88] T. Prasad, E. A. Shabeena, D. Vinod, T. V. Kumary, and P. R. A. Kumar, "Characterization and in vitro evaluation of electrospun chitosan/polycaprolactone blend fibrous mat for skin tissue engineering," *Journal of Materials Science: Materials in Medicine*, vol. 26, pp. 1–13, 11 2015.

[89] J. Sims-Mourtada, R. A. Niamat, S. Samuel, C. Eskridge, and E. B. Kmiec, "Enrichment of breast cancer stem-like cells by growth on electrospun polycaprolactone-chitosan nanofiber scaffolds," *International Journal of Nanomedicine*, vol. 9, pp. 995–1003, 2 2014.

[90] I. Steyaert, L. V. D. Schueren, H. Rahier, and K. D. Clerck, "An alternative solvent system for blend electrospinning of polycaprolactone/chitosan nanofibres," *Macromolecular Symposia*, vol. 321-322, pp. 71–75, 12 2012.

[91] O. Urbanek, P. Sajkiewicz, F. Pierini, M. Czerkies, and D. Kołbuk, “Structure and properties of polycaprolactone/chitosan nonwovens tailored by solvent systems,” *Biomedical Materials (Bristol)*, vol. 12, 2 2017.

[92] O. A. Monteiro and C. Airoldi, “Some studies of crosslinking chitosan–glutaraldehyde interaction in a homogeneous system,” *International Journal of Biological Macromolecules*, vol. 26, no. 2, pp. 119–128, 1999.

[93] V. Guarino, I. Cruz-Maya, R. Altobelli, W. K. A. Khodir, L. Ambrosio, M. A. A. Pèrez, and A. A. Flores, “Electrospun polycaprolactone nanofibres decorated by drug loaded chitosan nano-reservoirs for antibacterial treatments,” *Nanotechnology*, vol. 28, 11 2017.

[94] W. K. W. A. Khodir, V. Guarino, M. A. Alvarez-Perez, C. Cafiero, and L. Ambrosio, “Trapping tetracycline-loaded nanoparticles into polycaprolactone fiber networks for periodontal regeneration therapy,” *Journal of Bioactive and Compatible Polymers*, vol. 28, pp. 258–273, 5 2013.

[95] Špela Zupančič, L. Casula, T. Rijavec, A. Lapanje, M. Luštrik, A. M. Fadda, P. Kocbek, and J. Kristl, “Sustained release of antimicrobials from double-layer nanofiber mats for local treatment of periodontal disease, evaluated using a new micro flow-through apparatus,” *Journal of Controlled Release*, vol. 316, pp. 223–235, 12 2019.

[96] M. Demir, F. Büyükserin, and E. Bayrak, “Development and characterization of metronidazole-loaded and chitosan-coated pcl electrospun fibres for potential applications in guided tissue regeneration,” *Trends Biomater. Artif. Organs*, vol. 35, pp. 255–263, 2021.

[97] K. T. Shalumon, S. Sowmya, D. Sathish, K. P. Chennazhi, S. V. Nair, and R. Jayakumar, “Effect of incorporation of nanoscale bioactive glass and hydroxyapatite in pcl/chitosan nanofibers for bone and periodontal tissue engineering,” *Journal of Biomedical Nanotechnology*, vol. 9, pp. 430–440, 3 2013.

[98] M. Gümüşderelioğlu, E. Sunal, T. T. Demirtaş, and A. S. Kiremitçi, “Chitosan-based double-faced barrier membrane coated with functional nanostructures and loaded with bmp-6,” *Journal of Materials Science: Materials in Medicine*, vol. 31, 1 2020.

[99] L. Zhang, Y. Dong, N. Zhang, J. Shi, X. Zhang, C. Qi, A. C. Midgley, and S. Wang, “Potentials of sandwich-like chitosan/polycaprolactone/gelatin scaffolds for guided tissue regeneration membrane,” *Materials Science and Engineering C*, vol. 109, 4 2020.

[100] W. Jiang, L. Li, D. Zhang, S. Huang, Z. Jing, Y. Wu, Z. Zhao, L. Zhao, and S. Zhou, “Incorporation of aligned pcl-peg nanofibers into porous chitosan scaffolds improved the orientation of collagen fibers in regenerated periodontium,” *Acta Biomaterialia*, vol. 25, pp. 240–252, 10 2015.

[101] B. C. Heng, S. Zhu, J. Xu, C. Yuan, T. Gong, and C. Zhang, "Effects of decellularized matrices derived from periodontal ligament stem cells and shed on the adhesion, proliferation and osteogenic differentiation of human dental pulp stem cells in vitro," *Tissue and Cell*, vol. 48, no. 2, pp. 133–143, 2016.

[102] Y. Jiang, J. M. Liu, J. P. Huang, K. X. Lu, W. L. Sun, J. Y. Tan, B. X. Li, L. L. Chen, and Y. M. Wu, "Regeneration potential of decellularized periodontal ligament cell sheets combined with 15-deoxy-Δ12,14-prostaglandin j2 nanoparticles in a rat periodontal defect," *Biomedical Materials (Bristol)*, vol. 16, 7 2021.

[103] A. Farag, C. Vaquette, C. Theodoropoulos, S. M. Hamlet, D. W. Hutmacher, and S. Ivanovski, "Decellularized periodontal ligament cell sheets with recellularization potential," *Journal of Dental Research*, vol. 93, pp. 1313–1319, 12 2014.

[104] A. Farag, S. M. Hashimi, C. Vaquette, P. M. Bartold, D. W. Hutmacher, and S. Ivanovski, "The effect of decellularized tissue engineered constructs on periodontal regeneration," *Journal of Clinical Periodontology*, vol. 45, pp. 586–596, 5 2018.

[105] J. C. Silva, M. S. Carvalho, X. Han, K. Xia, P. E. Mikael, J. M. Cabral, F. C. Ferreira, and R. J. Linhardt, "Compositional and structural analysis of glycosaminoglycans in cell-derived extracellular matrices," *Glycoconjugate Journal*, vol. 36, pp. 141–154, 4 2019.

[106] D. Garna, M. Kaur, F. J. Hughes, and M. Ghuman, "Comparison of the expression of periodontal markers in dental and bone marrow-derived mesenchymal stem cells." *The Open Dentistry Journal*, vol. 14, pp. 196–202, 5 2020.

[107] S. Yamada, M. Tomoeda, Y. Ozawa, S. Yoneda, Y. Terashima, K. Ikezawa, S. Ikegawa, M. Saito, S. Toyosawa, and S. Murakami, "Plap-1/asporin, a novel negative regulator of periodontal ligament mineralization*," *Journal of Biological Chemistry*, vol. 282, no. 32, pp. 23 070–23 080, 2007.

[108] M. S. Carvalho, J. C. Silva, C. M. Hoff, J. M. Cabral, R. J. Linhardt, C. L. da Silva, and D. Vashishth, "Loss and rescue of osteocalcin and osteopontin modulate osteogenic and angiogenic features of mesenchymal stem/stromal cells," *Journal of Cellular Physiology*, vol. 235, pp. 7496–7515, 10 2020.

[109] C. Gao, L. Fu, Y. Yu, X. Zhang, X. Yang, and Q. Cai, "Strategy of a cell-derived extracellular matrix for the construction of an osteochondral interlayer," *Biomaterials Science*, 2022.

[110] S. R. Banavar, S. Y. Rawal, I. C. Paterson, G. Singh, F. Davamani, S. P. Khoo, and E. L. Tan, "Establishing a technique for isolation and characterization of human periodontal ligament derived mesenchymal stem cells," *The Saudi Dental Journal*, vol. 33, no. 7, pp. 693–701, 2021.

[111] S. Novello, S. Tricot-Doleux, A. Novella, P. Pellen-Mussi, and S. Jeanne, "Influence of periodontal ligament stem cell-derived conditioned medium on osteoblasts," *Periodontal Ligament Stem Cell-Derived Conditioned Medium on Osteoblasts. Pharmaceutics, MDPI*, vol. 2022, p. 729, 2022.

[112] I. C. Gay, S. Chen, and M. MacDougall, "Isolation and characterization of multipotent human periodontal ligament stem cells," *Orthodontics and Craniofacial Research*, vol. 10, pp. 149–160, 2007.

[113] Z. X. Yang, Z.-B. Han, Y. R. Ji, Y. W. Wang, L. Liang, Y. Chi, S. G. Yang, L. N. Li, W. F. Luo, J. P. Li, D. D. Chen, W. J. Du, X. C. Cao, G. S. Zhuo, T. Wang, and Z. C. Han, "Cd106 identifies a subpopulation of mesenchymal stem cells with unique immunomodulatory properties," *PLOS ONE*, vol. 8, no. 3, pp. 1–12, 03 2013.

[114] W. Zhu and M. Liang, "Periodontal ligament stem cells: Current status, concerns, and future prospects," *Stem Cells International*, vol. 2015, 2015.

[115] J. D. Schiffman and C. L. Schauer, "Cross-linking chitosan nanofibers," *Biomacromolecules*, vol. 8, pp. 594–601, 2 2007.

[116] X. Yang, X. Chen, and H. Wang, "Acceleration of osteogenic differentiation of preosteoblastic cells by chitosan containing nanofibrous scaffolds," *Biomacromolecules*, vol. 10, pp. 2772–2778, 10 2009.

[117] C. Dong, F. Qiao, G. Chen, and Y. Lv, "Demineralized and decellularized bone extracellular matrix-incorporated electrospun nanofibrous scaffold for bone regeneration," *Journal of Materials Chemistry B*, vol. 9, pp. 6881–6894, 9 2021.

[118] A. Padalhin, R. Ventura, B. Kim, T. Sultana, C. M. Park, and B. T. Lee, "Boosting osteogenic potential and bone regeneration by co-cultured cell derived extracellular matrix incorporated porous electrospun scaffold," *Journal of Biomaterials Science, Polymer Edition*, vol. 32, pp. 779–798, 2021.

[119] Y. Fu, L. Liu, R. Cheng, and W. Cui, "Ecm decorated electrospun nanofiber for improving bone tissue regeneration," *Polymers*, vol. 10, 3 2018.

[120] J. Du and M. Li, "Functions of periostin in dental tissues and its role in periodontal tissues' regeneration," *Cellular and Molecular Life Sciences*, vol. 74, pp. 4279–4286, 12 2017.

[121] M. Komaki, K. Iwasaki, H. Arzate, A. S. Narayanan, Y. Izumi, and I. Morita, "Cementum protein 1 (cemp1) induces a cementoblastic phenotype and reduces osteoblastic differentiation in periodontal ligament cells," *Journal of Cellular Physiology*, vol. 227, pp. 649–657, 1 2012.

Appendix

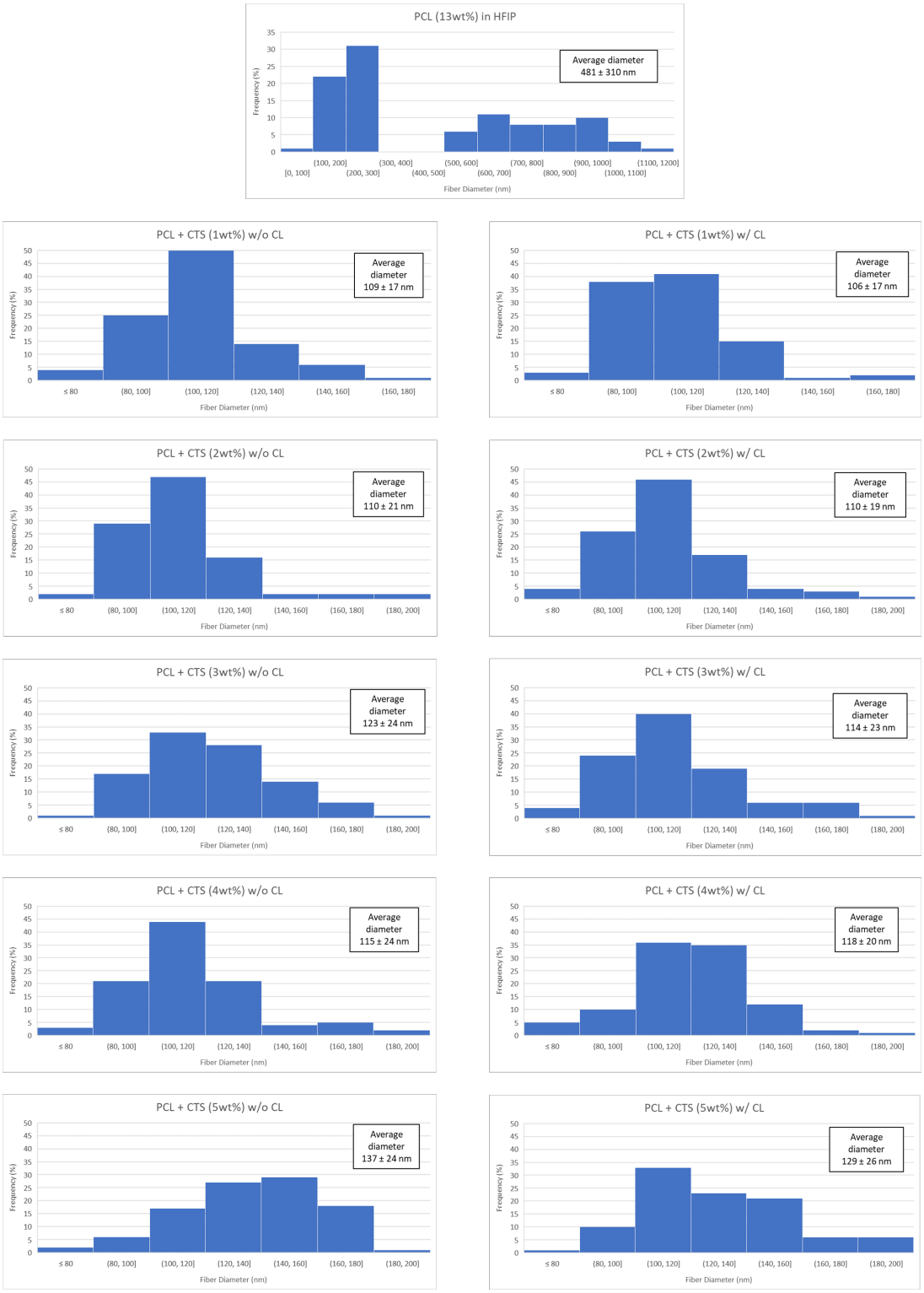

Figure A.1: Fiber diameter distribution of PCL and PCL-CTS electrospun scaffolds prepared with 1%, 2%, 3%, 4% and 5% CTS solutions, with (w/) and without (w/o) crosslinking (CL).

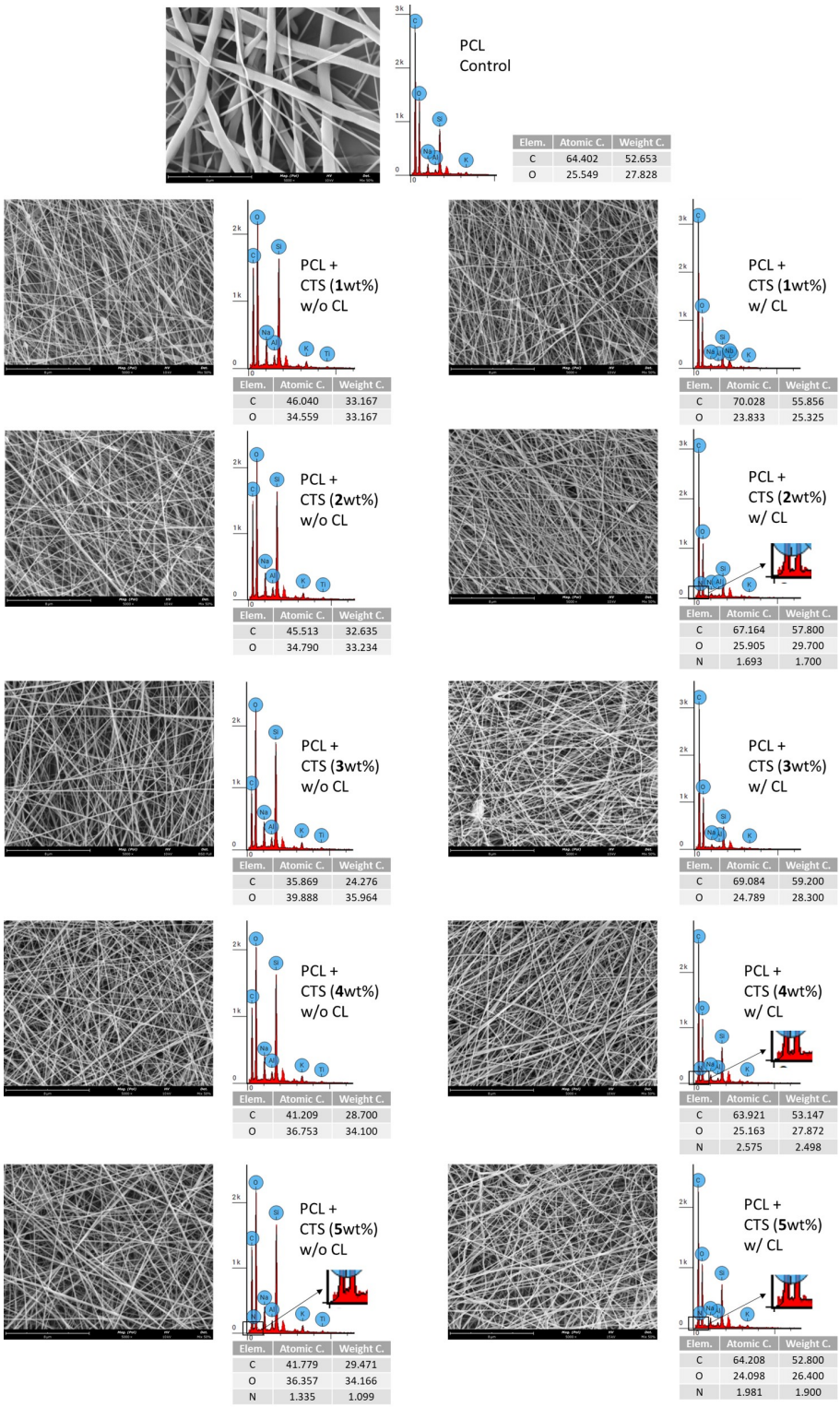

Figure A.2: SEM images, EDX spectra, atomic and weight percentages of carbon (C), oxygen (O) and nitrogen (N) of PCL and PCL-CTS electrospun scaffolds, prepared with 1%, 2%, 3%, 4% and 5% CTS solutions, with (w/) and without (w/o) crosslinking (CL). Scale bar 8 µm.

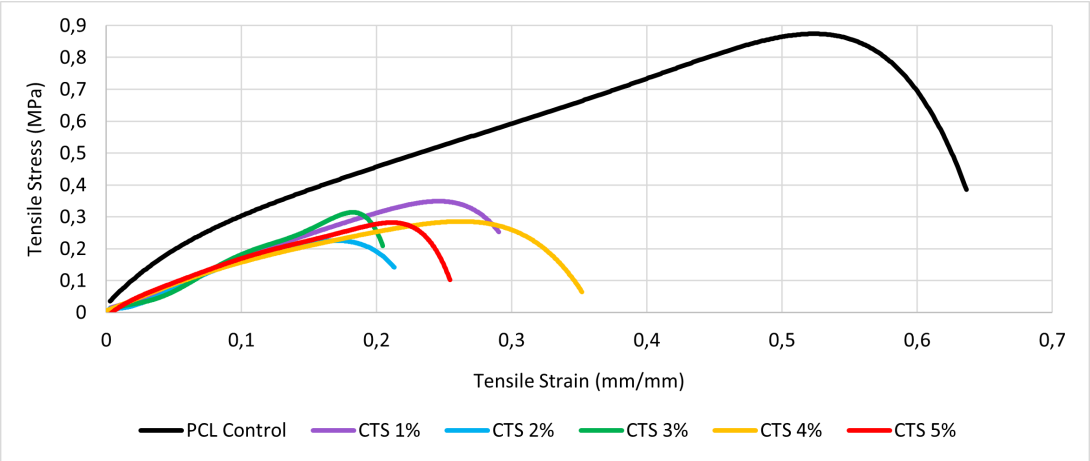

Figure A.3: Representative stress-strain curves of PCL and PCL-CTS electrospun scaffolds, prepared with 1%, 2%, 3%, 4% and 5% CTS solutions, without crosslinking.

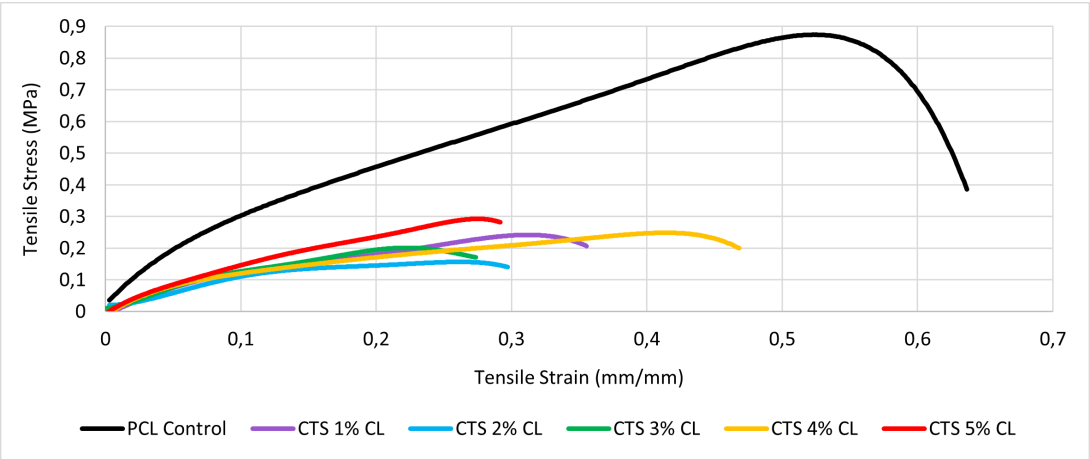

Figure A.4: Representative stress-strain curves of PCL and PCL-CTS electrospun scaffolds prepared with 1%, 2%, 3%, 4% and 5% CTS solutions, with crosslinking (CL).

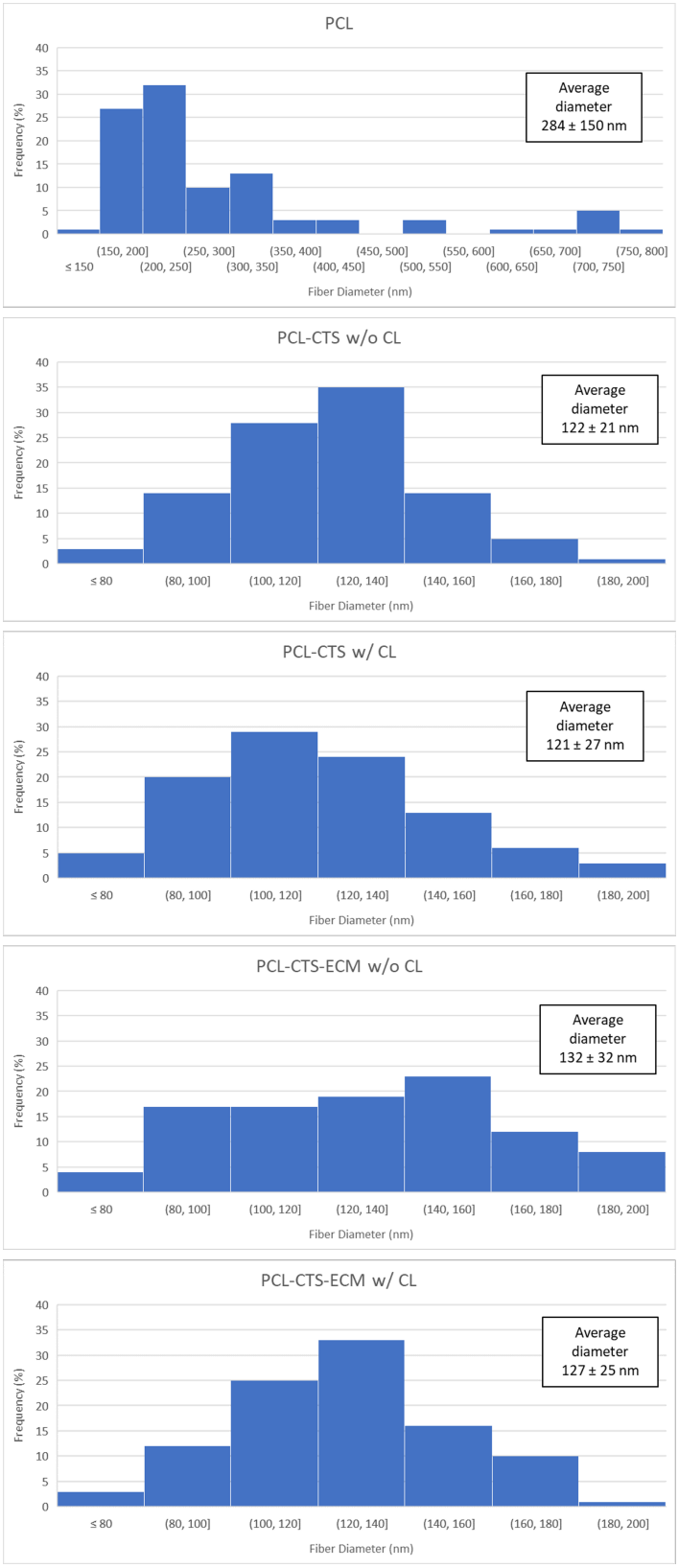

Figure A.5: Fiber diameter distribution of PCL, PCL-CTS and PCL-CTS-ECM electrospun scaffolds prepared with 5% CTS solution, with (w/) and without (w/o) crosslinking (CL).

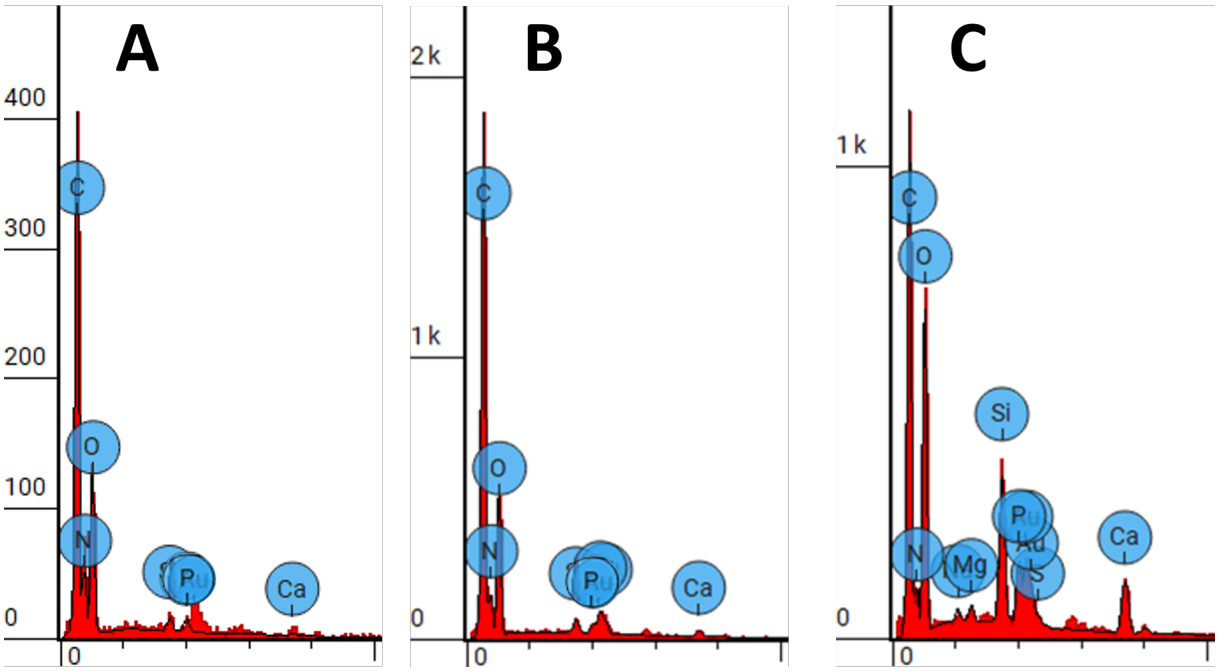

Figure A.6: EDX spectra obtained from the analysis of the spots outlined red in fig. 4.32 of PCL (A), PCL-CTS (B) and PCL-CTS-ECM (C) electrospun scaffolds after 21 days of PDLSCs osteogenic differentiation.